Some Effects of Mechanical Damping on the Self-Induced Aeroelastic Oscillations of an Axial Compressor Blade

I. M. DAVIDSON

(National Gas Turbine Establishment)

SUMMARY: By a slight modification to den Hartog's classical theory of harmonically forced vibration off resonance it is shown that, with such distorted forcing wave forms as might be encountered in the stalling or choking flutter of an aerofoil in cascade, the influence of damping on the amplitude of motion can still be assessed with considerable accuracy by the assumption of an equivalent harmonic excitation. The result is valid for any amount of Coulomb damping at which motion is significant in the presence of any "velocity" damping coefficient up to that defined by a logarithmic decrement of about 1·3, the formal conclusion of the argument being stated in Section 4.

1. Introduction

Among the stress components experienced by the blading of an axial compressor one of the most important is the periodic bending stress produced by such oscillations as are due partly to mechanical forcing through the disc or casing, partly to aerodynamic forcing by periodically incident wakes, and in the worst practical instances to self-induced aeroelastic oscillation of the blades involved. Such self-induced oscillations cannot safely be assumed to bear any simple relationship to flutter as it is known in the aircraft field, for they arise most often in a single degree of freedom and in an air stream which is not only unsteady but often manifestly periodic in nature. An attempt has been made[1] to demonstrate that such an instability could occur with a cascade in incompressible potential flow, but only with such assumptions as to render the conclusions inapplicable in practice.

Generally there is, even in the presence of significant aerodynamic forcing, no serious oscillation until the blading is driven beyond a critical combination of incidence and Mach number. In the possible operating range of a typical axial compressor there may be two or more such regions, one corresponding to stalling and another to choking flutter. Since the periodicity of the field in which the cascade is situated will have both incidence and Mach number components it may often produce a triggering effect, but one which need have no bearing on the subsequent oscillatory stress.

Originally received June 1953.
[The Aeronautical Quarterly, Vol. VI, May 1955]

When a multi-stage compressor is throttled the incidence on its blading increases, but at a different rate in each stage. Thus, long before there is any one-dimensional instability of the general stream through the compressor some individual stage will stall, usually not as a whole, but in patches or cells which may move around the annulus at some fraction of the shaft speed[2]. The effect is of philosophical importance because it constitutes a marked distinction between the behaviour of infinite and finite but unbounded cascades. In practice it means that stalling flutter will often occur in regular but discrete bursts, while the blading in cascades other than that which is stalling will be subjected to what might with licence be described as periodically recurring, sharp-edged gusts.

However, although each blade in the affected cascade may flutter only in bursts, it will be oscillating continuously as a result of the mechanical forcing transmitted through the disc or casing from other blades in the cascade. In the face of such physical complexity there is little hope of studying in detail the variation with time of the gas load on any one blade, so that the practical solution must lie in the adoption of a panacea either for the elimination of the operational circumstances in which flutter is possible, or for the mitigation of its effects when they occur. One possibility is the incorporation in the blade or its root fixing of artificially enhanced mechanical damping, and the principal object of this paper is a demonstration of the fact that the effects of such damping can be accurately assessed without reference to the aerodynamic mechanism of the flutter.

Before proceeding it is desirable to consider in a little more detail the differences between an aerodynamically forced oscillation and one which is self-induced. One practical distinction is that a damped blade may have quite a "broadly tuned" resonance curve and so could be forced (mechanically or aerodynamically) to oscillate over a wide frequency range, while in flutter the same blade would exhibit only its natural frequency. A more important distinction concerns the harmonic or overtone frequencies, for a blade can be forced not only in the region of its fundamental frequency but also in the region of one or more of its harmonics. For example, in the presence of the forcing wave form of Fig. 4 and Table II a typical blade would exhibit simultaneously its fundamental frequency, certainly its first, and perhaps also its second overtone—just like a musical instrument. In flutter, however, the energy will be extracted from the air stream principally in the region of the blade tip and the co-existence of an overtone mode would clearly upset the whole process. Thus, even when the periodic gas bending moment varies temporally in accordance with Fig. 4 and Table II, the blade will perform only in its fundamental mode and only at its fundamental frequency. This point is vital to the whole analysis and is why the results do not apply in instances of mechanically or aerodynamically forced vibration.

Finally, to those skilled in the art of flutter as it is understood in the aircraft field, the mathematical approach and in particular the initial equations of this paper may seem a little strange. The answer might be said to lie in the fact that, whatever may be the form of its aerodynamic excitation, the motion of a fluttering cascade blade is known from observation to be very nearly sinusoidal.

NOTATION

A_n	lifting moment Fourier coefficient
B_n	lifting moment Fourier coefficient
c	"velocity" damping coefficient
F	Coulomb damping coefficient
k	effective stiffness
m	effective mass
n	term number in series
p	height of forcing pulse
P_n	lifting moment Fourier coefficient
t	time
x	displacement of blade tip
X	semi-amplitude of blade tip
X_+	positive part-amplitude of blade tip
X_-	negative part-amplitude of blade tip
γ	"velocity" damping factor
Γ	magnification factor
δ	logarithmic decrement
Δ	"F" vector phase lead
ν	term number in series
ρ	relative natural frequency
ϕ	a phase angle
ψ_n	a phase angle
ω	natural frequency in rad./sec.

2. The Basic Theory

2.1. THE EXACT THEORY

Consider a single cascade blade which is oscillating in its fundamental flexural mode in an air stream of unknown state with a tip amplitude of $(X_+ - X_-)$ about its rest position as in Fig. 1 so that, whatever the aerodynamic circumstances, the periodic gas bending moment which it experiences is defined at any time t by the series:—

$$\text{Periodic lifting moment} = \sum_{n=1,2,3}^{\infty} A_n \cos n\omega t + \sum_{n=1,2,3}^{\infty} B_n \sin n\omega t. \quad . \quad . \quad . \quad . \quad (1)$$

The period of this motion is $2\pi/\omega$ and the Fourier coefficients are in general functions of X_+, X_- and the velocity and state of the air stream.

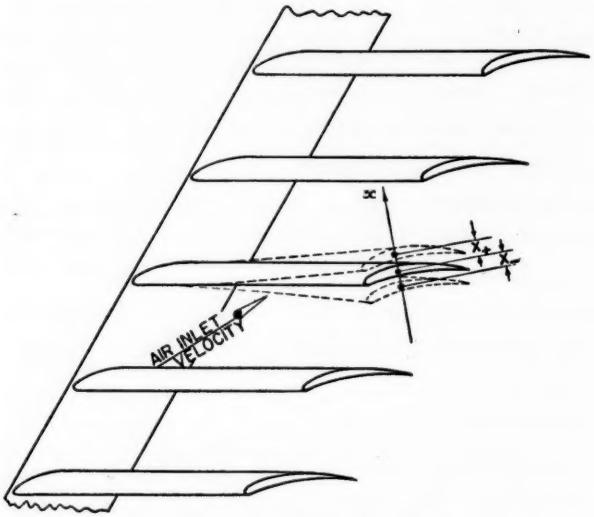

Fig. 1.
The physical system.

In general, it will be necessary to assume for the mechanical damping of the blade and its root, and so on, both "velocity" and Coulomb components, the latter being represented for the moment by the square-topped wave:—

$$\text{Coulomb damping moment} = \frac{4F}{\pi} \sum_{\nu=1,3,5}^{\infty} \frac{1}{\nu} \sin \nu \omega t \quad . \quad . \quad (2)$$

which has a semi-amplitude of F. It should be observed that this assumption is valid only if, for $dx/dt=0$ at $t=0$, we also have $dx/dt=0$ at $t=\pi/\omega$, and to this extent the equation of motion must anticipate its own solution. Should it transpire that there are regions in which the solution will not satisfy these conditions simultaneously, the Fourier series representing the Coulomb damping moment will become generally indeterminate. However, for any numerical example, an exact solution could still be obtained by an iterative process involving the unknown coefficients.

With these assumptions the equation of motion of the blade tip is then

$$m\frac{d^2x}{dt^2} + c\frac{dx}{dt} + kx = \sum_{n=1,2,3}^{\infty} A_n \cos(n\omega t + \phi) + \sum_{n=1,2,3}^{\infty} B_n \sin(n\omega t + \phi) + \frac{4F}{\pi} \sum_{\nu=1,3,5}^{\infty} \frac{1}{\nu} \sin \nu \omega t \quad . \quad . \quad . \quad (3)$$

where m, c and k are respectively the effective mass, "velocity" damping coefficient and stiffness of the blade. The constant phase angle, ϕ, is introduced to satisfy for

simplicity the boundary condition $dx/dt=0$ when $t=0$, and the coefficients m, c, k and F must be cast in moment form to satisfy both equation (3) and the physical system of Fig. 1. As shown in Appendix I, the "steady state" solution of equation (3) is then

$$x=\frac{1}{k}\sum_{n=1,2,3}^{\infty}\frac{P_n}{\{(1-n^2\rho^2)^2+4n^2\gamma^2\rho^2\}^{\frac{1}{2}}}\cos(n\omega t+\psi_n)+$$
$$+\frac{4F}{\pi k}\sum_{\nu=1,3,5}^{\infty}\frac{1}{\nu}\frac{1-\nu^2\rho^2}{(1-\nu^2\rho^2)^2+4\nu^2\gamma^2\rho^2}\sin\nu\omega t-$$
$$-\frac{4F}{\pi k}\sum_{\nu=1,3,5}^{\infty}\frac{2\gamma\rho}{(1-\nu^2\rho^2)^2+4\nu^2\gamma^2\rho^2}\cos\nu\omega t \quad . \quad (4)$$

where $P_n=+(A_n^2+B_n^2)^{\frac{1}{2}}$

$$\tan(\phi-\psi_n)=\frac{2n\gamma\rho A_n+(1-n^2\rho^2)B_n}{(1-n^2\rho^2)A_n-2n\gamma\rho B_n} \quad . \quad . \quad . \quad . \quad (5)$$

and ϕ is given by

$$\sum_{n=1,2,3}^{\infty}n\frac{(1-n^2\rho^2)A_n-2n\gamma\rho B_n}{(1-n^2\rho^2)^2+4n^2\gamma^2\rho^2}\sin\phi-\sum_{n=1,2,3}^{\infty}n\frac{2n\gamma\rho A_n+(1-n^2\rho^2)B_n}{(1-n^2\rho^2)^2+4n^2\gamma^2\rho^2}\cos\phi$$
$$=\frac{4F}{\pi}\sum_{\nu=1,3,5}^{\infty}\frac{1-\nu^2\rho^2}{(1-\nu^2\rho^2)^2+4\nu^2\gamma^2\rho^2} \quad . \quad . \quad (6)$$

However, since this value of ϕ satisfies the condition $dx/dt=0$ when $t=0$, we can write for the positive part of the amplitude of motion

$$X_+=\frac{1}{k}\sum_{n=1,2,3}^{\infty}\frac{P_n\cos\psi_n}{\{(1-n^2\rho^2)^2+4n^2\gamma^2\rho^2\}^{\frac{1}{2}}}-\frac{4F}{\pi k}\sum_{\nu=1,3,5}^{\infty}\frac{2\gamma\rho}{(1-\nu^2\rho^2)^2+4\nu^2\gamma^2\rho^2} \quad . \quad (7)$$

In this solution the non-dimensional parameters γ and ρ are defined by

$$\gamma=\frac{c}{2(mk)^{\frac{1}{2}}} \quad \text{and} \quad \rho=\frac{\omega}{(k/m)^{\frac{1}{2}}} \quad . \quad . \quad . \quad . \quad (8)$$

That is, γ is the ratio of the actual "velocity" damping coefficient to that which would effect critical damping in the absence of any Coulomb force, and ρ is the ratio of the frequency of oscillation to the natural frequency of the undamped blade. Unless they are actually negligible, the aerodynamic and centrifugal contributions to k and the aerodynamic contribution to m must naturally be considered in the estimation of the natural frequency.

2.2. The Physical Significance of the Exact Theory

Since the ultimate aim is the use in practice of an equivalent harmonic excitation, the most important feature of the exact solution is the rate of convergence of its series, for only if this is rapid will any reasonable approximation be achieved. There is thus a temptation to assume $\rho=1$, but a fairly rapid convergence is still

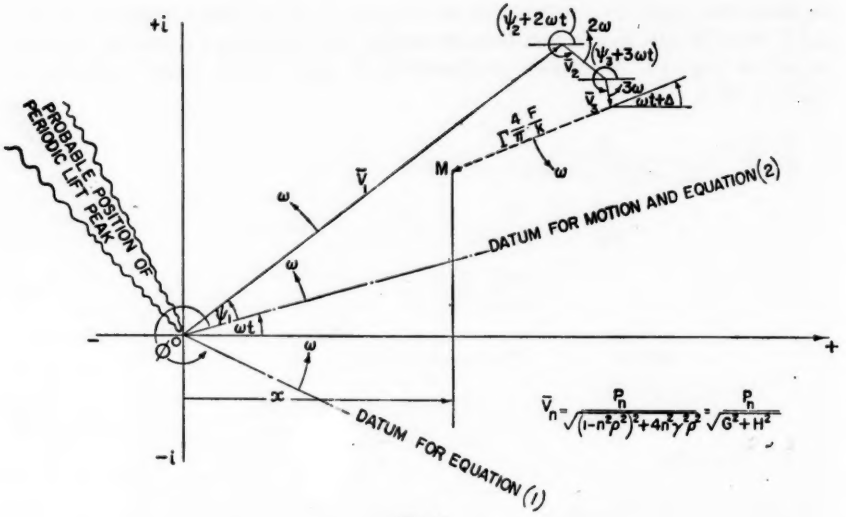

Fig. 2.
The exact solution.

obtained when ρ is given a value corresponding to oscillation at the natural frequency of the fully damped blade. This assumption, which is probably the closest approach that can be made to physical reality, is effected by writing

$$\rho = +(1-\gamma^2)^{\frac{1}{2}} \quad . \quad . \quad . \quad . \quad . \quad (9)$$

so that the solution becomes a function only of the parameters

$$\frac{A_n}{k}, \frac{B_n}{k}, \frac{F}{k} \quad \text{and} \quad \gamma.$$

In this form it can be applied directly and with equal facility to either flexural or torsional motion, for, apart from γ which is non-dimensional, the remaining parameters are effectively those steady deflections or twists which would result at the blade tip from the application of the moments A_n, B_n and F.

Apart from the fact that its "F" vector anticipates a subsequent approximation (*see* Section 2.3), an interpretation of the solution for a typical instance is displayed in Fig. 2. However, if the offending vector were replaced by a series of rapidly diminishing ones, each with an appropriate phase angle and speed of rotation, the exact solution would be represented. From Fig. 2 the physical significance of ϕ and ψ_n is clear because, unless the condition $dx/dt=0$ when $t=0$ can be satisfied, the square wave series for the Coulomb damping will be invalid and must be replaced by a generally indeterminate function of ωt. However, in numerical work ϕ is essentially the phase angle between the datum of the Fourier series representing the aerodynamic excitation and that representing the motion of the blade tip. That

it is therefore not in general the physical angle by which the peak of the exciting force leads the time of maximum tip deflection is more clearly shown in the example of Fig. 4.

The example of Fig. 2 is one in which the excitation comprises three significant harmonics, but in order to study the influence of the Coulomb damping it is desirable firstly to consider a case of simple harmonic forcing. In such circumstances ψ_1 would shrink to about two or three degrees and, Δ remaining unaltered, the point marked M would lie precisely on the motion datum line and we should have approximately

$$x \simeq \left[\frac{P_1/k}{\{(1-\rho^2)^2+4\gamma^2\rho^2\}^{\frac{1}{2}}} - \Gamma\frac{4}{\pi}\frac{F}{k}\right]\cos\omega t,$$

where Γ is a single-valued function of γ. The physical effect of the damping is therefore to reduce the amplitude of the motion without distorting its simple harmonic wave form which is invariant with respect to both γ and F.

However, in the example displayed it is evident that, as the value of F is increased for a given value of γ, the vector $\overline{OM}$ will in general attain zero magnitude at one or more values of ωt while, at $t=0$, X_+ is still real and finite. The physical meaning of this is that, as shown by den Hartog[3] for simple harmonic forcing off resonance, the motion will proceed, but with one or more stops during each cycle. This, of course, destroys the validity of the series assumed for the Coulomb damping and so sets a limit to the relative values of γ and F which can be considered by the simple theory.

Finally, it appears from the diagram of Fig. 2 that, with the values of ϕ and ψ_n arranged as shown to give $dx/dt=0$ at $t=0$, it will not in general be possible to satisfy the condition $dx/dt=0$ at $t=\pi/\omega$ and, moreover, that X_+ and X_- will not be equal. However, provided that there is only "velocity" damping the solution is still exact, but in the presence of Coulomb damping the equation of motion itself is wrong and the general theory becomes invalid. Nevertheless, as is shown in Section 3.3, a simple approximate method happens in practice to yield fairly accurate results.

2.3. A Simplifying Approximation

Consider now the magnitude of the Coulomb damping term of equation (4), namely,

$$\text{Coulomb term} = \frac{4F}{\pi k}\sum_{\nu=1,3,5}^{\infty}\frac{1}{\nu}\frac{1-\nu^2\rho^2}{(1-\nu^2\rho^2)^2+4\nu^2\gamma^2\rho^2}\sin\nu\omega t - \\ - \frac{4F}{\pi k}\sum_{\nu=1,3,5}^{\infty}\frac{2\gamma\rho}{(1-\nu^2\rho^2)^2+4\nu^2\gamma^2\rho^2}\cos\nu\omega t.$$

The rapidity with which these series converge depends upon the value of γ and is greatest for $\gamma \rightarrow 0$, so that we should consider first an example in which γ is as great as it is likely to be in practice, say 0·2.

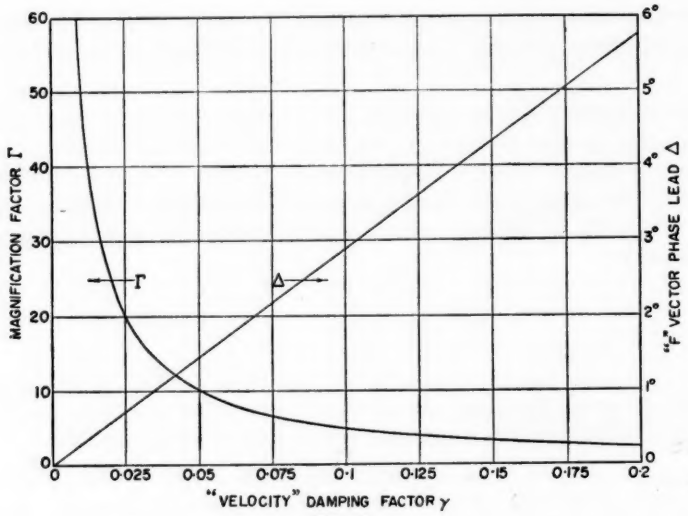

Fig. 3.
The magnification factor.

We then have numerically,

$$\text{Coulomb term} = -\frac{4F}{\pi k}\left\{2{\cdot}538\cos(\omega t+5°50')+0{\cdot}044\cos(3\omega t-80°45')+\right.$$
$$\left.+0{\cdot}009\cos(5\omega t-83°40')+\ldots\ldots\ldots\right\}$$
$$\simeq -2{\cdot}538\frac{4F}{\pi k}\cos(\omega t+5°50').$$

In making this approximation the error incurred at $t=0$ is only 0·2 per cent. and, for any value of t, the maximum error in the length of the "F" vector as shown in Fig. 2 is 1·6 per cent. Since this latter inaccuracy cannot affect the amplitude directly—but only through the validity of the Coulomb damping series of equation (2) when the amplitude is necessarily negligible—and the 0·2 per cent. error at $t=0$ will affect ϕ and ψ_n but little, the exact solution can safely be replaced for all practical purposes by

$$x=\frac{1}{k}\sum_{n=1,2,3}^{\infty}\frac{P_n}{\{(1-n^2\rho^2)^2+4n^2\gamma^2\rho^2\}^{\frac{1}{2}}}\cos(n\omega t+\psi_n)-\Gamma\frac{4F}{\pi k}\cos(\omega t+\Delta) \quad (10)$$

where ϕ is given by

$$\sum_{n=1,2,3}^{\infty} n\frac{(1-n^2\rho^2)A_n-2n\gamma\rho B_n}{(1-n^2\rho^2)^2+4n^2\gamma^2\rho^2}\sin\phi-\sum_{n=1,2,3}^{\infty} n\frac{2n\gamma\rho A_n+(1-n^2\rho^2)B_n}{(1-n^2\rho^2)^2+4n^2\gamma^2\rho^2}\cos\phi=\Gamma\frac{4F}{\pi}\sin\Delta \quad (11)$$

TABLE I
Γ AND Δ OF THE APPROXIMATE SOLUTION

γ	0·01	0·025	0·05	0·10	0·15	0·20
Γ	50·00	20·00	10·01	5·019	3·362	2·538
Δ	0	0°43′	1°26′	2°53′	4°20′	5°50′

and the functions Γ and Δ have the values given in Table I and plotted in Fig. 3. As is more evident in Section 4, Γ is merely the so-called magnification factor of orthodox forced vibration theory.

3. A Limiting Example

3.1. Principal Features of the Example

From the arguments of Sections 2.2 and 2.3 it follows that, when excited at resonance by a simple harmonic force, a blade will itself execute very nearly simple harmonic motion for all values of F at which the motion is significant and for all values of γ up to about 0·2. In practice, any perturbation from simple harmonic motion must therefore be due to the higher harmonic content of the excitation and the form of the solution indicates that all such perturbations will increase in magnitude with γ. The limits of approximation to the exact theory must therefore be found by studying an example in which the excitation is wildly non-harmonic and the damping coefficients are varied throughout the practical range. The chosen example is illustrated in Fig. 4 and, when it is expressed as a Fourier series, significant coefficients of the exciting moment are as listed in Table II.

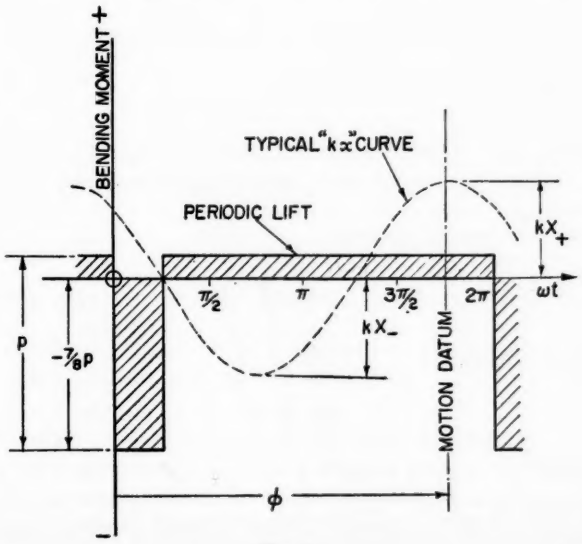

Fig. 4.
A limiting example.

KRESGE-HOOKER
WAYNE
UNIVERSITY
SCIENTIFIC LIBRARY

TABLE II
MOMENT COEFFICIENTS FOR THE LIMITING EXAMPLE

n	1	2	3	4	5	6	7	8	100
A_n/p	−0·225	−0·159	−0·075	0	+0·045	+0·053	+0·032	0	0
B_n/p	−0·093	−0·159	−0·181	−0·159	−0·109	−0·053	−0·013	0	−0·006
P_n/p	0·243	0·225	0·196	0·159	0·118	0·075	0·035	0	0·006

Although physically impossible, this example can be thought of as an idealised case of stalling flutter in which the instantaneous lift, which is invariant with respect to x except at the points $\omega t=0$ and $\pi/4$, is known exactly and the problem is to estimate the amplitude and wave form of the resultant blade motion. Near the positive peak displacement there occurs, on the upper surface of the blade, a sudden separation of the boundary layer which lasts for a time $\pi/(4\omega)$ and produces a reduction of magnitude p in the root gas bending moment. Oscillation would occur at maximum amplitude when, due to the inertia of the separating air stream, the lift pulse lags behind the positive peak displacement by an amount ϕ which is precisely such as to satisfy the theory of Section 2. It will be observed that the first coefficient of the series accounts for only a small fraction of the total exciting moment and, whereas this may generally be so in stalling flutter, the example has been chosen with the intention that it shall in this respect be as bad as any case likely to arise in practice. Although relatively large, the hundredth harmonic is nevertheless unimportant, since what appears to matter is the distribution of magnitude amongst the first three or four harmonics only.

3.2. SOLUTION FOR $\gamma=0{\cdot}01$

Since for pure "velocity" damping we have, by definition[4],

$$\text{Logarithmic decrement}=\delta=2\pi\frac{\gamma}{(1-\gamma^2)^{\frac{1}{2}}} \quad . \quad . \quad . \quad . \quad . \quad . \quad . \quad (12)$$

the value of 0·01 for γ yields a logarithmic decrement of 0·0628 as compared with the value for a typical compressor blade without root damping of about 0·001. The exact solution for $F=0$ (*see* Appendix II) is then as in Table III, so that we have for the positive part of the amplitude,

$$X_+=12{\cdot}17\frac{p}{k}(1-0{\cdot}00220-0{\cdot}00139-0{\cdot}00080-0{\cdot}00040-0{\cdot}00020-0{\cdot}00004\ldots\ldots)$$

$$=12{\cdot}17\frac{p}{k}(1-0{\cdot}0050).$$

TABLE III
EXACT SOLUTION OF EXAMPLE FOR $\gamma=0{\cdot}01$ AND $F=0$

n	1	2	3	4	5	6	7
$\dfrac{P_n/p}{\{(1-n^2\rho^2)^2+4n^2\gamma^2\rho^2\}^{\frac{1}{2}}}$	12·17	0·0749	0·0245	0·0106	0·0049	0·0021	0·0007
ψ_n	+0°50′	−110°59′	−133°46′	−156°24′	−178°24′	+158°29′	+135°36′

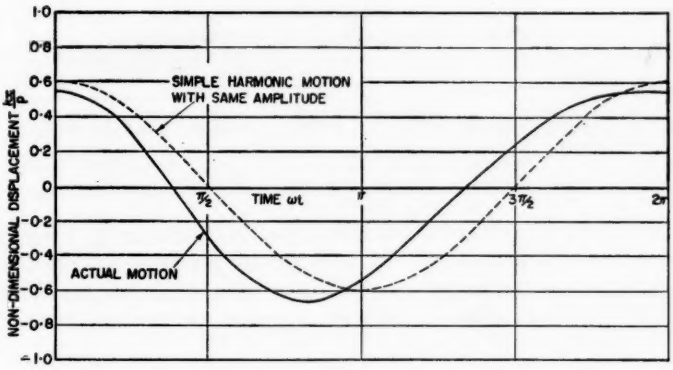

Fig. 5.
The motion without Coulomb damping for $\gamma=0{\cdot}2$.

Moreover, although $dx/dt \neq 0$ when $t=\pi/\omega$, the error involved in overlooking this fact is clearly negligible because of the small value of ψ_1, so with considerable accuracy we can write

$$X_- = -12{\cdot}17\,\frac{p}{k}\,(1-0{\cdot}0014)$$

and deduce for the amplitude of motion

$$(X_+ - X_-) = 24{\cdot}34\,\frac{p}{k}\,(1-0{\cdot}0018) = 24{\cdot}30\,\frac{p}{k}\,.$$

Despite its relatively small magnitude, the fundamental harmonic of the excitation thus gives rise to over 99·8 per cent. of the amplitude of motion, and the distortion from simple harmonic motion at the blade tip is likely to be negligible for all practical purposes. From equation (10) we can thus write with excellent approximation,

$$x \simeq \left[\frac{(X_+ - X_-)_{F=0}}{2} - \frac{200}{\pi}\,\frac{F}{k}\right]\cos\omega t,$$

whence the Coulomb damping moment required to reduce the amplitude to zero with the excitation unaltered is defined by $F=0{\cdot}191\,p$.

3.3. Solution for $\gamma=0{\cdot}20$

For $F=0$ this amount of "velocity" damping gives a logarithmic decrement of 1·282 and may reasonably be considered as beyond anything which will be necessary or perhaps even possible in future practice. The solution is defined by Table IV and, because of the relatively slow convergence of the series (*see* Appendix II), the wave form is distorted as shown in Fig. 5.

TABLE IV

EXACT SOLUTION OF EXAMPLE FOR $\gamma=0{\cdot}20$ AND $F=0$

n	1	2	3	4	5	6	7
P_n/p	0·618	0·0763	0·0252	0·0110	0·00511	0·00223	0·00075
$\{(1-n^2\rho^2)^2+4n^2\gamma^2\rho^2\}^{\frac{1}{2}}$							
ψ_n	+25°14′	−77°42′	−106°50′	−131°54′	−155°42′	−179°7′	+157°23′

The boundary conditions for which equation (2) is valid are no longer satisfied, dx/dt being zero for $\omega t=0$ and $+155°$, so that in the presence of Coulomb damping an exact solution can be found only by means of a rather lengthy computation. However, for $F=0$ the values of Table IV are exact and the amplitude of motion is therefore given by

$$X_+=0{\cdot}559\frac{p}{k}(1+0{\cdot}0291-0{\cdot}0131-0{\cdot}0131-0{\cdot}0083-0{\cdot}0040-0{\cdot}0012+\ldots\ldots)$$

$$=0{\cdot}559\frac{p}{k}(1-0{\cdot}0107)$$

$$X_-=-0{\cdot}618\frac{p}{k}(1+0{\cdot}0455)$$

and $$(X_+-X_-)=1{\cdot}177\frac{p}{k}(1+0{\cdot}0188)=1{\cdot}555\frac{p}{k}.$$

Thus, even under such disadvantageous conditions, the fundamental harmonic of the excitation would still account for over 98 per cent. of the periodic gas bending stress at the blade root.

The error involved in the equation of motion when Coulomb damping is added is illustrated in Fig. 6, where it is assumed that the damping increment ΔF is too small seriously to affect either ϕ, ψ_n or the amplitude of motion. If equation (10) be assumed valid, the calculated dissipation of energy due to any amount of Coulomb damping clearly cannot exceed that obtaining in fact and, for the small amount ΔF, we can write

$$\text{Actual dissipation per cycle}=2\Delta F(X_+-X_-)$$

$$\text{Calculated dissipation per cycle}=\Delta F\{[X_+-X_-]-[(x)_{\pi/\omega}-X_-]+[X_+-(x)_{\pi/\omega}]\}$$

$$\text{so that}\quad\frac{\text{calculated dissipation}}{\text{actual dissipation}}=0{\cdot}910.$$

Now, if we make the gross assumption that they are valid, equations (10), (11) and (5) give the value of F required to stop the motion with the excitation unaltered as $0{\cdot}158p$ and the resultant change in ϕ and ψ_n as about $+6{\cdot}9°$. The consequent change in the sum of the P_n vectors of Fig. 2 would thus be small, so that the difference between the Coulomb damping actually required to stop the motion and its calculated value of $0{\cdot}158p$ would be due principally to the appearance in the series replacing that of equation (2) of an appreciable second harmonic term.

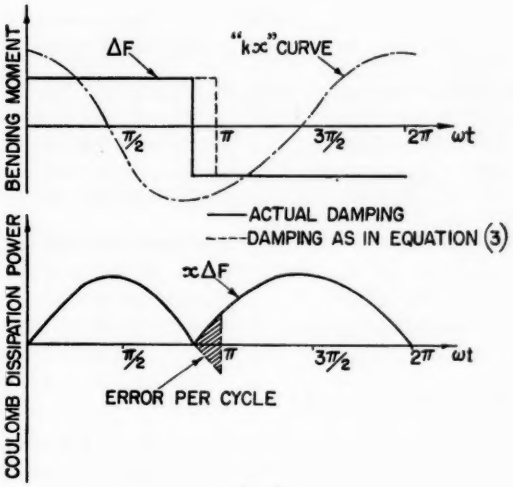

Fig. 6.
The Coulomb damping inaccuracy.

However, this term would produce such a small vector in the field of Fig. 2 that the exact critical value of F could reasonably be expected to lie some ten or at the most twenty per cent. below $0{\cdot}158\,p$.

3.4. The Practical Effects

Suppose that in practice a blade with a value for γ of 0·01 and no Coulomb damping is still found to exhibit a vibration with a tip semi-amplitude of, say, 0·010 inches. If it is desired to reduce or eliminate this amplitude by an increase in damping, the form of the invariant excitation being unknown, there is no reasonable alternative to the assumption that the latter is harmonic. This being assumed, equation (10) reduces to

$$x \simeq \Gamma\left(\frac{P}{k} - \frac{4}{\pi}\frac{F}{k}\right)\cos\omega t. \qquad . \quad . \quad . \quad . \quad (13)$$

Whence P/k is found to be 0·0020 inches.

Now the results of calculations based on equation (13) will vary in accuracy as the unknown excitation varies in harmonic content and, since the example of Section 3.1 is as bad in this respect as anything likely to be encountered in practice, the maximum possible errors of such calculations can be found directly by comparison with the results of Sections 3.2 and 3.3. Such a process yields the results of Table V.

It thus appears that, in all practical instances of self-induced oscillation in one degree of freedom, estimations of the variation of amplitude with damping can safely be performed on the assumption that the unknown excitation is of simple harmonic form. The errors resulting from this superficially gross assumption are not only acceptable but in most instances actually negligible and, whenever the object is a reduction in amplitude, the error appears to be "on the safe side."

TABLE V

COMPARISON OF APPROXIMATE AND EXACT THEORY

Circumstances	*Result from Exact Theory*	*Result from Equation* (13)	*Error*
$\gamma=0{\cdot}01$, $F=0$	Amplitude = 0·020 in.	Amplitude = 0·020 in.	Datum
$\gamma=0{\cdot}01$, Amplitude = 0	$\frac{F}{k} \simeq 157$ micro-in.	$\frac{F}{k} = 157$ micro-in.	less than 1%
$\gamma=0{\cdot}20$, $F=0$	Amplitude = 950 micro-in.	Amplitude = 1,016 micro-in.	+7%
$\gamma=0{\cdot}20$, Amplitude = 0	$\frac{F}{k} \simeq 120$ to 130 micro-in.	$\frac{F}{k} = 157$ micro-in.	+20 to 30%

4. The Approximate Formula

Should an aerofoil or blade be observed to oscillate aeroelastically in a single degree of freedom with a finite amplitude and a frequency defined by ω rad./sec., it can be assumed to be excited by a periodic lifting moment of the form

$$\text{Excitation} = P\cos(\omega t + \phi) \qquad . \quad . \quad . \quad . \quad (14)$$

where the appropriate phase angle, ϕ, can for most practical purposes be taken as 90° and P is in general a function of the blade tip amplitude and of the velocity and state of the air stream. Provided only that the variation of P with the semi-amplitude, X, is known, the variation of X with damping can then be estimated from the equation

$$X \simeq \Gamma\left(\frac{P}{k} - \frac{4}{\pi}\frac{F}{k}\right) \qquad . \quad . \quad . \quad . \quad . \quad . \quad (15)$$

where $$\Gamma = \frac{1}{2\gamma(1-\frac{1}{4}\gamma^2)^{\frac{1}{2}}} \simeq \frac{1}{2\gamma} \simeq \frac{\pi}{\delta}.$$

The entities P/k and F/k are respectively those static deflections of the blade tip which would result from the steady application of P and the Coulomb frictional moment F, k being effectively the stiffness of the blade in its fundamental mode. The non-dimensional parameter γ is the ratio of the actual "velocity" damping coefficient to that which would effect critical damping with $F=0$, δ is the logarithmic decrement corresponding to γ, and values of the magnification factor Γ are given in Table I and Fig. 3.

Provided that γ does not exceed about 0·2, this value giving a logarithmic decrement of 1·282, the errors involved in the use of equation (15) will in practice be negligible, typical worst values being given in Table V. Moreover, by a simple change of co-ordinates, equation (15) can be applied with equal facility and accuracy to both flexural and torsional oscillations.

5. Concluding Remarks

The formal conclusion of this investigation is stated in Section 4 and, whereas it is valid for self-induced aeroelastic oscillations, it must not be applied to instances of simple forced vibration, even when the forcing is purely aerodynamic. This is because of the basic postulate that the aerofoil or blade deflects in its fundamental mode and that this deflection is changed only in magnitude and not in form by the presence in the excitation of predominant higher harmonics.

Before the method can be applied to the estimation of amplitudes, a knowledge of the variation of P with X is of course essential, but this in no way affects the validity and accuracy of equation (15). Indeed, whereas throughout the argument it is implied that the method primarily concerns stalling or choking conditions where the amplitude of motion is finite, there is no reason why equation (15) should not be used to define the critical conditions for the onset in one degree of freedom of the diverging oscillation of a damped cascade blade, should such a phenomenon be discovered in practice (*see*, for example, Ref. 1). In such an instance, however, not only the centrifugal but also the aerodynamic contribution to stiffness might have to be taken into account.

Acknowledgment

This paper deals mainly with work which was done at the National Gas Turbine Establishment and the author acknowledges the permission of the Chief Scientist, Ministry of Supply, to publish it.

References

1. Bellenot, Ch. and Lalive d'Epinay, J. Self Induced Vibrations of Turbo-machine Blades. *Brown Boveri Review*, October 1950.

2. Pearson, H. The Aerodynamics of Compressor Blade Vibration. *Fourth Anglo-American Aeronautical Conference*, London, 1953. Royal Aeronautical Society, 1954.

3. den Hartog, J. P. Forced Vibration with Combined Coulomb and Viscous Friction. Transactions of the American Society of Mechanical Engineers, Vol. 53, p. 107, 1931.

4. Kimball, A. L. Vibration Damping, including the Case of Solid Friction. Transactions of the American Society of Mechanical Engineers, Vol 51(1), p. 227, 1929.

Appendix I

Solution of the Equation of Motion

As given in Section 2.1, the equation of motion of the blade tip is

$$m\frac{d^2x}{dt^2}+c\frac{dx}{dt}+kx=\sum_{n=1,2,3}^{\infty}A_n\cos(n\omega t+\phi)+\sum_{n=1,2,3}^{\infty}B_n\sin(n\omega t+\phi)+\frac{4F}{\pi}\sum_{\nu=1,3,5}^{\infty}\frac{1}{\nu}\sin\nu\omega t \quad . \quad . \quad . \quad (3)$$

Now the general solution of this equation comprises two parts, of which the first is an exponentially decaying term and the second is that which is known in forced vibration theory as the "steady forced vibration" solution. Only the latter is of interest here and, being a particular integral of equation (3), it is obtained by writing

$$x=\sum_{n=1,2,3}^{\infty} J_n \cos n\omega t+\sum_{n=1,2,3}^{\infty} K_n \sin n\omega t+\sum_{\nu=1,3,5}^{\infty} L_\nu \sin \nu\omega t+\sum_{\nu=1,3,5}^{\infty} M_\nu \cos \nu\omega t \quad . \qquad (16)$$

On differentiating equation (16), substitution in equation (3) and a comparison of coefficients gives

$$\left.\begin{aligned}
(k-mn^2\omega^2)J_n+nc\omega K_n&=A_n\\
(k-mn^2\omega^2)K_n-nc\omega J_n&=B_n\\
(k-m\nu^2\omega^2)L_\nu-\nu c\omega M_\nu&=\frac{4}{\pi}\frac{F}{\nu}\\
(k-m\nu^2\omega^2)M_\nu+\nu c\omega L_\nu&=0
\end{aligned}\right\} \quad . \quad . \quad . \quad . \qquad (17)$$

whence

$$J_n=\frac{(k-n^2m\omega^2)A_n-nc\omega B_n}{(k-n^2m\omega^2)^2+n^2c^2\omega^2}=\frac{(1-n^2\rho^2)A_n-2n\gamma\rho B_n}{(1-n^2\rho^2)^2+4n^2\gamma^2\rho^2}\times\frac{1}{k}$$

$$K_n=\frac{nc\omega A_n+(k-n^2m\omega^2)B_n}{(k-n^2m\omega^2)^2+n^2c^2\omega^2}=\frac{2n\gamma\rho A_n+(1-n^2\rho^2)B_n}{(1-n^2\rho^2)^2+4n^2\gamma^2\rho^2}\times\frac{1}{k}$$

$$L_\nu=\frac{4}{\pi}\times\frac{F}{\nu}\times\frac{k-\nu^2m\omega^2}{(k-\nu^2m\omega^2)^2+\nu^2c^2\omega^2}=\frac{4}{\pi}\times\frac{F}{\nu}\times\frac{1-\nu^2\rho^2}{(1-\nu^2\rho^2)^2+4\nu^2\gamma^2\rho^2}\times\frac{1}{k}$$

$$M_\nu=-\frac{4F}{\pi}\times\frac{c\omega}{(k-\nu^2m\omega^2)^2+\nu^2c^2\omega^2}=-\frac{4F}{\pi}\times\frac{2\gamma\rho}{(1-\nu^2\rho^2)^2+4\nu^2\gamma^2\rho^2}\times\frac{1}{k}.$$

However, it is convenient in practice to combine the first two terms of the solution vectorially so that equation (16) becomes,

$$x=\sum_{n=1,2,3}^{\infty}(J_n^2+K_n^2)^{\frac{1}{2}}\cos\left(n\omega t-\tan^{-1}\frac{K_n}{J_n}\right)+\sum_{\nu=1,3,5}^{\infty}L_\nu\sin\nu\omega t+\sum_{\nu=1,3,5}^{\infty}M_\nu\cos\nu\omega t \quad . \quad . \qquad (18)$$

and, on making this addition, the final "steady state" solution of the equation of motion is found to be

$$\begin{aligned}
x=\frac{1}{k}\sum_{n=1,2,3}^{\infty}&\frac{P_n}{\{(1-n^2\rho^2)^2+4n^2\gamma^2\rho^2\}^{\frac{1}{2}}}\cos(n\omega t+\psi_n)+\\
&+\frac{4F}{\pi k}\sum_{\nu=1,3,5}^{\infty}\frac{1}{\nu}\frac{1-\nu^2\rho^2}{(1-\nu^2\rho^2)^2+4\nu^2\gamma^2\rho^2}\sin\nu\omega t-\\
&-\frac{4F}{\pi k}\sum_{\nu=1,3,5}^{\infty}\frac{2\gamma\rho}{(1-\nu^2\rho^2)^2+4\nu^2\gamma^2\rho^2}\cos\nu\omega t \quad . \quad . \qquad (4)
\end{aligned}$$

where $P_n=+(A_n^2+B_n^2)^{\frac{1}{2}}$

and $\psi_n=\phi-\tan^{-1}\frac{K_n}{J_n}$.

Only ϕ now remains to be evaluated and, by definition, this is done by applying to the solution the boundary condition $dx/dt=0$ when $t=0$, whence

$$\sum_{n=1,2,3}^{\infty} n\frac{(1-n^2\rho^2)A_n-2n\gamma\rho B_n}{(1-n^2\rho^2)^2+4n^2\gamma^2\rho^2}\sin\phi-\sum_{n=1,2,3}^{\infty} n\frac{2n\gamma\rho A_n+(1-n^2\rho^2)B_n}{(1-n^2\rho^2)^2+4n^2\gamma^2\rho^2}\cos\phi$$
$$=\frac{4F}{\pi}\sum_{\nu=1,3,5}^{\infty}\frac{1-\nu^2\rho^2}{(1-\nu^2\rho^2)^2+4\nu^2\gamma^2\rho^2} \quad . \quad . \quad (6)$$

Appendix II

Numerical Solution for the Limiting Example

The system under consideration is illustrated in Fig. 4 and the Fourier coefficients of its exciting moment are given in Table II of Section 3.1. For the purposes of computation it is convenient to write

$$1-n^2\rho^2=G \text{ and } 2n\gamma\rho=H,$$

and to know that $\rho=(1-\gamma^2)^{\frac{1}{2}}$.

Example 1. $\gamma=0{\cdot}01$.

TABLE VI

(1)	n	1	2	3	4	5	6	7
(2)	G^2+H^2	0·0004	9·002	64	22·5	576	1225	2304
(3)	GA_n	0	0·477	0·600	0	−1·080	−1·855	−1·536
(4)	HB_n	−0·00186	−0·00636	−0·01086	−0·01272	−0·01090	−0·00636	−0·00182
(5)	(3)−(4)	0·00186	0·483	0·611	0·01272	−1·069	−1·849	−1·534
(6)	HA_n	−0·00450	−0·00636	−0·00450	0	0·00450	0·00636	0·00448
(7)	GB_n	0	0·477	1·448	2·385	2·616	1·855	0·624
(8)	(6)+(7)	−0·00450	0·471	1·444	2·385	2·621	1·861	0·629
$\tan(\phi-\psi_n)=$	(8)/(5)	−2·419	0·9751	2·363	187·5	−2·452	−1·0065	−0·4100
$(\phi-\psi_n)$		−67°32′	44°17′	67°4′	89°42′	112°11′	134°49′	157°42′
$n\frac{GA_n-HB_n}{G^2+H^2}=\frac{(5)}{(2)}n$		4·650	0·1073	0·0286	0·0002	−0·0093	−0·0091	−0·0047
$n\frac{HA_n+GB_n}{G^2+H^2}=\frac{(8)}{(2)}n$		−11·25	0·1046	0·0677	0·0424	0·0228	0·0091	0·0019

From Table VI, since $A_8=B_8=0$, we have

$$\sum_{n=1,2,3}^{8} n\frac{GA_n-HB_n}{G^2+H^2}=4{\cdot}763 \text{ and } \sum_{n=1,2,3}^{8} n\frac{HA_n+GB_n}{G^2+H^2}=-11{\cdot}00$$

whence, for $F=0$, equation (6) gives

$$4{\cdot}736\sin\phi+11{\cdot}00\cos\phi=0,$$

so that the numerical value of ϕ is $-66°42'$.

As is evident in Fig. 4, this superficially peculiar value arises as a result of the position in time of the excitation series datum and has no physical importance.

In reality, the physical angle by which the peak of the exciting pulse leads the maximum deflection of the blade is given by

Physical angle of lead $= \pi - (66°42') -$ (semi-pulse width)

$$= \frac{7\pi}{8} - 66°42'$$

$$= 90°48'.$$

The vectorial solution, as illustrated in Fig. 2, would then be defined by the coefficients of Table II of Section 3.1 and the following phase angles:—

n	1	2	3	4	5	6	7
ψ_n	0°50′	−110°59′	−133°46′	−156°24′	−178°53′	158°29′	135°36′

EXAMPLE 2. $\gamma = 0{\cdot}20$.

The corresponding results for this amount of damping are as follows:—

TABLE VII

(1)	n	1	2	3	4	5	6	7
(2)	G^2+H^2	0·15526	8·6795	59·751	208·67	532·8	1131·8	2126·2
(3)	GA_n	−0·00900	0·45156	0·57300	0	−1·03500	−1·7787	−1·4733
(4)	HB_n	−0·03646	−0·12458	−0·21268	−0·24931	−0·21364	−0·12466	−0·03566
(5)	(3)−(4)	0·02746	0·57614	0·78568	0·24931	−0·82136	−1·6540	−1·4376
(6)	HA_n	−0·08820	−0·12458	−0·08813	0	0·08820	0·12466	0·08778
(7)	GB_n	−0·00372	0·45156	1·3828	2·2832	2·5070	1·7787	0·59852
(8)	(6)+(7)	−0·09192	0·32698	1·2947	2·2832	2·5952	1·9034	0·68630
$\tan(\phi-\psi_n)=(8)/(5)$		−3·3474	0·56754	1·64787	9·1581	−3·1596	−1·15079	−0·47739
$(\phi-\psi_n)$		−73°22′	29°34′	58°45′	83°46′	107°34′	130°59′	154°29′
$n\dfrac{GA_n-HB_n}{G^2+H^2}=\dfrac{(5)}{(2)}n$		0·1769	0·1328	0·0395	0·0048	−0·0077	−0·0088	−0·0047
$n\dfrac{HA_n+GB_n}{G^2+H^2}=\dfrac{(8)}{(2)}n$		−0·5920	0·0754	0·0650	0·0438	0·0244	0·0101	0·0023

Thus, for $F=0$,

$$0{\cdot}3326 \sin\phi + 0{\cdot}3712 \cos\phi = 0,$$

whence $\phi = -48°8'$ and the physical angle by which the exciting pulse leads the maximum blade displacement is 109°22′. As before, the solution is then defined by the coefficients of Table II of Section 3.1 and the following phase angles:—

n	1	2	3	4	5	6	7
ψ_n	25°14′	−77°42′	−106°50′	−131°54′	−155°42′	−179°7′	157°23′

The Drag of Non-Planar Thickness Distributions in Supersonic Flow

E. W. GRAHAM, B. J. BEANE and R. M. LICHER

(Douglas Aircraft Company, Inc., Santa Monica, California)

SUMMARY: For many conventional aircraft, the thickness of the wing and fuselage can be represented approximately by source distributions in the plane of the wing and on the axis of the fuselage. Such aircraft may be considered as having essentially planar thickness distributions. However, missiles with cruciform wings, biplane arrangements, " ring " wings and so on, require non-planar source distributions to represent the wing and fuselage thickness. For this reason, the term " spatial thickness distribution " is used.

To simplify the investigation of spatial thickness distributions, a singularity representing an element of volume is introduced. It is shown that the optimum distribution of such elements in a prescribed space gives rise to a minimum wave drag value consistent with that obtained for a Sears-Haack optimum body of revolution.

It is also shown that the interference of lift and side force elements, with the optimum distribution of volume elements alone, makes it possible to reduce the drag of a given volume below the Sears-Haack " minimum." Such interference effects (among lift force, side force, and volume elements) apparently account for the nearly zero drag of finite aspect ratio Busemann biplanes, and the zero drag of Ferri's axially symmetric central body plus outer shell.

1. Introduction

The distribution of lift on an aircraft in supersonic flight can be represented by the use of elementary horseshoe vortices (lifting elements). The thickness of the wing, fuselage and other components can be represented by source distributions. These singularities satisfy the linearised equation for supersonic flow.

Many conventional aircraft can be represented fairly well by distributions of sources and lifting elements in a single horizontal plane. In such cases there is no interference between the sources and lifting elements, and the problems of reducing drag due to lift and drag due to thickness can be studied separately.

However, the investigation of more general types of aircraft requires the use of singularity distributions which cannot be confined to a single horizontal plane. The term " spatial distribution " is introduced to cover this broader class. In

Received September 1954

addition to lifting elements and sources it is necessary to consider side force elements, which are simply lifting elements rotated through 90° so that the forces are directed to one side instead of vertically.

In the most general case, these singularities (sources, lifting elements and side force elements) have interference drag terms, so that the drag due to thickness, for example, cannot be studied independently of the lift and side forces on the aircraft.

In this paper, the thickness drag is considered first and the interference effects caused by lift and side force are then discussed.

NOTATION

a, b semi-minor and semi-major axes of an ellipse

c length of a cylinder, or length of body, or wing chord

C_D drag coefficient

d distance between source and sink

D drag force

$f( )$, f_0, $F( )$ intensity of singularity distribution

K a constant

l length of body

$l(x)$ chordwise radial load distribution on shell

m mass of fluid introduced per unit time

M free stream Mach number

q dynamic pressure

r co-ordinate normal to streamwise direction, or radial co-ordinate on circular plan form wing

R semi-span of circular plan form wing

S cross-sectional area

t thickness

U_0 free stream velocity

V volume

x co-ordinate in streamwise direction ($X = \alpha x/R$)

y co-ordinate in spanwise direction ($Y = by/R$)

$\alpha = 1-(r/R)^2$

$\beta = \sqrt{(M^2-1)}$

μ angular inclination of the trace of the Mach planes on the xy-plane, relative to the y-axis

ξ co-ordinate in the streamwise direction or co-ordinate perpendicular to trace of Mach planes in the xy-plane

η co-ordinate parallel to trace of Mach planes in the xy-plane

$\varphi = 1 - \left(\frac{x}{R \sec \mu}\right)^2$

ϕ potential

ϕ_s potential of a unit source

ϕ_v potential of a unit dipole

θ polar co-ordinate on wing plan form or angular co-ordinate from the xy-plane

ρ_0 free stream density

$( )_{opt}$ optimum

$( )_{min}$ minimum

Dashes denote differentiation

2. The Singularity Representing an Element of Volume

The investigation of lift distributions is simplified by the use of a singularity which represents an element of lift. This singularity is the elementary horseshoe vortex. The intensity of lift corresponds to the strength of the singularity and the location of the lift force is identical with that of the bound vortex. The study of volume (or thickness) distributions is similarly simplified by identifying the singularity which corresponds to an element of volume.

Consider a source and sink of equal strength and located on the same streamwise line. In each unit of time a certain quantity of fluid is introduced into the flow pattern by the source and the same quantity is removed by the sink. The volume occupied by the fluid flowing from source to sink depends on the strength of the source and sink and the distance between them, and also depends on the velocity and density of the fluid flowing from source to sink. However, if the volume is to be considered a linear function of the strength of the singularities, then the mean value of density times velocity must be unaffected by the perturbation velocities created by the source and sink. This means that in a linearised treatment of the problem the fluid flowing from source to sink may be considered to have free stream density and velocity.

Let m = mass of fluid introduced per unit time

d = distance between source and sink

ρ_0 = free stream density

U_0 = free stream velocity.

Then the volume occupied by the fluid is $\frac{md}{\rho_0 U_0}$.

Since the volume is proportional to *md*, doubling the intensity of source and sink and halving the distance between them should produce a shorter, but thicker, volume of the same magnitude. This suggests proceeding to the limiting case (as in incompressible flow) where the source and sink are combined in a dipole with axis in the free stream direction. This singularity should represent an element of volume, although the fineness ratio of the element is zero.

The potential for a unit source at $(\xi, 0)$ in supersonic flow is

$$\phi_s = \frac{-1}{2\pi\sqrt{\{(x-\xi)^2 - \beta^2 r^2\}}}$$

where $\beta = \sqrt{(M^2-1)}$,

x and ξ are co-ordinates in the streamwise direction and r is radial distance from the x-axis.

Differentiating with respect to x gives

$$\phi_{sx} = \frac{+(x-\xi)}{2\pi[(x-\xi)^2 - \beta^2 r^2]^{\frac{3}{2}}} = +\phi_v,$$

where ϕ_v is the potential for the unit dipole or an element of volume equal to $1/U_0$.

3. The Distribution of Volume Elements

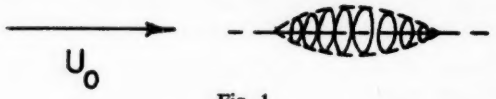

Fig. 1.

For a distribution of volume elements along the ξ-axis with intensity $f(\xi)$, starting at $\xi = 0$, the potential is

$$\phi = \frac{+1}{2\pi}\int_0^{x-\beta r} \frac{f(\xi)(x-\xi)\,d\xi}{[(x-\xi)^2 - \beta^2 r^2]^{\frac{3}{2}}}.$$

Integration by parts gives

$$\phi = \left[\frac{+f(\xi)}{2\pi\sqrt{\{(x-\xi)^2 - \beta^2 r^2\}}}\right]_0^{x-\beta r} - \frac{1}{2\pi}\int_0^{x-\beta r} \frac{f'(\xi)\,d\xi}{\sqrt{\{(x-\xi)^2 - \beta^2 r^2\}}}.$$

The first term in the expression for the potential is infinite, and apparently corresponds to the "roughness" of the body, which is an assembly of blunt elements (*see* Fig. 1).

The smoothly faired body (indicated by broken lines) is all that we are concerned with, and this creates the finite part of the potential. This finite part is also the potential for a source distribution of intensity equal to $+f'(\xi)$. This source distribution can be used to construct a body of revolution extending from $-l/2$ to $+l/2$. The volume of this body, computed from the surface shape obtained from slender-body theory, is equal to

$$\int_{-l/2}^{+l/2} f(\xi)\, d\xi / U_0.$$

This is consistent with the total volume corresponding to the sum of the volume elements.

Similarly, a planar distribution of volume elements should give a wing with a thickness distribution whose total volume computed from the surface shape is equal to the sum of the volume elements.

The concept of the volume element is not particularly useful in studying bodies of revolution and planar wings, since these cases are relatively simple. However, the use of the volume element does help to clarify problems involving more general spatial distributions of thickness.

The points to be emphasised are that fixing the sum of the volume elements fixes the total volume and fixing the distribution of volume elements determines the drag. It is therefore possible to study the drag of a distribution of volume elements without calculating the exact shape of the corresponding body. This is analogous to the fact that the drag of a distribution of *lifting* elements can be studied without calculating the twist and camber of the corresponding wing surfaces.

4. The Drag of Volume Distributions on a Streamwise Line

A body of revolution may be constructed from a distribution of volume elements along a streamwise line, or from the equivalent distribution of sources. The body constructed from volume elements is an "infinitely rough" body and has infinite drag. However, discarding the infinite part of the potential leaves a "smooth" body (with finite drag) which is equivalent in every respect to the body created by a source distribution.

If $f(x)$ is the intensity of the volume element distribution for a body of revolution of length l, then the drag is given by[1]

$$D = \frac{-\rho_0}{4\pi} \int_{-l/2}^{+l/2} \int_{-l/2}^{+l/2} f''(x_1) f''(x_2) \log |x_1 - x_2|\, dx_1\, dx_2.$$

To maintain constant total volume according to linearised theory,

$$\int_{-l/2}^{+l/2} f(x)\, dx = \text{constant}.$$

The body shape giving minimum drag for a given length and volume has been determined by Sears[1] and Haack[2] independently. The corresponding $f(x)$ (which is proportional to the cross-sectional area) is given by

$$f_{\text{opt}}(x) = \frac{16}{3\pi}\left[1-(2x/l)^2\right]^{\frac{3}{2}}\left[\frac{\int_{-l/2}^{+l/2} f(\xi)\,d\xi}{l}\right].$$

Thus, the optimum distribution of volume elements along the axis corresponds to the *cube* of an elliptical distribution. (For lifting elements the optimum distribution is elliptical).

The value of the minimum drag is

$$D_{\min} = \frac{8q}{\pi}\left(\frac{l}{2}\right)^2\left[\frac{\int_{-l/2}^{+l/2} f(x)\,dx}{U_0(l/2)^3}\right]^2$$

$$= \frac{8q}{\pi}\left(\frac{l}{2}\right)^2\left[\frac{\text{volume}}{(l/2)^3}\right]^2.$$

5. The Drag of Volume Distributions in Space

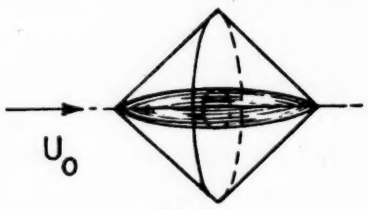

Fig. 2.

If the volume elements are not confined to a single streamwise line, then the drag contributions at different angles, θ, on Hayes's cylindrical control surface[3] are not necessarily the same. For any one angle, θ, the drag is given by

$$\frac{\partial D}{\partial \theta} = \frac{-\rho_0}{8\pi^2}\int_{-l/2}^{+l/2}\int_{-l/2}^{+l/2} f''(x_1,\theta)\,f''(x_2,\theta)\log|x_1-x_2|\,dx_1\,dx_2.$$

Here $f(x, \theta)$ is determined by the use of "Mach planes" for the angle θ. All the volume elements intercepted by any one "Mach plane" are transferred (in the plane) to the streamwise axis. The resulting distribution along the axis is $f(x, \theta)$. The problem of finding the minimum drag contribution *at the one angle* θ is then equivalent to the Sears-Haack problem. If $f(x, \theta)$ corresponds to the cube of an elliptical distribution for *all* θ, then the total drag is a minimum, and the drag

contribution at each θ is a minimum and corresponds to that of an equivalent Sears-Haack body.

It is not always possible to get such a perfect minimum. For example, if the space within which thickness may be distributed corresponds to that which can be utilised in a "planar" wing of rectangular plan form, then it is not possible for the drag contributions at all angles θ to be made a minimum simultaneously. However, if the available space corresponds to that occupied by a "planar" wing of *elliptical* plan form, it is possible to get a "perfect" minimum. The optimum distribution of thickness for such a wing was first determined by R. T. Jones[4]. (In Appendix I of this paper, the optimum thickness distribution for a wing of elliptical plan form and constant volume is determined by a slightly different procedure). Jones found that for minimum drag with constant volume the aerofoil sections should have constant curvature in the streamwise direction. The resulting thickness distribution, viewed from any angle on Hayes's cylindrical control surface, gives an equivalent body of revolution having the Sears-Haack optimum shape. However, these various equivalent bodies, corresponding to different angles on the control surface, have different lengths, so there is no *one* Sears-Haack body which corresponds exactly to the elliptical wing.

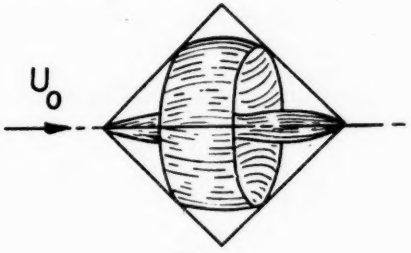

Fig. 3.

If we consider the optimum distribution of thickness within a space which has axial symmetry about a streamwise axis, then it is possible for all the equivalent Sears-Haack bodies to have the same length. For example, consider that a double Mach cone bounds the space within which thickness is to be distributed (Fig. 2). The Sears-Haack body placed on the axis has the same drag contribution at every angle on the cylindrical control surface and, of course, the "equivalent" body of revolution for any angle θ is identical with the real body. However, a "ring" wing (which carries no radial forces) plus a central body of revolution (Fig 3) can be designed to have exactly the same drag as the Sears-Haack body (*see* Appendix II(A)). The equivalent bodies of revolution are all identical with the Sears-Haack body.

In obtaining the minimum drag values just discussed, only volume elements were used. However, it will be shown in the next section that lift and side force elements have interference drag with the optimum distribution of volume elements. Consequently, the drag for a given volume can be reduced below the Sears-Haack value.

6. Interference Between Lift and Side Force Elements and an Optimum Distribution of Volume Elements

Consider a Sears-Haack body placed on the axis of a double Mach cone, and place a lifting element as shown in Fig. 4. The interference drag between body and lifting element is composed of two parts, the effect of the body nose on the lifting element and the effect of the lifting element on the tail of the body.

The nose of the body corresponds to a source distribution and produces an upwash velocity at the lifting element. This causes negative drag. The lifting element produces a positive pressure at the tail of the body. This also causes negative drag so the total interference drag is negative. (This argument, of course, applies not only to the Sears-Haack shape but to other shapes also).

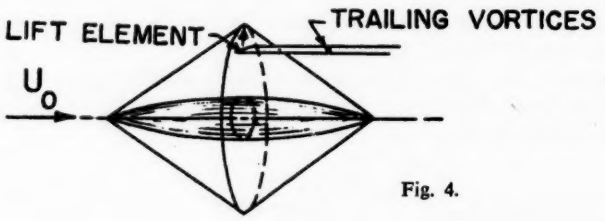

Fig. 4.

The total drag of the combination is equal to the drag of the Sears-Haack body alone plus the drag of the lifting element alone plus the interference drag. The drag of the lifting element alone is proportional to the square of the lift it carries. However, the interference drag is proportional to the first power of the lift on the element and to the first power of the strength of those sources and sinks in the body which are affected by interference. The lift carried by the element can, therefore, always be made small enough so that the drag of the element alone is less (in absolute magnitude) than the interference drag. Thus, the total drag of the combination can be made less than the drag of the Sears-Haack body alone.

This suggests placing elements of lift and side force in a ring about the Sears-Haack body, and so arranged that the force on each element is directed radially outward from the body. This process may be used to construct a central body plus cylindrical shell which has zero drag (Appendix II(B)). Such a system has been investigated by Ferri[5]; its two-dimensional analogue is the Busemann biplane.

It therefore appears that the optimum distribution in space of volume elements alone yields minimum drag values consistent with the Sears-Haack values. However, the optimum distribution of volume elements *plus* lifting and side force elements should give *zero* drag for any total volume.

References

1. Sears, William R. On Projectiles of Minimum Wave Drag. *Quarterly of Applied Mathematics*, Vol. IV, No. 4, 1947.

2. Haack, W. Geschossformen Kleinsten Wellenwiderstandes. Bericht 139 der Lilienthal-Gesellschaft fur Luftfahrt, 1941.

3. HAYES, WALLACE D. Linearized Supersonic Flow. North American Aviation, Inc., Los Angeles, Report No. A.L. 222, 1947.

4. JONES, R. T. Theoretical Determination of the Minimum Drag of Airfoils at Supersonic Speeds. *Journal of the Aeronautical Sciences*, Vol. 19, No. 12, December 1952.

5. FERRI, A. Application of the Method of Characteristics to Supersonic Rotational Flow. N.A.C.A. Report 841, 1946.

6. HILDEBRAND, F. B. *Methods of Applied Mathematics*. Prentice-Hall, 1952.

Appendix I

OPTIMUM THICKNESS DISTRIBUTION FOR ELLIPTICAL PLAN FORM

It is desired to find the optimum thickness distribution for a planar wing of elliptic plan form and given volume; this problem was first solved by R. T. Jones[4]. A geometrically simpler problem, which will be examined first, is to find the optimum thickness distribution for a circular wing of given volume. The method of Hayes[3], in which the drag is evaluated by summing increments of drag at each angular station around a cylindrical control surface far away from the body, will be used. For the total drag to be a minimum, the increment of drag at each angular station should also be a minimum. Hayes's method substitutes for the actual planar distribution, as viewed at each angular station, an " equivalent " thickness distribution concentrated along an axis parallel to the free stream direction. It is known that the optimum thickness distribution for such an equivalent body is that of the Sears-Haack body[1, 2]. For each angular station the equivalent body is constructed by finding the cross-sectional area of the wing intercepted by a series of planes inclined at the Mach angle to the free stream direction. The area cut out by a given Mach plane is then concentrated, at the intersection of the Mach plane and longitudinal (streamwise) axis, such that the volume of the equivalent body is equal to the volume of the actual wing.

If the thickness distribution of the circular plan form is axially symmetric, then the equivalent bodies at each angular station will have the same shape (although different " fineness ratios ") due to symmetry. If $t(r)$ is the thickness distribution which is to be the optimum for a given volume V, then

$$V=2\pi\int_0^R t(r)r\,dr \qquad . \quad . \quad . \quad . \quad . \quad (1)$$

where R is the radius of the circular wing and r, θ are polar co-ordinates from the wing centre (Fig. 5). The area cut out at each point along the ξ-axis by planes normal to that axis is

$$S(\xi)=\int_{-\sqrt{(R^2-\xi^2)}}^{+\sqrt{(R^2-\xi^2)}} t\,d\eta=2\int_{\xi}^{R}\frac{t(r)r\,dr}{\sqrt{(r^2-\xi^2)}} \qquad . \quad . \quad . \quad . \quad . \quad (2)$$

The equivalent lineal distribution along the x-axis is

$$S(x)=2\cos\mu\int_{x\cos\mu}^{R}\frac{t(r)r\,dr}{\sqrt{(r^2-x^2\cos^2\mu)}} \qquad . \quad . \quad . \quad (3)$$

with $$\int_{-R\sec\mu}^{R\sec\mu} S(x)\,dx=V.$$

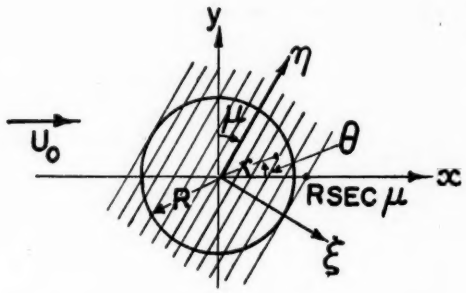

Fig. 5.

For minimum drag, this distribution should be[1]

$$S(x)\sim\left[1-\left(\frac{x}{R\sec\mu}\right)^2\right]^{\frac{3}{2}}.$$

Thus the integral equation to be solved for $t(r)$ is

$$K\left[1-\left(\frac{x}{R\sec\mu}\right)^2\right]^{\frac{3}{2}}=2\cos\mu\int_{x\cos\mu}^{R}\frac{t(r)\,r\,dr}{\sqrt{(r^2-x^2\cos^2\mu)}}, \qquad (4)$$

where K is a constant dependent upon the given wing volume. By a suitable transformation of co-ordinates, equation (4) may be written in the form

$$\frac{K}{R\cos\mu}\varphi^{\frac{3}{2}}=\int_0^{\varphi}\frac{t(\alpha)\,d\alpha}{\sqrt{(\varphi-\alpha)}} \qquad (5)$$

where $$\varphi=1-\left(\frac{x}{R\sec\mu}\right)^2$$

$$\alpha=1-\left(\frac{r}{R}\right)^2.$$

Equation (5) is called Abel's equation and its solution is well known, *cf.* Ref. 6.

The solution to equation (5) is

$$t(r)=\frac{3K}{4R\cos\mu}\left[1-\left(\frac{r}{R}\right)^2\right]$$

and substitution of this in equation (1) determines K; then

$$t(r)=\frac{2V}{\pi R^2}\left[1-\left(\frac{r}{R}\right)^2\right]. \qquad (6)$$

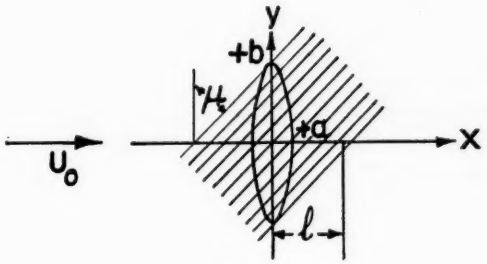

Fig. 6.

Equation (6) thus gives the distribution of thickness which will result in minimum drag for the circular plan form wing of given volume.

To apply the circular plan form solution to the original problem of finding the optimum thickness for an unyawed elliptic plan form, we make the following change of co-ordinates:—

$$\left.\begin{aligned} X &= ax/R \\ Y &= by/R \end{aligned}\right\} \quad . \quad . \quad . \quad . \quad . \quad . \quad . \quad . \quad (7)$$

The circular wing is then transformed into an elliptic wing whose equation is

$$\left(\frac{X}{a}\right)^2 + \left(\frac{Y}{b}\right)^2 = 1.$$

It can be verified that the thickness distribution

$$t = \frac{2V}{\pi ab}\left[1 - \left(\frac{X}{a}\right)^2 - \left(\frac{Y}{b}\right)^2\right]. \quad . \quad . \quad . \quad . \quad . \quad (8)$$

obtained from equation (6) through the transformation of equation (7) is the optimum for this more general case; that is, the equivalent lineal distribution for equation (8) with a set of Mach planes inclined at the angle μ as shown in Fig. 6 is

$$S(X) = \frac{8V}{3\pi l}\left[1 - \left(\frac{X}{l}\right)^2\right]^{\frac{3}{2}} \quad . \quad . \quad . \quad . \quad . \quad (9)$$

where $\qquad l = \sqrt{(a^2 + b^2 \tan^2 \mu)}.$

Since equation (9) represents a Sears-Haack body, the thickness given by equation (8) is optimum for the unyawed elliptic wing.*

Determination of the total drag in this optimum case involves an integration of the drag increments from these Sears-Haack bodies as seen at each angular reference station. If the reference station is at an angle θ from the horizontal, then the Mach planes cut the elliptic plan form at an angle μ defined as[3]

$$\tan \mu = \sqrt{(M^2 - 1)} \cos \theta \quad . \quad . \quad . \quad . \quad . \quad (10)$$

*Within the accuracy of linearised theory, this thickness distribution corresponds to constant curvature in the streamwise direction.

and the total drag is $$D = \int_0^{2\pi} \frac{dD}{d\theta}\, d\theta.$$

The increment of drag at each reference station is[3]

$$\frac{dD}{d\theta} = \frac{-q}{4\pi} \int_0^{\lambda} \int_0^{\infty} \frac{d^2S}{dx^2} \frac{d^2S}{d\xi^2} \log|x-\xi|\, dx\, d\xi$$

$$= \frac{4qV^2}{\pi^2 l^4} \quad . \quad . \quad . \quad . \quad . \quad . \quad . \quad . \quad . \quad (11)$$

and the total drag for the optimum thickness distribution of equation (8) is

$$D_{opt} = \frac{4qV^2}{\pi a^3 b} \left\{ \frac{(M^2-1)+2\,a^2/b^2}{[(M^2-1)+a^2/b^2]^{\frac{3}{2}}} \right\} \quad . \quad . \quad . \quad . \quad . \quad (12)$$

Defining $$t = t_0 (1 - X^2/a^2 - Y^2/b^2)$$

and $$D = C_D q \pi a b,$$

then $$C_{D\,opt} = \frac{[(M^2-1)+2a^2/b^2]\, t_0^{\,2}}{[(M^2-1)+a^2/b^2]^{\frac{3}{2}}\, a^2} \quad . \quad . \quad . \quad . \quad . \quad . \quad (13)$$

This result agrees with that given by Jones[4].

Appendix II

(A) Ring-Wing and Central Body of Revolution Combination Having Drag of Sears-Haack Body

Consider a ring-wing plus a central body of revolution contained within the volume bounded by a double Mach cone. Because of the axial symmetry of this particular system, the equivalent body of revolution is independent of the angle θ on the cylindrical control surface. In this case, if the local radial force on the wing is everywhere zero, the drag of the equivalent body of revolution is, according to Hayes's formula, identical to the drag of the original system. Thus, a ring-wing (which carries no radial force) plus a central body of revolution will have exactly the same drag as a Sears-Haack body if the equivalent body of revolution is a Sears-Haack body.

To design such a system, we may select any smooth, slender profile for the ring-wing and compute the cross-sectional areas cut from this wing by a set of parallel Mach planes. These areas must then be subtracted from the cross-sectional areas which would be cut from a central Sears-Haack body by the corresponding Mach planes. The resulting area difference defines the area distribution (in the Mach planes) of the correct central body. (This area must be projected normal to the flow direction to obtain the cross-sectional area of the central body defined in the usual way). This body, together with the ring-wing originally selected, is an optimum distribution of thickness within the double Mach cone volume.

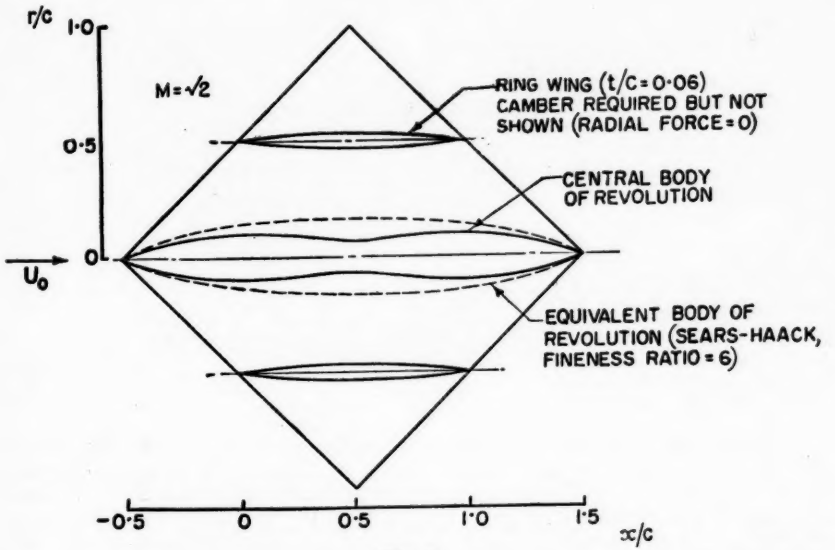

Fig. 7.
Cross-sectional view of ring-wing and central body. (An optimum distribution of thickness within the double Mach cone volume).

As an example, consider a ring-wing with thickness distribution corresponding to a bi-parabolic arc profile. The camber necessary for zero local radial force need not be determined, since it does not affect the shape of the central body. Assume that the wing is six per cent. thick and located half-way between the axis and the apex of the volume. If the central body of revolution is designed so that the equivalent Sears-Haack body is of fineness ratio 6, the resulting shape of the central body of revolution is as shown in Fig. 7.

(B) Ring-Wing and Central Body of Revolution Having Zero Drag

The theoretical minimum drag value for a distribution of thickness elements that has no interference with lift or side force elements is the drag of a Sears-Haack body. Part (A) of this Appendix illustrates a system which attains this minimum drag value for thickness elements contained within a double Mach cone volume. However, it was pointed out previously that interferences between thickness distributions and distributions of lift or side force may provide negative drag contributions which reduce the theoretical minimum wave drag of a system to zero. For the double Mach cone volume, the remaining portion of this Appendix illustrates a central body of revolution which, together with a certain distribution of radial forces on a cylindrical shell, has zero wave drag. The method used here to design such a system makes use of certain equivalences between sources and line distributions of elementary vortex shells.* (These equivalences will be discussed in a later paper).

*A vortex shell is defined to be a closed vortex line in a plane normal to the flow direction. The present application assumes infinitesimal rectangular vortex shells distributed uniformly along a streamwise line.

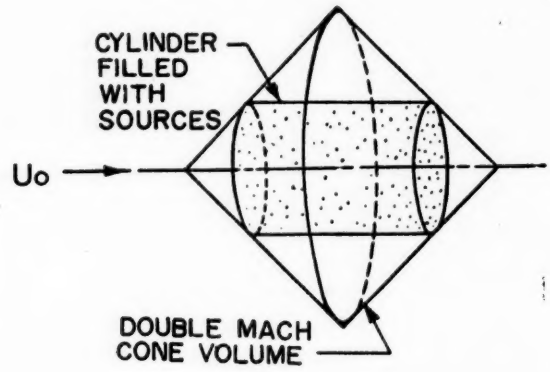

Fig. 8.

Consider an axially symmetric, continuous distribution of sources filling a cylindrical space contained within the double Mach cone volume (Fig. 8). A set of parallel Mach planes cutting this source distribution determines an equivalent lineal source distribution according to the method of Hayes[3]. For convenience, this equivalent lineal source distribution will be denoted by $F(x)$. Because of the axial symmetry of this case, $F(x)$ is independent of the angle θ on the distant control surface. A central body of revolution which is represented by the negative of $F(x)$ will just cancel the velocities induced at the distant control surface by the original sources. The drag of the combined system is then zero. The remaining step is to relate the original source distribution to a distribution of radial forces around the boundary of the cylindrical space. It can be shown that a source and a sink of equal strength, lying on the same line parallel to the flow direction, have exactly the same effect at the distant control surface as a line of constant-strength elementary vortex shells connecting the source and the sink. If such vortex shells are considered to replace the original source distribution, the forces on adjoining shells inside the cylinder are seen to cancel one another, while the forces on the outer sides of the shells next to the boundary of the cylindrical space determine the radial force. A cylindrical shell having this radial load distribution plus a central body of revolution which corresponds to the source distribution $-F(x)$ constitute a system having zero drag.

As an example, suppose that a cylinder within a double Mach cone volume is considered to contain a source distribution which varies linearly with axial distance but is independent of radial distance. That is, the source strength per unit area inside the cylinder is

$$f = -f_0\left(1 - 2\frac{x}{c}\right),$$

where x is measured from the leading edge of the cylinder, c is the cylinder length, and f_0 is the strength of the sources at the rear face of the cylinder. The equivalent lineal source strength corresponding to this original distribution is given by

$$\frac{\beta^2}{c^2}F(x) = \left(\frac{\beta R}{c}\right)^2 f_0\left[-\left(1-2\frac{x}{c}\right)\left\{\frac{x}{\beta R}\sqrt{\left[1-\left(\frac{x}{\beta R}\right)^2\right]} + \cos^{-1}\left(\frac{-x}{\beta R}\right)\right\} + \right.$$

$$\left. + \frac{4}{3}\left(\frac{\beta R}{c}\right)\left\{1-\left(\frac{x}{\beta R}\right)^2\right\}^{\frac{3}{2}}\right]; -\beta R \leqslant x \leqslant +\beta R,$$

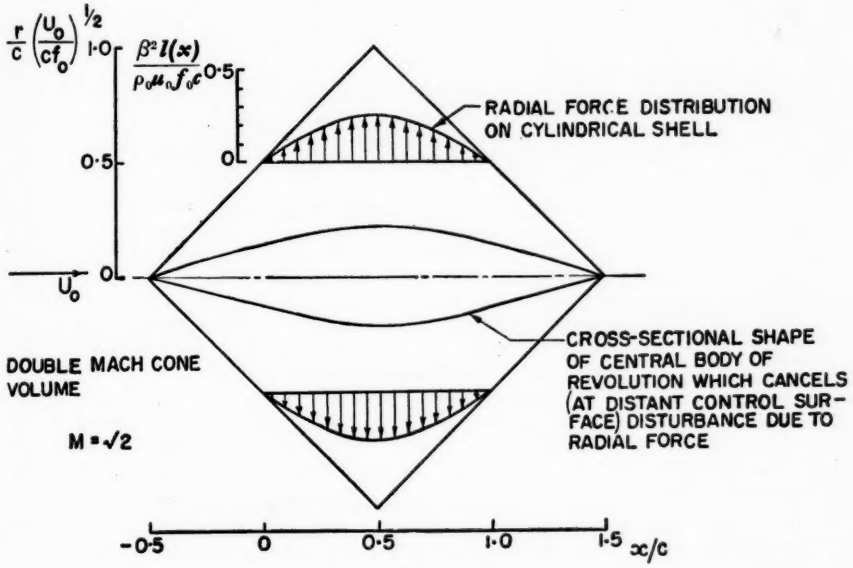

Fig. 9.
Central body of revolution and radial force distribution having zero wave drag.

and $$\frac{\beta^2}{c^2}F(x)=\left(\frac{\beta R}{c}\right)^2 f_0\left[-\pi\left(1-2\frac{x}{c}\right)\right];\ \beta R\leqslant x\leqslant c-\beta R,$$

where R is the cylinder radius. Now, if the negative of this source distribution is assumed to represent a body of revolution, then within the accuracy of slender-body theory the area distribution of the central body is

$$S(x)=-\frac{1}{U_0}\int_{-\beta R}^{x}F(x)\,dx.$$

For illustration, the dimensions of the cylinder are assumed to be such that $\beta R/c=1/2$; that is, the radius is half the distance between the axis and the apex of the double Mach cone volume. The shape of the central body of revolution which cancels the effect of the original source distribution for this case is shown in Fig. 9. The distribution of radial force which can replace the original linearly varying source distribution is

$$l(x)=\frac{\rho_0 U_0}{\beta^2}f_0\int_0^x\left(1-2\frac{x}{c}\right)dx=\frac{\rho_0 U_0}{\beta^2}f_0 c\left(\frac{x}{c}\right)\left(1-\frac{x}{c}\right).$$

Supersonic Flow Past Slender Bodies With Discontinuous Profile Slope

L. E. FRAENKEL and H. PORTNOY

(*Imperial College*)

SUMMARY: Ward's slender-body theory is extended to derive first approximations to the external forces on slender bodies of general cross section with discontinuous profile slope. Two classes of body are considered: bodies whose profile (typified by the local radius) is continuous between the nose and base, and certain bodies whose profile is discontinuous, such as bodies with annular or side air intakes and wing-bodies on which the wing has an unswept leading edge. (Where air intakes are concerned, it is assumed that they are sharp-edged and that there is no "spillage" of the internal flow).

The following conclusions apply to the former class of bodies. The variation of drag with Mach number is found to depend only on the discontinuities in the longitudinal rate of change of the cross-sectional area, and is thus independent of cross-sectional shape. The drag itself is unchanged if the direction of the flow is reversed. The expressions for lift and moment assume the same forms as for smooth pointed bodies, the lift depending only on conditions at the base of the body.

The general theory is applied to winged bodies of revolution with an unswept wing leading edge: the results bear a marked resemblance to those obtained by Ward. The results for wings alone are seen to be applicable, with one modification, to subsonic as well as to supersonic speeds.

1. Introduction

In this paper we extend Ward's slender-body theory[1] to derive first approximations to the aerodynamic forces in steady supersonic flow on slender bodies of general cross section whose profiles have discontinuous slope. (By the word "profile" we mean the boundary of a section of the body by a plane through its longitudinal axis). The discontinuities must lie approximately in planes normal to the direction of the undisturbed flow. Lighthill[2] first treated this problem for the particular case of bodies of revolution by introducing some results of the quasi-cylinder theory. In Ref. 3 bodies of elliptic cross section were considered, and it was shown that for a first approximation to the forces the introduction of a quasi-cylinder theory was not absolutely necessary; a modified form of Ward's simple velocity potential was used in a particular manner to obtain the results. It is this approach which is generalised in the present paper, and it is found that the method may also be used for certain bodies whose actual profile is discontinuous.

Received September 1954

The physical effect of the discontinuities is that in short regions behind them the flow is roughly analogous to that on a wing with a sharp supersonic leading edge, and the pressure is of a greater magnitude there than it is on smooth, pointed bodies. Consequently these regions, although short, make contributions to the aerodynamic forces which are of the order of the total forces. The mathematical effect on the slender-body approximation has been discussed in Ref. 4 and elsewhere: this solution now provides only an asymptotic approximation, valid when the distance downstream from a discontinuity is large compared with the thickness of the body, and it fails completely in the important regions of relatively large pressure behind the discontinuities. This difficulty is overcome by relating the integral over the body of the $\partial\varphi/\partial s$ term in the pressure to the values of the potential φ itself at points immediately upstream and far downstream of a discontinuity, where the approximation is valid.

NOTATION

$a_n(s)$	coefficients in the slender-body potential
$b(s)$	wing semi-span
$b_0(s)$	function in the slender-body potential
B	$\sqrt{(M^2-1)}$, where M is free stream Mach number
C, C_{i+}	body contour in a plane $s=$constant, $s=e_i+$
D	drag force
e_i	values of s at which R, dv/ds are discontinuous ($i=0, 1, 2, \ldots m$)
F, G	complex lateral force $X+iY$ as given by ϕ, φ
l	length of body
l_1	value of s at maximum span of wing
M_x, M_y	moments about x- and y-axes
M_z	complex moment M_x+iM_y
(r, θ, s)	cylindrical co-ordinates
$R(\theta, s)$	value of r on body surface
R_s, R_θ	partial differentials of R with respect to s and θ
$R_1(s)$	radius of body of revolution
$\mathscr{R}$	real part of
$S(s)$	cross-sectional area of body
t	maximum thickness of body
U	free stream velocity
$w(z, s)$	complex function such that $\mathscr{R}w=\phi$
(x, y, s)	Cartesian co-ordinates
X, Y	forces in positive x-, y-directions
z, z_1	complex variables $x+iy$, $(x+\alpha s)+iy$

$z_g(s)$	complex co-ordinate of centre of area of cross section
α	angle of incidence
$\beta(s)$	effective wing semi-span, $(b^2-R_1^2)/b$
∇_2	two-dimensional gradient operator in plane $s=$constant
ν	normal outward from body in plane $s=$constant
$d\nu/ds$	streamwise body slope, $RR_s(R^2+R_\theta^2)^{-\frac{1}{2}}$
ρ	density in the free stream
τ	circumferential variable, $d\tau=(R^2+R_\theta^2)^{\frac{1}{2}}\,d\theta$
φ	exact linearised perturbation potential
ϕ	asymptotic slender-body potential
ϕ_1	$\varphi-\phi$
ϕ_h	*see* equation (3)

2. The Slender-body Solution

Let (x, y, s) and (r, θ, s) be Cartesian and cylindrical co-ordinates such that an undisturbed stream at infinity, of velocity U, flows in the direction of increasing s, and such that the origin of the frame is at the centre of area of the nose cross section of the body. Let the complete velocity potential of the field be $\Phi=U(s+\varphi)$.

Consider a body subject to the restrictions specified by Ward[1], except that its streamwise slope $d\nu/ds$ and its profile may be discontinuous at stations $s=e_i+O(t^2)$, $(i=0, 1, \ldots m)$, which must be spaced well apart $(e_{i+1}-e_i=O(1))$. We take $e_0=0$, $e_m=l$, and specify that l is $O(1)$. The following conventions are also used:—

$$\left(\frac{d\nu}{ds}\right)_{s=0-}=\left(\frac{d\nu}{ds}\right)_{s=l+}=0,$$

$$f(x, y, e_i+)-f(x, y, e_i-)=\Delta f_i.$$

The linearised equation for the velocity potential is

$$\nabla_2{}^2\varphi=B^2\frac{\partial^2\varphi}{\partial s^2}, \qquad (1)$$

where ∇_2 denotes the two-dimensional gradient operator in a plane $s=$constant; and the boundary condition on a slender body is

$$\frac{\partial\varphi}{\partial\nu}\simeq\frac{d\nu}{ds}. \qquad (2)$$

We assume the existence of a perturbation potential φ which satisfies equations (1) and (2) exactly, and which also satisfies the appropriate conditions at infinity and on the wave fronts emanating from the discontinuities.

The asymptotic, slender-body solution ϕ, valid near the body for $s-e_i \gg O(t)$, is

$$\phi(r,\theta,s)=\mathscr{R}w(z,s)=\phi_h(r,\theta,s)+b_0(s), \quad . \quad . \quad . \quad (3)$$

where ϕ_h is harmonic in (r,θ), satisfies the boundary condition (2), and is such that $\left[\phi_h-\frac{1}{2\pi}S'(s)\log r\right]\to 0$ as $r\to\infty$; and

$$b_0(s)=\frac{1}{2\pi}\left\{S'(s)\log\frac{B}{2}-\int_{\sigma=0-}^{s}\log(s-\sigma)\,dS'(\sigma)\right\}. \quad . \quad . \quad (4)$$

Here a Stieltjes integral has replaced the Riemann integral of Ref. 1. ϕ_h may be expanded in series outside a circular cylinder enclosing the body:—

$$\left.\begin{aligned}&\phi_h=\mathscr{R}\left[a_0(s)\log z+\sum_{n=1}^{\infty}a_n(s)z^{-n}\right],\quad r>R_{\max},\\ &\text{where}\quad a_0(s)=\frac{1}{2\pi}S'(s).\end{aligned}\right\} \quad . \quad . \quad (5)$$

The coefficients $a_n(s)$ are $O(t^{n+2})$ and are in general discontinuous at $s=e_i$.

It may be shown[4] that if we write $\varphi=\phi+\phi_1$, then there exists some finite positive number K such that

$$\text{for}\qquad s-e_i\leqslant Kt,\quad \phi_1\ \text{ is }\ O\left(t^2\log\frac{t}{s-e_i}\right),$$

$$\text{while for}\qquad s-e_i\geqslant Kt,\quad \phi_1\ \text{ is }\ O\left(\frac{t^4}{(s-e_i)^2}\log\frac{t}{s-e_i}\right).$$

The arguments leading to this last result include an assumption which is supported by known particular cases.

3. The Drag Force

The drag integral is first expressed in terms of φ, and cast into a form which permits substitution of the asymptotic potential ϕ. The drag of a segment of the body between $s=e_i$ and $s=e_{i+1}$ may be written

$$\frac{D_{i,i+1}}{\frac{1}{2}\rho U^2}=\int_{e_i}^{e_{i+1}}ds\oint_C\left[-2\frac{\partial\varphi}{\partial s}-(\nabla_2\varphi)^2\right]\frac{dy}{ds}\,d\tau+O(t^5). \quad . \quad . \quad (6)$$

The O-term results from the fact that in the initial region $s-e_i\leqslant O(t)$, where $\partial\varphi/\partial s$ is $O(t)$, the error of $\partial\varphi/\partial s$ is $O(t^2)$, because φ is only a solution of the linearised equation.

We introduce the total derivative of the integral around the body contour of $\varphi(\partial\varphi/\partial\nu)$. Let C denote the body contour in a plane $s=$constant, C' the projection of C on the plane $s+\delta s=$constant, and C'' the body contour in the plane $s+\delta s=$constant. Then*

$$\frac{d}{ds}\oint_C \varphi\frac{\partial\varphi}{\partial\nu}\,d\tau = \lim_{\delta s\to 0}\frac{1}{\delta s}\left\{\oint_{C''-C'}\varphi\frac{\partial\varphi}{\partial\nu}\,d\tau+\oint_{C'-C}\varphi\frac{\partial\varphi}{\partial\nu}\,d\tau\right\}$$

$$=\lim_{\delta s\to 0}\frac{1}{\delta s}\left\{\oint_{C'}\left[\varphi(\nabla_2{}^2\varphi)+(\nabla_2\varphi)^2\right]\cdot\frac{d\nu}{ds}\,\delta s\,d\tau+\oint_C\left[\frac{\partial\varphi}{\partial s}\frac{\partial\varphi}{\partial\nu}+\varphi\frac{\partial^2\varphi}{\partial\nu\,\partial s}\right]\delta s\,.\,d\tau\right\} \quad . \quad . \quad . \quad . \quad (7)$$

where we have used Green's theorem for the first integral, and the fact that C' is geometrically the same as C, but is displaced a distance δs, in the second. Proceeding to the limit $\delta s\longrightarrow 0$, and substituting for $\nabla_2{}^2\varphi$ and $\partial\varphi/\partial\nu$ from equations (1) and (2) respectively gives

$$-\oint_C\frac{\partial\varphi}{\partial s}\frac{d\nu}{ds}\,d\tau=-\frac{d}{ds}\oint_C\varphi\frac{\partial\varphi}{\partial\nu}\,d\tau+\oint_C\left[B^2\varphi\frac{\partial^2\varphi}{\partial s^2}\frac{d\nu}{ds}+(\nabla_2\varphi)^2\frac{d\nu}{ds}+\varphi\frac{\partial^2\varphi}{\partial\nu\,\partial s}\right]d\tau. \quad (8)$$

Inserting this result into (6), we now have

$$\frac{D_{i,i+1}}{\frac{1}{2}\rho U^2}=-2\oint_{C_{(i+1)-}}\left(\varphi\frac{d\nu}{ds}\right)_{s=e_{i+1}-}d\tau+2\oint_{C_{i+}}\left(\varphi\frac{d\nu}{ds}\right)_{s=e_i+}d\tau+\int_{e_i}^{e_{i+1}}ds\oint_C\left[2\varphi\frac{\partial^2\varphi}{\partial\nu\,\partial s}+\right.$$

$$\left.+(\nabla_2\varphi)^2\frac{d\nu}{ds}+2B^2\varphi\frac{\partial^2\varphi}{\partial s^2}\frac{d\nu}{ds}\right]d\tau+O(t^5). \quad . \quad . \quad (9)$$

In this expression the contribution of $2B^2\varphi(\partial^2\varphi/\partial s^2)(d\nu/ds)$ is at most $O(t^5)$. In the second integral we substitute

$$\varphi(r,\theta,e_i+)=\phi(r,\theta,e_i-)+O(t^4(\log^2 t),$$

since φ (as opposed to ϕ) is continuous, and in the remaining terms we may substitute $\varphi\simeq\phi$: the error is still $O(t^5)$ (*see* the Appendix).

The integral over the body surface may now be transformed, by the two-dimensional form of Green's theorem, into an integral over the surface of a circular cylinder $r=r_2>R_{\max}$, $e_i<s<e_{i+1}$, (Fig. 1), on which the series expansion of ϕ converges. We have

$$2\oint_C\phi\frac{\partial^2\phi}{\partial\nu\,\partial s}\,d\tau=2\int_0^{2\pi}\phi\frac{\partial^2\phi}{\partial r\,\partial s}r_2\,d\theta-2\iint_A(\nabla_2\phi)\left(\nabla_2\frac{\partial\phi}{\partial s}\right)dS$$

$$=2\int_0^{2\pi}\phi\frac{\partial^2\phi}{\partial r\,\partial s}r_2\,d\theta-\frac{d}{ds}\iint_A(\nabla_2\phi)^2\,dS-\oint_C(\nabla_2\phi)^2\frac{d\nu}{ds}\,d\tau. \quad (10)$$

* The derivative $\partial^2\varphi/\partial\nu\partial s$ appearing in (7) may be defined as $(\underline{\nu}\cdot\nabla_2)(\partial\varphi/\partial s)$.

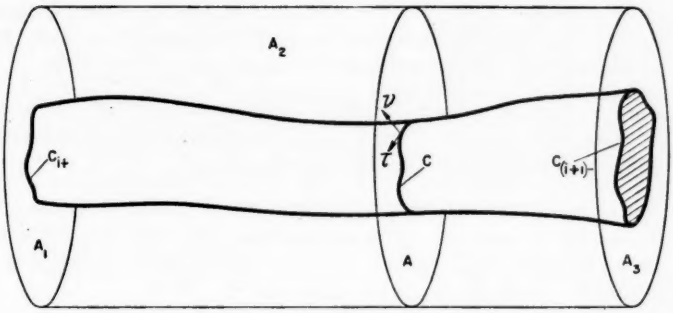

Fig. 1.

Inserting this expression into the double integral of (9), integrating with respect to s, and transforming the resulting integrals of $(\nabla_2\phi)^2$ over A_1 and A_3 into integrals around the boundaries of these areas, we obtain

$$\frac{D_{i,i+1}}{\frac{1}{2}\rho U^2} = -\oint_{C_{(i+1)-}} \left(\phi \frac{d\nu}{ds}\right)_{s=e_{i+1}-} d\tau + \oint_{C_{i+}} \left(2\phi_{s=e_i-} - \phi_{s=e_i+}\right)\left(\frac{d\nu}{ds}\right)_{s=e_i+} d\tau +$$

$$+2\int\int_{A_2} \phi \frac{\partial^2\phi}{\partial r\,\partial s}\,dS - \int_0^{2\pi}\left[\left(\phi\frac{\partial\phi}{\partial r}\right)_{s=e_{i+1}-} - \left(\phi\frac{\partial\phi}{\partial r}\right)_{s=e_i+}\right] r_2\,d\theta + O(t^5). \quad . \quad (11)$$

Substituting $\phi=\phi_h+b_0$ in the first two integrals of this expression, and using the series expansion of ϕ in the others, we now find

$$\frac{D_{i,i+1}}{\frac{1}{2}\rho U^2} = -\oint_{C_{(i+1)-}} \left(\phi_h \frac{d\nu}{ds}\right)_{s=e_{i+1}-} d\tau + \oint_{C_{i+}} \left[\left(2\phi_h\right)_{s=e_i-} - \left(\phi_h\right)_{s=e_i+}\right]\left(\frac{d\nu}{ds}\right)_{s=e_i+} d\tau +$$

$$+4\pi\left[\int_{e_i}^{e_{i+1}} a_0' b_0\,ds + a_0(e_i+)\,b_0(e_i-) - a_0(e_{i+1}-)\,b_0(e_{i+1}-)\right] + O(t^5). \quad . \quad (12)$$

This result in no way requires the profile function $R(\theta, s)$ to be continuous at $s=e_i$; it only requires the existence of a slender-body type of flow field immediately upstream of C_{i+}, on $s=e_i-$, $r=R(\theta, e_i+)$. We shall, however, only sum the drag of the m segments for bodies for which $R(\theta, s)$ is continuous in the range $0<s<l$. Performing this summation, and inserting the value of $b_0(s)$ given by equation (4), we obtain, after some reduction,

$$\frac{D}{\frac{1}{2}\rho U^2} = \frac{1}{2\pi}\,\mathscr{F}\int_{s=0-}^{l+}\int_{\sigma=0-}^{l+} \log\frac{1}{|s-\sigma|}\,dS'(s)\,dS'(\sigma) + \sum_{i=0}^{m}\left\{\frac{1}{2\pi}(\Delta S_i')^2 \log\frac{2}{B} + \right.$$

$$\left. + \oint_{C_i}\left[\left(\phi_h\right)_{s=e_i-}\left(\Delta\frac{d\nu}{ds}\right)_i - \left(\Delta\phi_h\right)_i\left(\frac{d\nu}{ds}\right)_{s=e_i+}\right] d\tau\right\} + O(t^5), \quad . \quad (13)$$

where $\mathscr{F}$ denotes the "finite part" of the double Stieltjes integral; that is, the points $s=\sigma=e_i$ are excluded from the area of integration (*see* Ref. 2). Two general conclusions may be drawn from this result:—

(*i*) The variation of drag with Mach number depends only on the discontinuities in the function $S'(s)$; it is independent of cross-sectional shape and of the area distribution between discontinuities.

(*ii*) The drag is unchanged if the direction of the stream is reversed: this is proved as follows. In reversed flow the signs of $S'(s)$, ϕ_h and $d\nu/ds$ are all changed, and values at $s=e_i+$ are replaced by values at $s=e_i-$. Hence it is only necessary to show that

$$\oint_{C_i}\left(\phi_h\right)_{s=e_i+}\left(\frac{\partial\phi}{\partial\nu}\right)_{s=e_i-}d\tau=\oint_{C_i}\left(\phi_h\right)_{s=e_i-}\left(\frac{\partial\phi}{\partial\nu}\right)_{s=e_i+}d\tau.$$

That this is in fact an identity may be shown by applying Green's theorem to the area between C_i and the circle $r=r_2$, $s=e_i$, and using the series expansion of ϕ on the circle.

4. The Lateral Forces and Moments

The complex lateral force due to a segment of the body is

$$\frac{F_{i,i+1}}{\frac{1}{2}\rho U^2}=\frac{(X+iY)_{i,i+1}}{\frac{1}{2}\rho U^2}=\int_{e_i}^{e_{i+1}}ds\oint_c\left[-2\frac{\partial\varphi}{\partial s}-(\nabla_2\varphi)^2\right]i\,dz+O(t^4). \quad . \quad (14)$$

Proceeding in a manner similar to that of equation (7) we find that

$$\begin{aligned}\frac{d}{ds}\oint_c\varphi\,dz&=\oint_c\left[\left(i\frac{\partial\varphi}{\partial x}-\frac{\partial\varphi}{\partial y}\right)\frac{d\nu}{ds}d\tau+\frac{\partial\varphi}{\partial s}dz\right]\\&=\oint_c\left[\left(\frac{\partial\varphi}{\partial s}+\frac{1}{2}(\nabla_2\varphi)^2\right)dz-\frac{1}{2}\left(\frac{\partial\varphi}{\partial x}+i\frac{\partial\varphi}{\partial y}\right)^2d\bar{z}\right],\end{aligned}$$

where we have used $(d\nu/ds)\,d\tau=(\partial\varphi/\partial\nu)d\tau=(\partial\varphi/\partial x)\,dy-(\partial\varphi/\partial y)\,dx$. Hence (14) becomes

$$\frac{F_{i,i+1}}{\frac{1}{2}\rho U^2}=-2i\left(\oint_c\varphi\,dz\right)\Big|_{s=e_i+}^{e_{i+1}-}-i\int_{e_i}^{e_{i+1}}ds\oint_c\left(\frac{\partial\varphi}{\partial x}+i\frac{\partial\varphi}{\partial y}\right)^2d\bar{z}+O(t^4). \quad . \quad (15)$$

We may again substitute $\varphi\simeq\phi$ into this expression, taking the value at $s=e_i-$ in the first term. The inner part of the double integral is then

$$\oint_c\left(\frac{\partial\overline{w}}{\partial\bar{z}}\right)^2d\bar{z},$$

which vanishes, since $\partial\overline{w}/\partial\bar{z}$ is a regular function of $\bar{z}$ outside C, and since the integral around an infinite contour vanishes. Taking the most general case where $R(\theta, e_i-) \neq R(\theta, e_i+)$ we find the lateral force up to some station s at a substantial distance downstream from a discontinuity. The difference between the integrals around the body contours immediately upstream and downstream of a discontinuity in R is transformed into an area integral by Stokes' theorem, and there results

$$\frac{F(s)}{\frac{1}{2}\rho U^2} = -2i\oint_C \phi_h\,dz - 2\sum_{i=0}^{m-1} H(s-e_i)\iint_{\Delta S_i}\left(\frac{\partial\overline{w}}{\partial\bar{z}}\right)_{s=e_i-} dS + O(t^4)$$

$$= 4\pi a_1 + 2\frac{d}{ds}(Sz_g) - 2\sum_{i=0}^{m-1} H(s-e_i)\iint_{\Delta S_i}\left(\frac{\partial\overline{w}}{\partial\bar{z}}\right)_{s=e_i-} dS + O(t^4), \quad (16)$$

where H is the Heaviside unit function, and the last step has been taken directly from Ref. 1. The total complex lateral force is obtained by evaluating this expression at $s=l-$.

To calculate the moments, let $G(s)$ denote the complex lateral force up to s as given by φ, and let $F(s)$ denote that given by ϕ. Then the total moment is

$$M_z = M_x + iM_y = i\int_0^l sG'(s)\,ds + O(t^4)$$

$$= i\left[lG(l) - \int_0^l G(s)\,ds\right] + O(t^4),$$

$G(s)$ being a continuous function. It is permissible to substitute $G(e_i) \simeq F(e_i-)$, $G(s) \simeq F(s)$, and hence

$$M_z = i\left[lF(l-) - \int_0^l F(s)\,ds\right] + O(t^4). \quad . \quad . \quad . \quad (17)$$

Thus for bodies on which $R(\theta, s)$ is continuous in the range $0 < s < l$, the expressions for lateral force and moment are unaffected by the discontinuities, and the lateral force still depends only on conditions at the base of the body.

The results of Refs. 2, 3 and 5 can, of course, be recovered from equations (12), (13), (16) and (17) as particular cases.

5. Winged Bodies of Revolution

In this section the results are applied, in the manner of Ref. 1, to calculate the forces on winged bodies of revolution at incidence. The novelty of the present treatment lies in the fact that the body geometry and the wing plan form may now include discontinuities (Fig. 2). The wing has zero thickness and total span $2b(s)$, and is mounted symmetrically on the body, the incidence of wing and body being defined by $z_g = -\alpha s$; the plan form of the configuration must be slender; and the

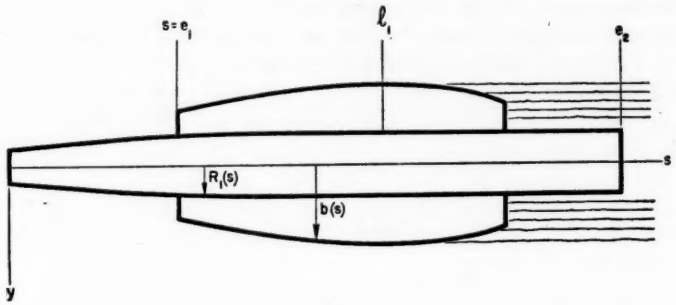

Fig. 2.

discontinuities must be separated by distances of $O(1)$. If $s=l_1$ denotes the station of maximum wing span, the radius of the body $R_1(s)$ (now measured from z_g), must be constant for $s \geqslant l_1$. In general it is necessary also to impose the restriction

$$b(s)\,b'(s) \geqslant R_1(s)\,R_1'(s), \quad e_1 < s \leqslant l_1, \qquad . \quad . \quad . \quad (18)$$

which ensures that the side edge of the wing is a "leading" rather than a "trailing" one with respect to the local flow, so that the vortices do not drift outboard of the wing, upstream of the maximum span. However, when $R_1'(s)=0$ for $s \geqslant e_1$, or when the wing alone is considered, this restriction is probably not necessary. In these latter cases the body does not deform the streamlines in the wing plane, and if $b'(s)$ is negative (so that $l_1=e_1$) the unknown flow over the foremost part of the wing only affects the vorticity in the most outboard part of the wake, the width of this part being $O(t^2)$.

The asymptotic potential of the wing-body is[1]

$$\left.\begin{aligned} \phi &= \mathscr{R}\left\{ a_0 \log z_1 + b_0(s) + \alpha\left[\left(z_1 + \frac{R_1^2(s)}{z_1}\right)^2 + \beta^2(s)\right]^{\frac{1}{2}} - \alpha z_1 \right\}, \quad 0 < s \leqslant l_1, \\ &= \mathscr{R}\left\{ b_0(l_1) + \alpha\left[\left(z_1 + \frac{R_1^2(l_1)}{z_1}\right)^2 + \beta^2(l_1)\right]^{\frac{1}{2}} - \alpha z_1 \right\}, \qquad l_1 \leqslant s < e_m, \end{aligned}\right\} \quad (19)$$

where

$$z_1 = z + \alpha s, \quad \beta(s) = \frac{b^2(s) - R_1^2(s)}{b(s)}. \qquad . \quad . \quad . \quad (20)$$

$\beta(s)$ might be called the "effective wing semi-span," (*see* next paragraph).

We insert this potential into equations (12), (16) and (17), noting that there is no coupling between the thickness and incidence terms in the resulting contour integrals, due to the anti-symmetry of the incidence terms. Writing D_0 for the drag of the body at zero incidence, we obtain

$$\frac{D}{\frac{1}{2}\rho U^2} \simeq \frac{D_0}{\frac{1}{2}\rho U^2} + \alpha^2 \left\{ S(0+) + S(l_1) + \pi\left[\beta^2(e_1+) + \beta^2(l_1)\right] \right\}, \qquad (21)$$

$$\frac{X}{\frac{1}{2}\rho U^2} \simeq 2\alpha \left\{ S(l_1) + \pi \beta^2 (l_1) \right\}, \qquad (22)$$

$$\frac{M_y}{\frac{1}{2}\rho U^2} \simeq 2\alpha \left\{ l_1 S(l_1) - \int_0^{l_1} S(s)\, ds + \pi \left[l_1 \beta^2 (l_1) - \int_{e_1}^{l_1} \beta^2 (s)\, ds \right] \right\}. \qquad (23)$$

The results for a wing alone may be of some interest. Such results are of course a particular case of those just given ($D_0 = S = 0$, $e_1 = 0$, $\beta = b$), and can also be obtained, for $b'(s) \geqslant 0$, from those for a body of elliptic cross section[3], by considering a body of suitable profile and length l_1, and letting the minor axis of the ellipse tend to zero.

The results for the lift and moment of a flat slender wing are valid for subsonic speeds also, since essentially they depend on only two facts: (*i*) that ϕ_h provides an asymptotic approximation to φ, ($b_0(s) = 0$ here), and (*ii*) that in the plane of the wing $\varphi = 0$ upstream of the leading edge. Both these remain true for subsonic speeds.

The drag result given here cannot be applied to subsonic speeds because the suction force at the unswept part of the leading edge cannot be calculated by the methods used. The subsonic drag can be found, however, by a well-known method. If we calculate it by considering the flow of momentum, as predicted by φ, through a large circular cylinder surrounding the wing, the contributions of the upstream face and of the curved surface of the cylinder vanish in the limit. There remains the contribution of the downstream face or "Trefftz plane." In this plane φ is harmonic in (r, θ) and the drag is

$$\frac{D}{\frac{1}{2}\rho U^2} = \iint (\nabla_2 \varphi)^2 \, dS = - \oint_{C_w} \varphi \frac{\partial \varphi}{\partial \nu} d\tau$$

$$\simeq - \oint_{C_w} \phi \frac{\partial \phi}{\partial \nu} d\tau,$$

where the contour C_w is taken around the wake. Hence

$$\frac{D}{\frac{1}{2}\rho U^2} \simeq \alpha^2 \pi b^2 (l_1), \qquad (24)$$

which is the same result as for a pointed wing.

Most of these results for a wing alone were originally suggested by the work of Jones[6], and were confirmed, for the case of a slender rectangular wing in supersonic flow, by Stewartson[7].

References

1. Ward, G. N. Supersonic Flow past Slender Pointed Bodies. *Quarterly Journal of Mechanics and Applied Mathematics*, Vol. 2, No. 1, pp. 75-97, March 1949.

2. Lighthill, M. J. Supersonic Flow past Slender Bodies of Revolution, the Slope of whose Meridian Section is Discontinuous. *Quarterly Journal of Mechanics and Applied Mathematics*, Vol. 1, No. 1, pp. 90-102, March 1948.

3. FRAENKEL, L. E. Supersonic Flow past Slender Bodies of Elliptic Cross-Section. A.R.C. 15,166. (To be published in the R. & M. series). 1952.

4. FRAENKEL, L. E. On the Unsteady Motion of a Slender Body through a Compressible Fluid. *The Aeronautical Quarterly*, Vol. VI, Part 1, pp. 59-80, February 1955.

5. WARD, G. N. The Supersonic Flow past a Slender Ducted Body of Revolution with an Annular Intake. *The Aeronautical Quarterly*, Vol. I, Part 4, pp. 305-318, February 1950.

6. JONES, R. T. Properties of Low-Aspect-Ratio Pointed Wings, at Speeds below and above the Speed of Sound. N.A.C.A. Report 835, 1945.

7. STEWARTSON, K. Supersonic Flow over an inclined Wing of Zero Aspect Ratio. *Proc. Camb. Phil. Soc.*, Vol. 46, Part 2, pp. 307-315, April 1950.

Appendix

In this Appendix we justify the substitution $\varphi=\phi$ in the term

$$\int_{e_i}^{e_{i+1}} ds \oint_C \varphi \frac{\partial^2 \varphi}{\partial \nu \partial s} d\tau$$

of equation (9). The proofs for other, similar substitutions proceed along the same lines. For convenience we put $e_i=0$, $e_{i+1}=l_2$.

We introduced the error ϕ_1 of the asymptotic potential in Section 2; we now establish the order of $\partial^2\phi_1/\partial\nu\partial s$ on the body. Differentiating along a line $\tau=$constant locally, we have

$$\frac{d}{ds}\left(\frac{\partial \phi_1}{\partial \nu}\right) = \frac{\partial^2 \phi_1}{\partial \nu \partial s} + \frac{\partial^2 \phi_1}{\partial \nu^2}\frac{d\nu}{ds}.$$

But φ and ϕ satisfy the same boundary condition; hence the left hand side of this equation vanishes. Applying the orders of ϕ_1 given in Section 2 to $\partial^2\phi_1/\partial\nu^2$, we now have

$$\frac{\partial^2 \phi_1}{\partial \nu \partial s} = O\left(\frac{t^3}{s^2}\log\frac{t}{s}\right), \text{ for } s \geqslant Kt.$$

In the region $s \leqslant Kt$, we may say that $\partial^2\phi_1/\partial\nu\partial s$ is $O(t)$ at most, since $\partial^2\varphi/\partial\nu\partial s$ and $\partial^2\phi/\partial\nu\partial s$ are both $O(t)$. Hence

$$\int_0^{l_2} ds \oint_C \varphi \frac{\partial^2 \varphi}{\partial \nu \partial s} d\tau = \int_0^{Kt} ds \oint_C \left[\phi + O\left(t^2 \log\frac{t}{s}\right)\right]\left[\frac{\partial^2 \phi}{\partial \nu \partial s} + O(t)\right] d\tau +$$

$$+ \int_{Kt}^{l_2} ds \oint_C \left[\phi + O\left(\frac{t^4}{s^2}\log\frac{t}{s}\right)\right]\left[\frac{\partial^2 \phi}{\partial \nu \partial s} + O\left(\frac{t^3}{s^2}\log\frac{t}{s}\right)\right] d\tau$$

$$= \int_0^{l_2} ds \oint_C \phi \frac{\partial^2 \phi}{\partial \nu \partial s} d\tau + O\left\{ t \int_0^{Kt} t^3 \left|\log\frac{t}{s}\right| ds + t \int_{Kt}^{l_2} \frac{t^5}{s^2}\log^2\frac{t}{s}\, ds \right\},$$

and the O-term is found to be $O(t^5)$.

The Buckling and Bending of Orthotropic Sandwich Panels With All Edges Simply-Supported

J. R. ROBINSON, B.Sc., A.F.R.Ae.S.

(Handley Page Limited)

SUMMARY: A formula is derived for the buckling in compression of an orthotropic sandwich panel, with all edges simply-supported. Two special types of symmetrical sandwiches, that of a sandwich having zero core flexural stiffnesses and of a corrugated core sandwich, are considered, and curves giving the critical buckling end load per inch are presented. An approximate theory is also given for the bending of sandwich panels under the action of an axial compressive load and a uniform lateral pressure. Curves are presented giving the maximum bending moments in a corrugated core sandwich panel.

1. Introduction

In the design of sandwich skins for aircraft wings, one of the important features is the buckling and bending of panels. The difference between sandwich theory and the normal plate theory is the low transverse shear stiffnesses which can no longer be neglected and must be included in all sandwich calculations. While most of the reports on sandwich construction deal with isotropic cores, this paper deals with an orthotropic core.

The assumption is made that the sandwich behaves essentially as a plate, so that it can be defined by the following physical constants:—

(*i*) the two flexural stiffnesses, D_x and D_y,

(*ii*) the twisting stiffness, D_{xy},

(*iii*) the two transverse shear stiffnesses, D_{Qx} and D_{Qy},

and (*iv*) the two Poisson's ratios, μ_y and μ_x, defined in terms of the curvatures.

The buckling and bending of an orthotropic sandwich panel, with all edges simply-supported will be considered. The mathematical theory is given in the Appendix, while in the main text the steps of the mathematical theory are explained and only the important equations are quoted.

The numbers beside the equations in the main text are those used in the Appendix.

Received November 1954.

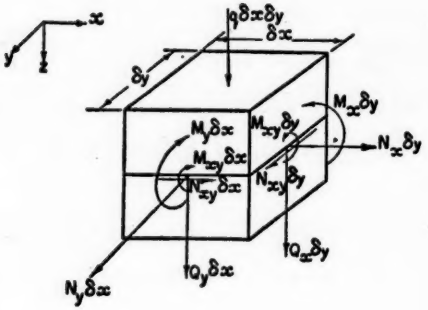

Fig. 1.
Forces and moments acting on differential element $\delta x\ \delta y$.

NOTATION

x, y, z rectangular co-ordinates; z is measured normal to the plane of the panel (*see* Fig. 1)

w deflection of the middle surface of the panel, measured in the z-direction (in.)

q lateral loading (lb./in.^{2})

Q_x internal shear force per unit width, acting in the z-direction in a cross section originally parallel to the yz-plane (lb./in.)

Q_y internal shear force per unit width, acting in the z-direction in a cross section originally parallel to the xz-plane (lb./in.)

M_x internal bending moment per unit width, acting in a cross section originally parallel to the yz-plane and about a line parallel to the y-axis (lb.in./in.)

M_y internal bending moment per unit width, acting in a cross section originally parallel to the xz-plane and about a line parallel to the x-axis (lb.in./in.)

M_{xy} internal twisting moment per unit width, acting in a cross section originally parallel to the yz-plane or xz-plane (lb.in./in.)

N_x internal tensile force per unit width, acting normal to a cross section originally parallel to the yz-plane (lb./in.)

N_y internal tensile force per unit width, acting normal to a cross section originally parallel to the xz-plane (lb./in.)

N_{xy} shear per unit length in the plane of the panel and parallel to the yz-plane and the xz-plane (lb./in.)

D_x, D_y flexural stiffnesses of the panel for bending about the y-axis and x-axis respectively $\left(= \dfrac{\text{bending moment/inch}}{\text{curvature}}\right)$ (lb.in.)

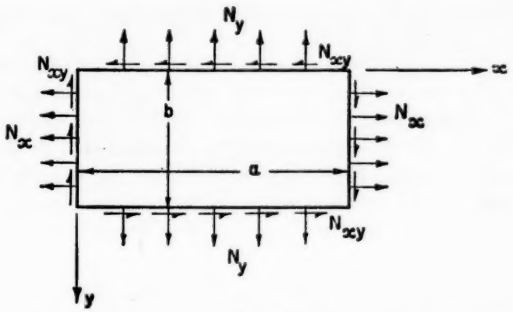

Fig. 2.
Rectangular plate with horizontal forces applied to the boundaries.

D_{xy} twisting stiffness of the panel for twisting about the x-axis and y-axis $\left(= \dfrac{\text{twisting moment/inch}}{\text{twist}} \right)$ (lb. in.)

D_{Qx}, D_{Qy} shear stiffnesses of the panel (lb. in.)

μ_x, μ_y Poisson's ratios for the panel (defined in terms of curvature)

μ Poisson's ratio for the face plates

a, b length and width respectively, of the rectangular panel (in.) (*see* Fig. 2)

m number of half waves in the x-direction

n number of half waves in the y-direction

A_{mn}, B_{mn}, C_{mn}, W_{mn}, q_{mn}, X_{mn}, Y_{mn}, Z_{mn} constants defined by equations (17)-(21) and (42)

$$P_y = \frac{4\pi^2 D_y}{b^2 (1 - \mu_x \mu_y)}$$

$$r = P_y/(4D_{Qy})$$

$$k = D_x/D_y$$

$$\varepsilon = D_{Qx}/D_{Qy}$$

$$\eta = D_{xy}/D_y$$

$$\beta = a/b$$

P_{cr} critical buckling end load per inch of the sandwich panel of infinite length (parallel to Ox), *i.e.* critical value of $-N_x$

α_x, α_y maximum bending moment parameters defined by

$$(M_x)_{max} = \alpha_x q b^2, \quad (M_y)_{max} = \alpha_y q b^2$$

2. Displacement and Equilibrium Equations for the Panel

By using the small deflection theory, including the shear terms, a set of six differential equations can be obtained, three of which express the equilibrium of an infinitesimal plate element and the other three relate the curvatures and twist of the element to the forces and moments acting on the element. A detailed derivation of these equations is given in Ref. 1 and only a brief one is given in the Appendix. These six equations can be reduced to the following three equations by eliminating the bending and twisting moments.

$$\left(D_{xy}+\frac{\mu_y D_x}{1-\mu_x\mu_y}\right)\frac{\partial^3 w}{\partial x\partial y^2}+\frac{D_x}{1-\mu_x\mu_y}\frac{\partial^3 w}{\partial x^3}=\frac{1}{1-\mu_x\mu_y}\frac{D_x}{D_{Qx}}\frac{\partial^2 Q_x}{\partial x^2}+$$
$$+\left\{\frac{1}{2}\frac{D_{xy}}{D_{Qy}}+\frac{\mu_y}{1-\mu_x\mu_y}\frac{D_x}{D_{Qy}}\right\}\frac{\partial^2 Q_y}{\partial x\partial y}+\frac{1}{2}\frac{D_{xy}}{D_{Qx}}\frac{\partial^2 Q_x}{\partial y^2}-Q_x \qquad (8)$$

$$\left(D_{xy}+\frac{\mu_x D_y}{1-\mu_x\mu_y}\right)\frac{\partial^3 w}{\partial x^2\partial y}+\frac{D_y}{1-\mu_x\mu_y}\frac{\partial^3 w}{\partial y^3}=\frac{1}{1-\mu_x\mu_y}\frac{D_y}{D_{Qy}}\frac{\partial^2 Q_y}{\partial y^2}+$$
$$+\left\{\frac{1}{2}\frac{D_{xy}}{D_{Qx}}+\frac{\mu_x}{1-\mu_x\mu_y}\frac{D_y}{D_{Qx}}\right\}\frac{\partial^2 Q_x}{\partial x\partial y}+\frac{1}{2}\frac{D_{xy}}{D_{Qy}}\frac{\partial^2 Q_y}{\partial x^2}-Q_y \quad . \qquad (9)$$

$$\frac{\partial Q_x}{\partial x}+\frac{\partial Q_y}{\partial y}=-\left(q+N_x\frac{\partial^2 w}{\partial x^2}+N_y\frac{\partial^2 w}{\partial y^2}+2N_{xy}\frac{\partial^2 w}{\partial x\partial y}\right). \quad . \qquad (10)$$

The problem now is to obtain a solution of these differential equations which satisfies the appropriate boundary conditions for the problem being considered.

3. Boundary Conditions

The boundary conditions for a simply-supported panel are:—

(*i*) no deflection normal to the plate, *i.e.* parallel to the z-axis,

(*ii*) no bending moments about the lines of support,

(*iii*) no displacement of the face plates along the lines of support.

4. Rectangular Panel Subjected to an End Load per inch, N_x, Parallel to the x-Axis and a Varying Lateral Loading

The first system of external loads to be considered will be an end load per inch, N_x, parallel to the x-axis and a lateral loading q of the form

$$q=q_{mn}\sin\frac{m\pi x}{a}\sin\frac{n\pi y}{b},$$

where m and n are integers.

The solution of the differential equations (8)-(10) for this system of external forces is of the form

$$\left.\begin{aligned} w &= A_{mn} \sin \frac{m\pi x}{a} \sin \frac{n\pi y}{b} \\ Q_x &= B_{mn} \cos \frac{m\pi x}{a} \sin \frac{n\pi y}{b} \\ Q_y &= C_{mn} \sin \frac{m\pi x}{a} \cos \frac{n\pi y}{b} \end{aligned}\right\} \quad . \quad . \quad . \quad . \quad (12)$$

These equations satisfy the boundary conditions for a simply-supported panel, and the constants A_{mn}, B_{mn} and C_{mn} can be obtained by substituting the equations (12) into equations (8)-(10). When these constants are known the deflections, internal forces, and moments of the plate can be obtained.

5. Buckling of an Orthotropic Sandwich Panel for Compression Parallel to *Ox*

The buckling load of the panel can now be obtained from the condition which makes the deflection w infinite. This gives the following expression for N_x in terms of the physical constants of the sandwich, the aspect ratio β of the panel, and the integers m and n.

$$\left(-\frac{4N_x}{P_y}\right)\frac{m^2}{\beta^2}\left[\frac{r^2}{\varepsilon}\left(1-\frac{\mu_x^2}{k}\right)\left\{\frac{\eta k}{2}\frac{m^4}{\beta^4}+\frac{m^2n^2}{\beta^2}\left(k-\eta\mu_x\right)+\frac{1}{2}\eta n^4\right\}+\right.$$

$$\left.+r\left\{\frac{m^2}{\beta^2}\left(\frac{k}{\varepsilon}+\eta\frac{(k-\mu_x^2)}{2k}\right)+n^2\left(1+\frac{\eta(k-\mu_x^2)}{2k\varepsilon}\right)\right\}+1\right]$$

$$=\frac{r(k-\mu_x^2)}{k}\left\{\frac{1}{2}k\eta\frac{m^4}{\beta^4}+\frac{m^2n^2}{\beta^2}\left(k-\eta\mu_x\right)+\frac{1}{2}\eta n^4\right\}\left\{\frac{n^2}{\varepsilon}+\frac{m^2}{\beta^2}\right\}+$$

$$+k\frac{m^4}{\beta^4}+\frac{2m^2n^2}{\beta^2}\frac{\eta(k-\mu_x^2)+k\mu_x}{k}+n^4. \quad . \quad (32)$$

In this equation, m and n are the number of half waves that the sandwich buckles into along and across the panel. The critical form of buckling across the panel will be when $n=1$, but that along the panel will depend on the aspect ratio β. By plotting $-N_x$ against β with various integers for m, the minimum values of $-N_x$ and hence the critical buckling end load per inch can be obtained.

6. Buckling in Compression of a Symmetrical Corrugated Core Sandwich Panel

One type of sandwich in present use is the corrugated core sandwich. Algebraic expressions for the elastic constants for this type of sandwich are given in Ref. 3. It can easily be proved that the shear stiffness along the corrugations is many times that across the corrugations, so that sufficient accuracy is obtained by putting

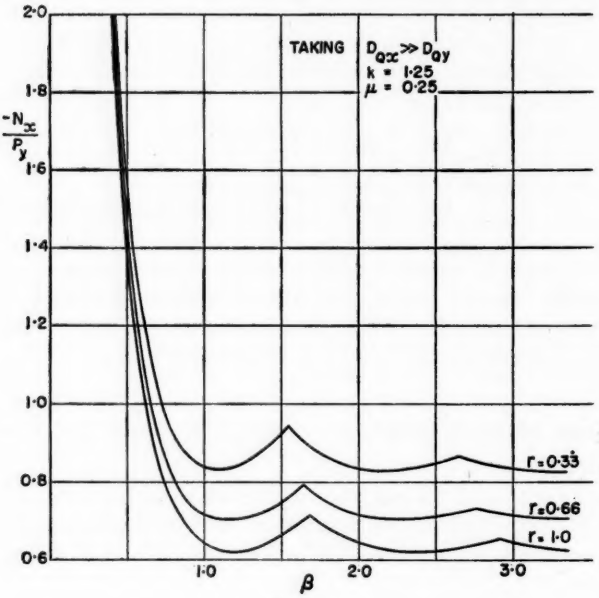

Fig. 3.
Compressive buckling end load per inch of a symmetrical corrugated core sandwich panel (all edges simply-supported).

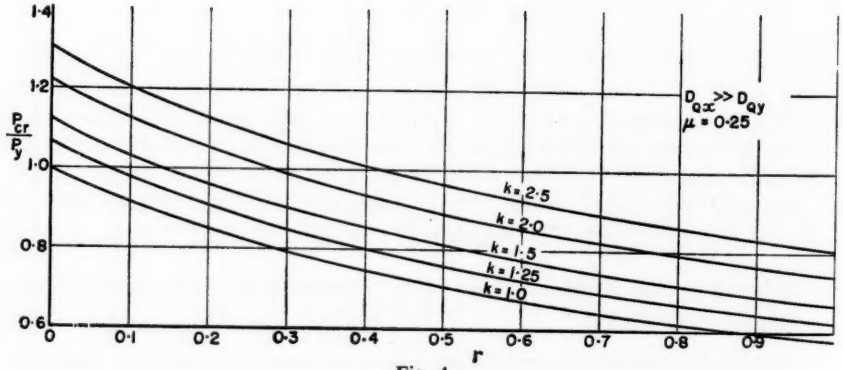

Fig. 4.
Compressive buckling end load per inch of an infinitely long corrugated core sandwich panel (all edges simply-supported).

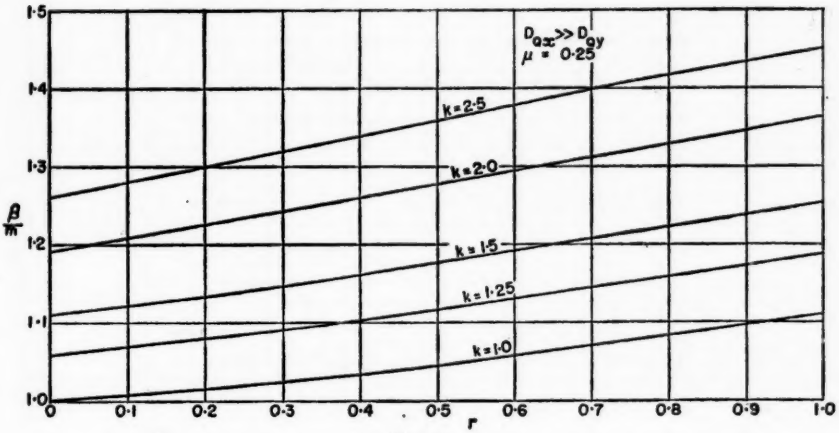

Fig. 5.
Critical value of β/m for an infinitely long corrugated core sandwich panel (all edges simply-supported).

ε equal to infinity. This is justified by Fig. 9. With the substitution, equation (32) then reduces to

$$\frac{-4N_x}{P_y} = \frac{\left[\begin{array}{l} \dfrac{r}{2}\dfrac{(k-\mu^2)}{k(1+\mu)}\left\{ k\,\dfrac{m^4}{\beta^4} + 2\dfrac{m^2}{\beta^2}\left(k+k\mu-\mu\right)+1 \right\} + \\ \quad + \dfrac{\beta^2}{m^2}\left(k\,\dfrac{m^4}{\beta^4} + 2\dfrac{m^2}{\beta^2}\dfrac{k-\mu^2+k\mu+k\mu^2}{k(1+\mu)}+1\right) \end{array}\right]}{1+r\left\{1+\dfrac{m^2}{\beta^2}\dfrac{k-\mu^2}{2k(1+\mu)}\right\}} \quad . \quad (37)$$

Figure 3 gives the buckling parameter $-N_x/P_y$ plotted against the panel aspect ratio β for three values of r, when the longitudinal flexural stiffness is 1·25 times the transverse flexural stiffness, which is representative of a typical corrugated core sandwich. The critical buckling end load per inch, P_{cr}, of an infinitely long panel of width b is obtained by minimising (37) with respect to β/m and is plotted in Fig. 4. The corresponding critical half wavelengths divided by the panel width are plotted in Fig. 5.

7. Buckling in Compression of a Symmetrical Sandwich Panel, Having Zero Core Flexural Stiffnesses

The other type in general use is the honeycomb core sandwich. This comes in the class of sandwiches having zero core flexural stiffnesses, that is the flexural stiffnesses D_x and D_y are equal. For this set of sandwiches equation (32) reduces to

$$-\frac{N_x}{P_y} = \frac{\dfrac{1}{4}\left(\dfrac{m}{\beta}+\dfrac{\beta}{m}\right)^2}{1+r\left[\dfrac{1+\dfrac{1}{\varepsilon}\dfrac{m^2}{\beta^2}+\dfrac{1}{2}\dfrac{r}{\varepsilon}\left(1-\mu\right)\left(1+\dfrac{m^2}{\beta^2}\right)^2}{1+\dfrac{1}{2}r\left(1-\mu\right)\left(\dfrac{1}{\varepsilon}+\dfrac{m^2}{\beta^2}\right)}\right]} \quad . \quad . \quad (38)$$

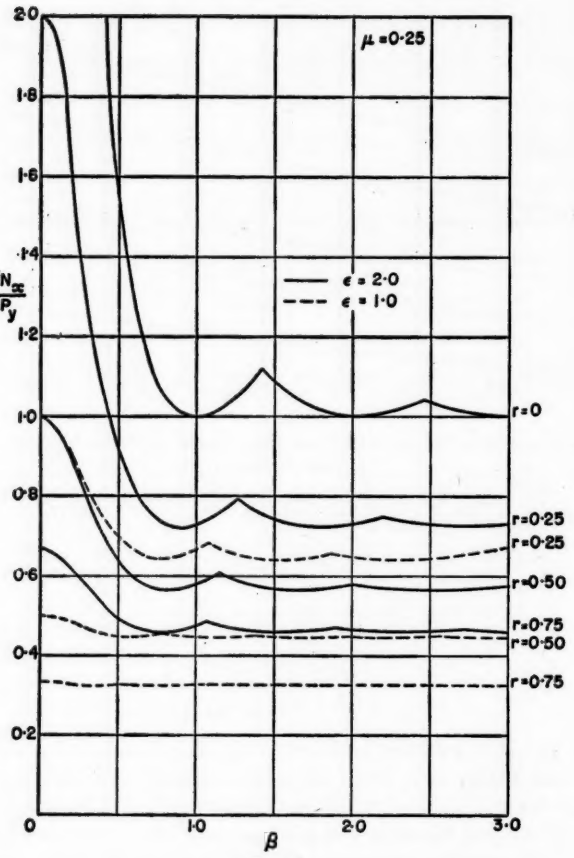

Fig. 6.

Compressive buckling end load per inch of a symmetrical sandwich panel having zero core flexural stiffnesses (all edges simply-supported).

Figure 6 gives the buckling parameter $-N_x/P_y$ plotted against the panel aspect ratio β for various values of r, which depends on the ratio of transverse flexural stiffness to transverse shear stiffness for two values of ε, the ratio of longitudinal to transverse shear stiffnesses. The critical buckling end load per inch, P_{cr}, of an infinitely long panel of width b is obtained by minimising (38) with respect to β/m and is plotted in Fig. 7. The critical value of β/m is plotted against r in Fig. 8. It is possible in minimising the expression for $-N_x$ in equation (38) to obtain negative values for $(\beta/m)^2$. In these cases, the minimum value of $-N_x$ is when β/m equals zero and depends only on the shear stiffnesses of the panel, and is plotted as a dotted line in Fig. 7. The values of P_{cr} corresponding to very small values of β/m are only of academic interest. This corresponds to the case of

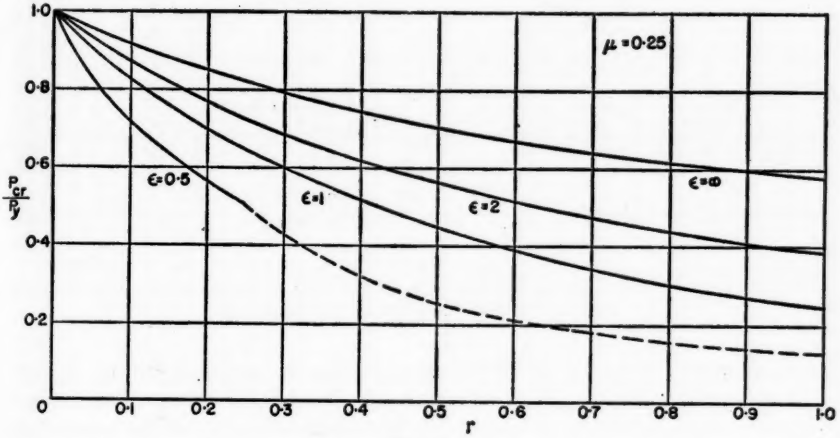

Fig. 7.

Compressive buckling end load per inch of an infintely long symmetrical sandwich panel having zero core flexural stiffnesses (all edges simply-supported).

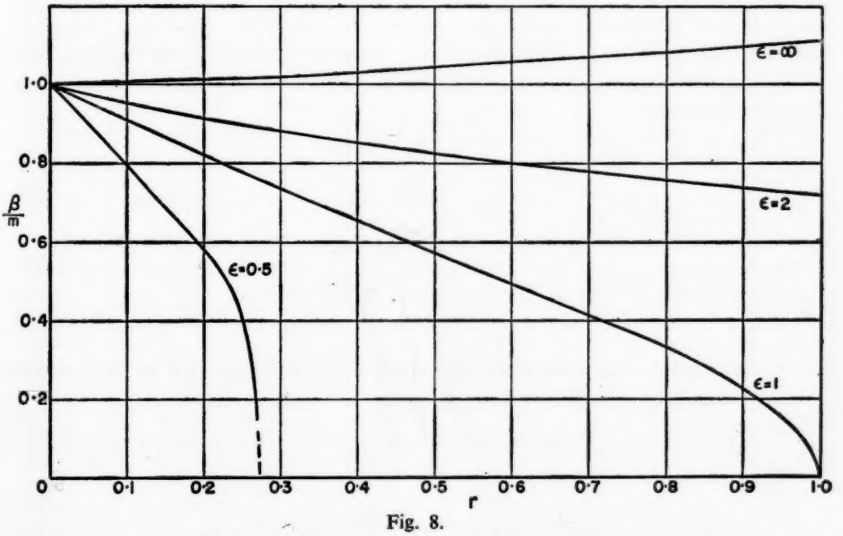

Fig. 8.

Critical value of β/m for an infinitely long symmetrical sandwich panel having zero core flexural stiffnesses (all edges simply-supported).

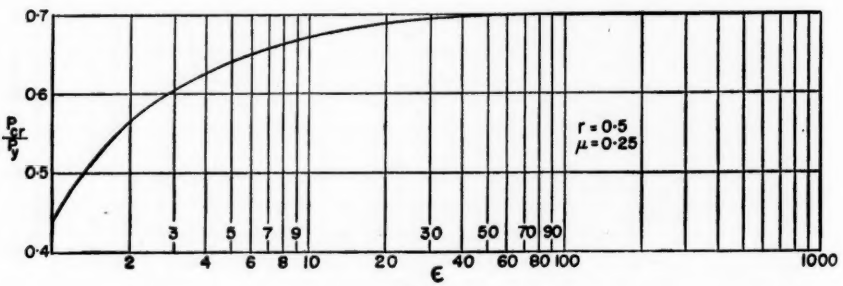

Fig. 9.
Variation of P_{cr}/P_y with ε for an infinitely long symmetrical sandwich panel having zero core flexural stiffnesses (all edges simply-supported).

anti-symmetrical wrinkling and the assumption that the sandwich can be regarded as a plate is no longer valid. For these conditions some of the other physical constants of the sandwich, particularly the modulus of elasticity of the core normal to the face plates and the flexural stiffnesses of the face plates alone, become important, while some of the physical constants used are no longer important. The wrinkling of sandwich panels has already been covered by several authors.

Figure 9 gives the critical buckling end load per inch, P_{cr}, of an infinitely long sandwich panel for a fixed value of r, which depends on the ratio of transverse flexural stiffness to transverse shear stiffness. From this it is seen that the maximum possible increase in P_{cr} by raising the ratio of longitudinal to transverse shear stiffnesses, ε, from 10 to a higher value, is less than five per cent. This fact allowed the simplification, by taking ε equal to infinity, of the calculation of the buckling loads for a symmetrical corrugated core sandwich panel with corrugations running parallel to the applied load.

For an isotropic core

$$P_{cr}=P_y/(1+r)^2. \qquad . \quad . \quad . \quad . \quad . \quad (40)$$

It has been shown in Ref. 5, that the formulae derived by several authors for the critical buckling end load per inch of an infinitely long sandwich panel with simply-supported edges and isotropic core reduce to this expression.

8. Rectangular Panel Subjected to End Load Parallel to the x-axis and Uniform Lateral Loading q

The uniform lateral loading can be represented by the double trigonometrical series

$$q=\sum_{m=1,3,5,\ldots}^{\infty}\ \sum_{n=1,3,5,\ldots}^{\infty} q_{mn}\sin\frac{m\pi x}{a}\sin\frac{n\pi y}{b}$$

where $$q_{mn}=\frac{16}{\pi^2}\frac{q}{mn}. \qquad . \quad . \quad . \quad . \quad . \quad . \quad (41)$$

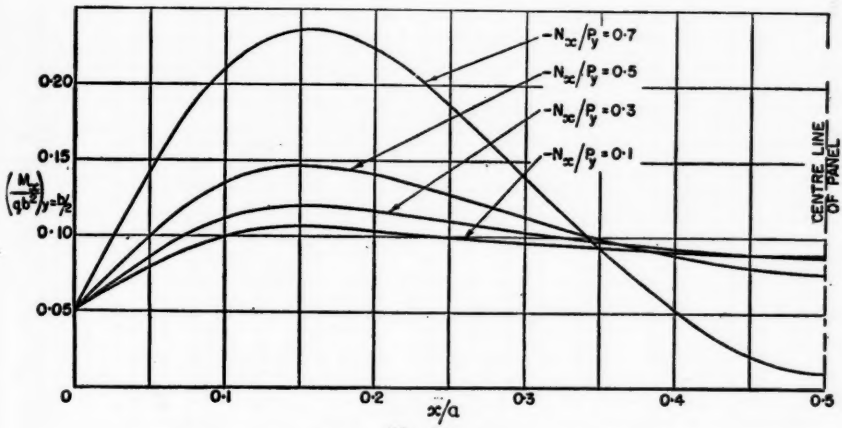

Fig. 10.
Values of $(M_x)_{y=b/2}$ for $k=1{\cdot}25$, $r=0{\cdot}333$, $\beta=3{\cdot}0$, and $\varepsilon=\infty$.

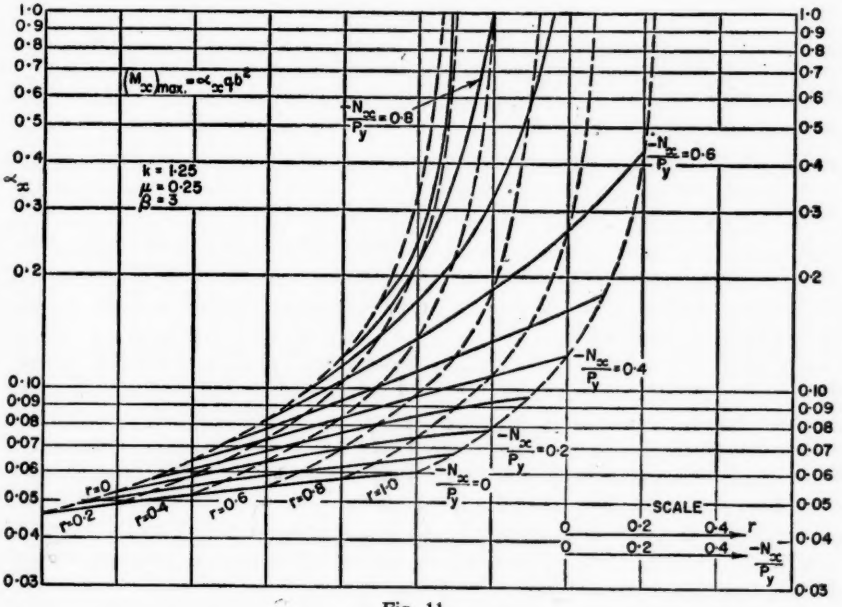

Fig. 11.
Maximum bending moment, $(M_x)_{max}$, in a rectangular corrugated core sandwich panel subjected to end load per inch parallel to the x-axis and a uniform lateral loading q (panel aspect ratio = 3·0).

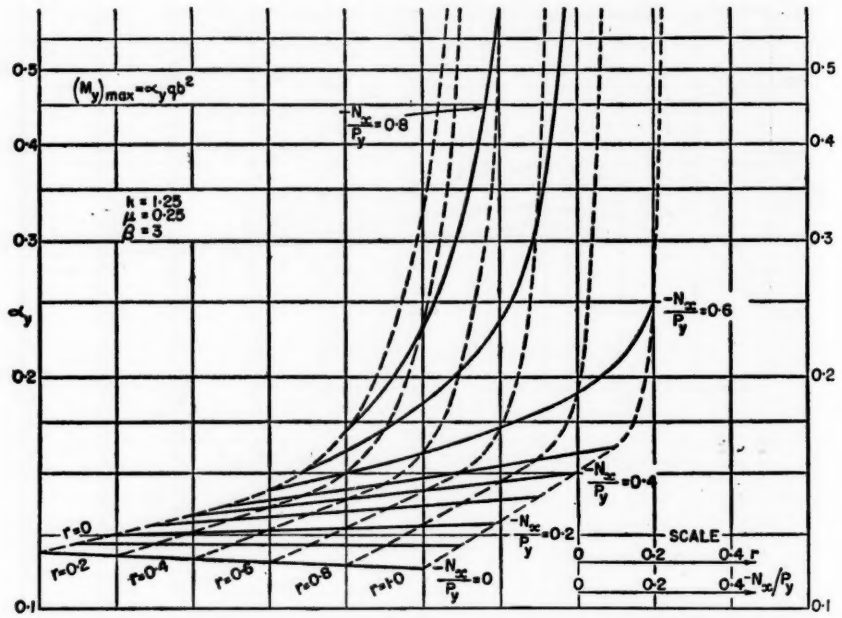

Fig. 12.

Maximum bending moment, $(M_y)_{max}$, in a rectangular corrugated core sandwich panel subjected to end load per inch parallel to the x-axis and a uniform lateral loading q (panel aspect ratio = 3·0).

Expressing the uniform loading in this manner allows the equations for the deflected surface, shear forces and bending moments to be obtained by taking the summation of the corresponding values previously obtained. In the Appendix expressions are derived for the bending moments M_x and M_y (equations (49) and (50) for a corrugated core panel and equations (54) and (55) for a panel having zero core stiffnesses). On the numerical side, only typical examples of the use of this method for corrugated core sandwich panels are given because of the large amount of computing work necessary in deriving each curve. Fig. 10 gives the bending moment about an axis parallel to the y-axis, $(M_x)_{y=b/2}$, at points along the centre line of a typical corrugated core panel of aspect ratio $\beta=3{\cdot}0$, for the case when r, which depends on the ratio of transverse flexural stiffness to transverse shear stiffness, equals $1/3$ and k, the ratio of longitudinal to transverse flexural stiffness equals 1·25, for various values of the end load parameter $-N_x/P_y$. For this case it is seen that the peak bending moment occurs at approximately one-sixth of the length of the panel from either end. The maximum values of the bending moments M_x and M_y can be expressed as

$$(M_x)_{max}=\alpha_x q b^2 \quad . \quad . \quad . \quad . \quad . \quad (52)$$

$$(M_y)_{max}=\alpha_y q b^2 \quad . \quad . \quad . \quad . \quad . \quad (53)$$

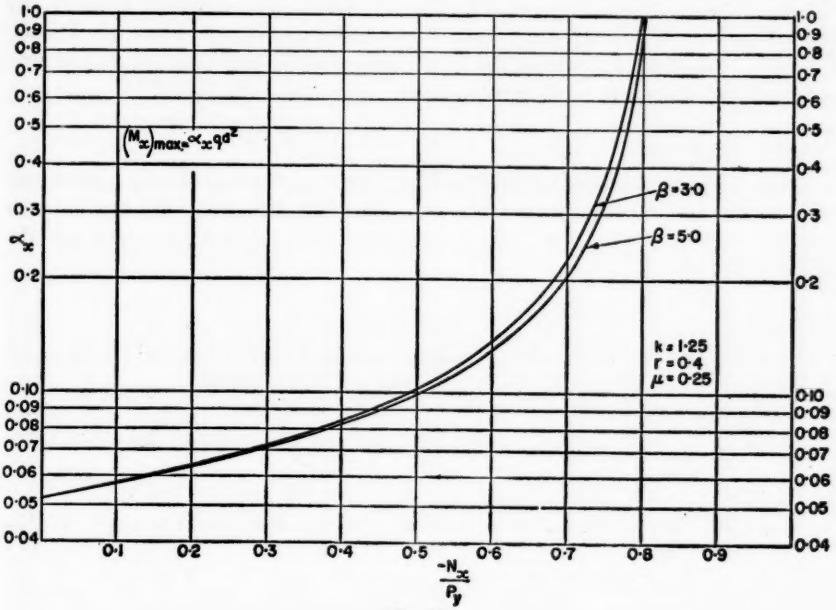

Fig. 13.

Maximum bending moment, $(M_x)_{max}$, in a rectangular corrugated core sandwich panel subjected to end load per inch parallel to the x-axis and a uniform lateral loading q.

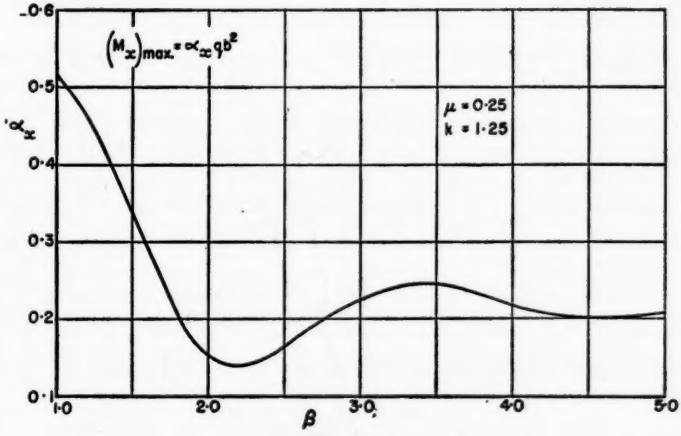

Fig. 14.

Maximum bending moment, $(M_x)_{max}$, in a rectangular corrugated core sandwich panel subjected to end load per inch parallel to the x-axis and a uniform lateral loading q ($r = 0{\cdot}4$, $-N_x/P_y = 0{\cdot}7$).

where α_x and α_y are functions of $-N_x/P_y$, r, k and β. The values of α_x and α_y are plotted in Figs. 11 and 12 for a typical corrugated core panel, where $\beta=3{\cdot}0$ and $k=1{\cdot}25$. The effect of changing the aspect ratio β of the panel on α_x only has been computed because of the work involved, and is shown in Figs. 13 and 14.

ACKNOWLEDGMENTS

The author is indebted to Handley Page Limited for permission to publish this theoretical work. He also thanks Mr. D. E. Lennard, B.Sc.(Eng.) for checking the theoretical work, and the computing section of the firm for their assistance with the numerical work.

REFERENCES

1. LIBOVE, C. and BATDORF, S. B. A General Small-Deflection Theory for Flat Sandwich Plates. N.A.C.A. Report 899 (formerly N.A.C.A. T.N. 1526), 1948.
2. TIMOSHENKO, S. *Theory of Elastic Stability*. McGraw-Hill, 1936.
3. LIBOVE and HUBKA. Elastic Constants for Corrugated Core Sandwich Plates. N.A.C.A. T.N. 2289, 1950.
4. HEMP, W. S. On a Theory of Sandwich Construction. R. & M. 2672, 1952.
5. TYSON, F. Metal Sandwich Construction. Royal Aeronautical Society Section Lecture on 2nd March 1954.

Appendix

Mathematical Theory

1. DISPLACEMENT AND EQUILIBRIUM EQUATIONS FOR THE PANEL

Consider a small element of the panel of length δx and width δy, cut from the unloaded panel by planes parallel to the xz- and the yz-planes. The internal forces which act on this small element are shown in Fig. 1. A detailed derivation of the displacement equations is given in Ref. 1 and only a brief one is given here.

The curvature $\partial^2 w/\partial x^2$ of the panel in the zx-plane is made up of three components:—

(*i*) that due to the bending moment M_x and equal to $-M_x/D_x$.

(*ii*) that due to the bending moment M_y and equal to $+\mu_y M_y/D_y$ (*i.e.* anticlastic curvature).

(*iii*) that due to the variation of the shear force Q_x and equal to $(\partial Q_x/\partial x)/D_{Qx}$.

The differential equation for the curvature $\partial^2 w/\partial x^2$ is obtained by summing these three components, and is

$$\frac{\partial^2 w}{\partial x^2} = -\frac{M_x}{D_x} + \mu_y \frac{M_y}{D_y} + \frac{1}{D_{Qx}} \frac{\partial Q_x}{\partial x} \quad . \quad . \quad . \quad (1)$$

Similarly the differential equation for the curvature $\partial^2 w/\partial y^2$ is

$$\frac{\partial^2 w}{\partial y^2} = +\mu_x \frac{M_x}{D_x} - \frac{M_y}{D_y} + \frac{1}{D_{Qy}} \frac{\partial Q_y}{\partial y} \quad . \quad . \quad . \quad . \quad . \quad (2)$$

The twist, $\partial^2 w/\partial x \partial y$, of the panel is also made up of three components:—

(*i*) that due to the twisting moment, M_{xy}, and equal to M_{xy}/D_{xy}.

(*ii*) that due to the variation of the shear force, Q_x, and equal to

$$\frac{1}{2}\frac{1}{D_{Qx}}\frac{\partial Q_x}{\partial y}$$

(*iii*) that due to the variation of the shear force, Q_y, and equal to

$$\frac{1}{2}\frac{1}{D_{Qy}}\frac{\partial Q_y}{\partial x}.$$

The differential equation of the curvature $\partial^2 w/\partial x\partial y$ is obtained by summing these three components and is

$$\frac{\partial^2 w}{\partial x\partial y}=\frac{M_{xy}}{D_{xy}}+\frac{1}{2}\frac{1}{D_{Qx}}\frac{\partial Q_x}{\partial y}+\frac{1}{2}\frac{1}{D_{Qy}}\frac{\partial Q_y}{\partial x} \quad . \quad . \quad . \quad . \quad (3)$$

The next step is to obtain the equilibrium equations. It will be assumed that the middle-plane stresses are constant throughout the panel. The equation for equilibrium of vertical forces is given at the top of page 305 of Ref. 2 as

$$\frac{\partial^2 M_x}{\partial x^2}-2\frac{\partial^2 M_{xy}}{\partial x\partial y}+\frac{\partial^2 M_y}{\partial y^2}=-\left(q+N_x\frac{\partial^2 w}{\partial x^2}+N_y\frac{\partial^2 w}{\partial y^2}+2N_{xy}\frac{\partial^2 w}{\partial x\partial y}\right) . \quad (4)$$

The equation for equilibrium of moments about the y- and x-axes is obtained from equations (188) and (189) of Ref. 2 as

$$Q_x=-\frac{\partial M_{xy}}{\partial y}+\frac{\partial M_x}{\partial x} \quad . \quad . \quad . \quad . \quad . \quad . \quad . \quad (5)$$

$$Q_y=-\frac{\partial M_{xy}}{\partial x}+\frac{\partial M_y}{\partial y} \quad . \quad . \quad . \quad . \quad . \quad . \quad . \quad (6)$$

These six equations (1)-(6) will be reduced to 3 equations by eliminating M_x, M_y and M_{xy}.

Eliminating M_y between (1) and (2) gives

$$\frac{\partial^2 w}{\partial x^2}+\mu_y\frac{\partial^2 w}{\partial y^2}=-(1-\mu_x\mu_y)\frac{M_x}{D_x}+\frac{1}{D_{Qx}}\frac{\partial Q_x}{\partial x}+\mu_y\frac{1}{D_{Qy}}\frac{\partial Q_y}{\partial y} \quad . \quad . \quad (7)$$

Substituting (3) and (7) in (5) gives

$$Q_x=-D_{xy}\frac{\partial^3 w}{\partial x\partial y^2}+\frac{1}{2}\frac{D_{xy}}{D_{Qx}}\frac{\partial^2 Q_x}{\partial y^2}+\frac{1}{2}\frac{D_{xy}}{D_{Qy}}\frac{\partial^2 Q_y}{\partial x\partial y}-\frac{D_x}{1-\mu_x\mu_y}\frac{\partial}{\partial x}\left(\frac{\partial^2 w}{\partial x^2}+\mu_y\frac{\partial^2 w}{\partial y^2}\right)+$$
$$+\frac{D_x}{1-\mu_x\mu_y}\left(\frac{1}{D_{Qx}}\frac{\partial^2 Q_x}{\partial x^2}+\mu_y\frac{1}{D_{Qy}}\frac{\partial^2 Q_y}{\partial x\partial y}\right)$$

i.e. $$\left(D_{xy}+\frac{\mu_y D_x}{1-\mu_x\mu_y}\right)\frac{\partial^3 w}{\partial x\partial y^2}+\frac{D_x}{1-\mu_x\mu_y}\frac{\partial^3 w}{\partial x^3}=\frac{1}{1-\mu_x\mu_y}\frac{D_x}{D_{Qx}}\frac{\partial^2 Q_x}{\partial x^2}+$$
$$+\left\{\frac{1}{2}\frac{D_{xy}}{D_{Qy}}+\frac{\mu_y}{1-\mu_x\mu_y}\frac{D_x}{D_{Qy}}\right\}\frac{\partial^2 Q_y}{\partial x\partial y}+\frac{1}{2}\frac{D_{xy}}{D_{Qx}}\frac{\partial^2 Q_x}{\partial y^2}-Q_x \quad . \quad (8)$$

Similarly, from (1), (2), (3) and (6),

$$\left(D_{xy}+\frac{\mu_x D_y}{1-\mu_x\mu_y}\right)\frac{\partial^3 w}{\partial x^2\partial y}+\frac{D_y}{1-\mu_x\mu_y}\frac{\partial^3 w}{\partial y^3}=\frac{1}{1-\mu_x\mu_y}\frac{D_y}{D_{Qy}}\frac{\partial^2 Q_y}{\partial y^2}+$$
$$+\left\{\frac{1}{2}\frac{D_{xy}}{D_{Qx}}+\frac{\mu_x}{1-\mu_x\mu_y}\frac{D_y}{D_{Qx}}\right\}\frac{\partial^2 Q_x}{\partial x\partial y}+\frac{1}{2}\frac{D_{xy}}{D_{Qy}}\frac{\partial^2 Q_y}{\partial x^2}-Q_y \quad . \quad (9)$$

and from (4), (5) and (6),

$$\frac{\partial Q_x}{\partial x}+\frac{\partial Q_y}{\partial y}=-\left(q+N_x\frac{\partial^2 w}{\partial x^2}+N_y\frac{\partial^2 w}{\partial y^2}+2N_{xy}\frac{\partial^2 w}{\partial x\partial y}\right) \quad . \quad . \quad (10)$$

By assuming general values for the middle-surface deflection w and the shear forces Q_x and Q_y which satisfy equations (8), (9), (10) and the relevant boundary conditions, it is possible to solve a number of bending and buckling problems of sandwich panels.

2. Boundary Conditions

The boundary conditions for a simply-supported edge parallel to the y-axis are

(*i*) no deflection parallel to the z-axis, *i.e.* $w=0$.

(*ii*) no bending moment about a y-axis, *i.e.* $M_x=0$.

(*iii*) *either* there is no y-displacement of points in the boundary, so that the shear angle $Q_y/D_{Qy}=0$; or the only support is applied to the middle surface of the boundary when $M_{xy}=0$.

The edge supports for sandwich panels are usually such that there is no displacement of the face plates along the line of support. Hence the boundary conditions for the rectangular panel shown in Fig. 2 are

(*i*) for the sides $x=0$ and $x=a$,

$$\left.\begin{aligned} w&=0\\ M_x&=0\\ Q_y/D_{Qy}&=0 \end{aligned}\right\} \quad . \quad . \quad . \quad . \quad . \quad . \quad . \quad (12)$$

(*ii*) for the sides $y=0$ and $y=b$,

$$\left.\begin{aligned} w&=0\\ M_y&=0\\ Q_x/D_{Qx}&=0 \end{aligned}\right\} \quad . \quad . \quad . \quad . \quad . \quad . \quad . \quad (11)$$

3. Rectangular Panel Subjected to an End Load per inch N_x Parallel to the x-axis and a Lateral Loading of the Form $q=q_{mn}\sin\frac{m\pi x}{a}\sin\frac{n\pi y}{b}$

The assumption will be made that the solution for the middle-surface deflection w and the shear angles Q_x/D_{Qx} and Q_y/D_{Qy} exists in the form

$$\left.\begin{aligned} w&=A_{mn}\sin\frac{m\pi x}{a}\sin\frac{n\pi y}{b}\\ Q_x&=B_{mn}\cos\frac{m\pi x}{a}\sin\frac{n\pi y}{b}\\ Q_y&=C_{mn}\sin\frac{m\pi x}{a}\cos\frac{n\pi y}{b} \end{aligned}\right\} \quad . \quad . \quad . \quad . \quad . \quad . \quad (13)$$

These satisfy the boundary conditions (11) and (12).

Substituting (13) in (8), (9) and (10) gives

$$A_{mn}\left\{\frac{mn^2\pi^3}{ab^2}\left(D_{xy}+\frac{\mu_y D_x}{1-\mu_x\mu_y}\right)+\frac{m^3\pi^3}{a^3}\frac{D_x}{1-\mu_x\mu_y}\right\}+$$
$$+B_{mn}\left\{-\frac{m^2\pi^2}{a^2}\frac{D_x}{1-\mu_x\mu_y}\frac{1}{D_{Qx}}-\frac{1}{2}\frac{n^2\pi^2}{b^2}\frac{D_{xy}}{D_{Qx}}-1\right\}-$$
$$-C_{mn}\left\{\frac{mn\pi^2}{ab}\left(\frac{1}{2}\frac{D_{xy}}{D_{Qy}}+\frac{\mu_y}{1-\mu_x\mu_y}\frac{D_x}{D_{Qy}}\right)\right\}=0 \quad . \quad (14)$$

$$A_{mn}\left\{+\frac{m^2n\pi^3}{a^2b}\left(D_{xy}+\frac{\mu_x D_y}{1-\mu_x\mu_y}\right)+\frac{n^3\pi^3}{b^3}\frac{D_y}{1-\mu_x\mu_y}\right\}+$$
$$+B_{mn}\left\{-\frac{mn\pi^2}{ab}\left(\frac{1}{2}\frac{D_{xy}}{D_{Qx}}+\frac{\mu_x}{1-\mu_x\mu_y}\frac{D_y}{D_{Qx}}\right)\right\}+$$
$$+C_{mn}\left\{-\frac{n^2\pi^2}{b^2}\frac{1}{1-\mu_x\mu_y}\frac{D_y}{D_{Qy}}-\frac{1}{2}\frac{m^2\pi^2}{a^2}\frac{D_{xy}}{D_{Qy}}-1\right\}=0 \quad (15)$$

$$A_{mn}\left\{N_x\frac{m^2\pi^2}{a^2}\right\}+B_{mn}\left\{\frac{m\pi}{a}\right\}+C_{mn}\left\{\frac{n\pi}{b}\right\}-q_{mn}=0 \quad . \quad (16)$$

Solving equations (14), (15) and (16) for A_{mn}, B_{mn} and C_{mn} gives

$$\frac{A_{mn}}{W_{mn}}=\frac{-B_{mn}}{X_{mn}}=\frac{C_{mn}}{Y_{mn}}=\frac{-q_{mn}}{Z_{mn}}, \quad . \quad . \quad . \quad (17)$$

where

$$W_{mn}=-\frac{1}{D_{Qx}D_{Qy}}\left[\frac{1}{2}\pi^4 D_{xy}\left(\frac{m^4}{a^4}\frac{D_x}{1-\mu_x\mu_y}-\frac{m^2n^2}{a^2b^2}\frac{(\mu_x D_y+\mu_y D_x)}{1-\mu_x\mu_y}+\right.\right.$$
$$\left.+\frac{n^4}{b^4}\frac{D_y}{1-\mu_x\mu_y}\right)+\frac{m^2n^2\pi^4}{a^2b^2}\frac{D_xD_y}{(1-\mu_x\mu_y)}\Big]-$$
$$-\pi^2\left[\frac{m^2}{a^2}\frac{1}{1-\mu_x\mu_y}\frac{D_x}{D_{Qx}}+\frac{n^2}{b^2}\frac{1}{1-\mu_x\mu_y}\frac{D_y}{D_{Qy}}\right]-\frac{1}{2}\pi^2 D_{xy}\left[\frac{m^2}{a^2}\frac{1}{D_{Qy}}+\frac{n^2}{b^2}\frac{1}{D_{Qx}}\right]-1 \quad (18)$$

$$X_{mn}D_{Qy}=\frac{1}{2}\frac{m^5}{a^5}\pi^5\frac{D_xD_{xy}}{1-\mu_x\mu_y}+\frac{m^3n^2}{a^3b^2}\pi^5\left[\frac{D_xD_y}{1-\mu_x\mu_y}-\frac{1}{2}D_{xy}\frac{(\mu_xD_y+\mu_yD_x)}{1-\mu_x\mu_y}\right]+$$
$$+\frac{1}{2}\frac{mn^4}{ab^4}\pi^5\frac{D_xD_{xy}}{1-\mu_x\mu_y}+\frac{mn^2}{ab^2}\pi^3 D_{xy}D_{Qy}+\frac{m\pi^3}{a}D_{Qy}\left(\frac{m^2}{a^2}\frac{D_x}{1-\mu_x\mu_y}+\frac{n^2}{b^2}\frac{\mu_yD_x}{1-\mu_x\mu_y}\right) \quad (19)$$

$$Y_{mn}D_{Qx}=-\frac{1}{2}\frac{n^5}{b^5}\pi^5\frac{D_yD_{xy}}{1-\mu_x\mu_y}-\frac{m^2n^3}{a^2b^3}\pi^5\left[\frac{D_xD_y}{1-\mu_x\mu_y}-\frac{1}{2}D_{xy}\frac{(\mu_xD_y+\mu_yD_x)}{1-\mu_x\mu_y}\right]-$$
$$-\frac{1}{2}\frac{m^4n}{a^4b}\pi^5\frac{D_xD_{xy}}{1-\mu_x\mu_y}-\frac{m^2n}{a^2b}\pi^3D_{xy}D_{Qx}-\frac{n\pi^3}{b}D_{Qx}\left(\frac{n^2}{b^2}\frac{D_y}{1-\mu_x\mu_y}+\frac{m^2}{a^2}\frac{\mu_xD_y}{1-\mu_x\mu_y}\right) \quad (20)$$

$$Z_{mn}=-N_x\frac{m^2\pi^2}{a^2}(+W_{mn})+\frac{m\pi}{a}X_{mn}-\frac{n\pi}{b}Y_{mn} \quad . \quad . \quad (21)$$

Hence the equations for the deflected surface and the shear forces are

$$\left.\begin{aligned} w &= -\frac{W_{mn}}{Z_{mn}} q_{mn} \sin\frac{m\pi x}{a} \sin\frac{n\pi y}{b} \\ Q_x &= \frac{X_{mn}}{Z_{mn}} q_{mn} \cos\frac{m\pi x}{a} \sin\frac{n\pi y}{b} \\ Q_y &= -\frac{Y_{mn}}{Z_{mn}} q_{mn} \sin\frac{m\pi x}{a} \cos\frac{n\pi y}{b} \end{aligned}\right\} \quad . \quad . \quad . \quad . \quad . \quad (22)$$

The bending moment M_x is, from (7),

$$M_x = -\frac{D_x}{1-\mu_x\mu_y}\left[\frac{\partial}{\partial x}\left(\frac{\partial w}{\partial x} - \frac{Q_x}{D_{Qx}}\right) + \mu_y \frac{\partial}{\partial y}\left(\frac{\partial w}{\partial y} - \frac{Q_y}{D_{Qy}}\right)\right] \quad . \quad (23)$$

Substituting (22) in (23) gives

$$M_x = -\frac{D_x}{1-\mu_x\mu_y}\left[+W_{mn}\frac{m^2\pi^2}{a^2} + X_{mn}\frac{m\pi}{a}\frac{1}{D_{Qx}} + \mu_y W_{mn}\frac{n^2\pi^2}{b^2} - \mu_y Y_{mn}\frac{n\pi}{bD_{Qy}}\right] \times$$

$$\times \frac{q_{mn}}{Z_{mn}} \sin\frac{m\pi x}{a} \sin\frac{n\pi y}{b}$$

$$i.e.\ M_x = -\frac{D_x}{1-\mu_x\mu_y}\left[W_{mn}\pi^2\left(\frac{m^2}{a^2} + \mu_y\frac{n^2}{b^2}\right) + \pi\left(\frac{m}{a}\frac{X_{mn}}{D_{Qx}} - \mu_y\frac{n}{b}\frac{Y_{mn}}{D_{Qy}}\right)\right] \times$$

$$\times \frac{q_{mn}}{Z_{mn}} \sin\frac{m\pi x}{a} \sin\frac{n\pi y}{b} \quad . \quad . \quad (24)$$

Similarly

$$M_y = -\frac{D_y}{1-\mu_x\mu_y}\left[W_{mn}\pi^2\left(\frac{n^2}{b^2} + \mu_x\frac{m^2}{a^2}\right) + \pi\left(-\frac{n}{b}\frac{Y_{mn}}{D_{Qy}} + \mu_x\frac{m}{a}\frac{X_{mn}}{D_{Qx}}\right)\right] \times$$

$$\times \frac{q_{mn}}{Z_{mn}} \sin\frac{m\pi x}{a} \sin\frac{n\pi y}{b} \quad . \quad . \quad (25)$$

The expressions for W_{mn}, X_{mn}, Y_{mn} and Z_{mn} are simplified by the following substitutions:—

$$\left.\begin{aligned} P_y &= \frac{4\pi^2 D_y}{b^2(1-\mu_x\mu_y)} \\ r &= P_y/4D_{Qy} \\ k &= D_x/D_y \\ \varepsilon &= D_{Qx}/D_{Qy} \\ \eta &= D_{xy}/D_y \\ \beta &= a/b \end{aligned}\right\} \quad . \quad . \quad . \quad . \quad . \quad . \quad . \quad (26)$$

Also from the generalisation of Maxwell's reciprocal law

$$\mu_x D_y = \mu_y D_x \quad . \quad . \quad . \quad . \quad . \quad . \quad . \quad (27)$$

Substituting (26) and (27) in (18), (19) and (20) gives

$$W_{mn} = -\frac{r^2}{\varepsilon}\left(1-\frac{\mu_x^2}{k}\right)\left[\frac{\eta}{2}k\frac{m^4}{\beta^4}+\frac{m^2n^2}{\beta^2}(k-\eta\mu_x)+\frac{\eta}{2}n^4\right]-$$

$$-r\left[\frac{m^2}{\beta^2}\left(\frac{k}{\varepsilon}+\frac{\eta(k-\mu_x^2)}{2k}\right)+n^2\left(1+\frac{\eta(k-\mu_x^2)}{2k\varepsilon}\right)\right]-1 \quad . \quad (28)$$

$$X_{mn} = \frac{1}{4}P_y r\frac{\pi m}{b\beta}\frac{k-\mu_x^2}{k}\left[\frac{1}{2}k\eta\frac{m^4}{\beta^4}+\frac{m^2n^2}{\beta^2}(k-\eta\mu_x)+\frac{1}{2}\eta n^4\right]+$$

$$+\frac{1}{4}P_y\frac{\pi m}{b\beta}\left[k\frac{m^2}{\beta^2}+n^2\left(\frac{\eta(k-\mu_x^2)+k\mu_x}{k}\right)\right] \quad . \quad (29)$$

$$Y_{mn} = -\frac{1}{4}P_y\frac{r}{\varepsilon}\frac{\pi n}{b}\frac{k-\mu_x^2}{k}\left[\frac{1}{2}k\eta\frac{m^4}{\beta^4}+\frac{m^2n^2}{\beta^2}(k-\eta\mu_x)+\frac{1}{2}\eta n^4\right]-$$

$$-\frac{1}{4}P_y\frac{\pi n}{b}\left[\frac{m^2}{\beta^2}\frac{\eta(k-\mu_x^2)+k\mu_x}{k}+n^2\right] \quad . \quad (30)$$

Hence the deflected shape, shear forces, and bending moments can be obtained by substituting equations (28)-(30) in equations (22), (24), and (25).

4. Buckling of an Orthotropic Sandwich Panel for Compression Parallel to Ox

The end load per inch, $-N_x$, which will cause the panel to buckle can be obtained by putting the denominator of the expression for w (equation (22)) equal to zero.

i.e.
$$-N_x\left(\frac{m^2\pi^2}{a^2}W_{mn}\right)=\pi\left(\frac{n}{b}Y_{mn}-\frac{m}{a}X_{mn}\right) \quad . \quad . \quad . \quad . \quad (31)$$

Substituting (28), (29) and (30) in (31) gives

$$-N_x\frac{m^2}{\beta^2}\left[\frac{r^2}{\varepsilon}\left(1-\frac{\mu_x^2}{k}\right)\left\{\frac{\eta k}{2}\frac{m^4}{\beta^4}+\frac{m^2n^2}{\beta^2}(k-\eta\mu_x)+\frac{1}{2}\eta n^4\right\}+r\left\{\frac{m^2}{\beta^2}\left(\frac{k}{\varepsilon}+\frac{\eta(k-\mu_x^2)}{2k}\right)+\right.\right.$$

$$\left.\left.+n^2\left(1+\frac{\eta(k-\mu_x^2)}{2k\varepsilon}\right)\right\}+1\right]$$

$$=\frac{r(k-\mu_x^2)}{4k}P_y\left\{\frac{1}{2}k\eta\frac{m^4}{\beta^4}+\frac{m^2n^2}{\beta^2}(k-\eta\mu_x)+\frac{1}{2}\eta n^4\right\}\left\{\frac{n^2}{\varepsilon}+\frac{m^2}{\beta^2}\right\}+$$

$$+\frac{1}{4}P_y\left\{k\frac{m^4}{\beta^4}+\frac{2m^2n^2}{\beta^2}\frac{\eta(k-\mu_x^2)+k\mu_x}{k}+n^4\right\} \quad . \quad (32)$$

The minimum value of $-N_x$ given in (32) is now required. The critical form of buckling in the y-direction will be when $n=1$.

This reduces (32) to

$$-\left(\frac{4N_x}{P_y}\right)\frac{m^2}{\beta^2}\left[\frac{r^2}{\varepsilon}\left(1-\frac{\mu_x^2}{k}\right)\left\{\frac{\eta k}{2}\frac{m^4}{\beta^4}+\frac{m^2}{\beta^2}(k-\eta\mu_x)+\frac{\eta}{2}\right\}+\right.$$
$$\left.+r\left\{\frac{m^2}{\beta^2}\left(\frac{k}{\varepsilon}+\frac{\eta(k-\mu_x^2)}{2k}\right)+\left(1+\frac{\eta(k-\mu_x^2)}{2k\varepsilon}\right)\right\}+1\right]$$
$$=\frac{r(k-\mu_x^2)}{k}\left\{\frac{1}{2}k\eta\frac{m^4}{\beta^4}+\frac{m^2}{\beta^2}(k-\eta\mu_x)+\frac{1}{2}\eta\right\}\left\{\frac{m^2}{\beta^2}+\frac{1}{\varepsilon}\right\}+$$
$$+k\frac{m^4}{\beta^4}+2\frac{m^2}{\beta^2}\frac{\eta(k-\mu_x^2)+k\mu_x}{k}+1 \quad . \quad . \quad (33)$$

By plotting $-N_x$ against β with various integers for m, the critical buckling value of $-N_x$ of the panel is obtained.

5. Buckling in Compression of a Symmetrical Corrugated Core Sandwich Panel

For a symmetrical corrugated core sandwich panel with the corrugations running parallel to Ox, the following substitution can be made in (33):—

$$\left.\begin{aligned}\mu_x&=\mu\\ D_{xy}&=D_y/(1+\mu)\end{aligned}\right\} \quad . \quad . \quad . \quad . \quad . \quad . \quad (34)$$

For other details of the Elastic Constants for a corrugated core sandwich *see* Ref. 3.

From (26) and (34),
$$\eta=\frac{1}{1+\mu} \quad . \quad . \quad . \quad . \quad . \quad . \quad (35)$$

Substituting (34) and (35) in (33) gives

$$-\frac{4N_x}{P_y}=\frac{\left[\begin{aligned}&\frac{r(k-\mu^2)}{2k(1+\mu)}\left\{1+\frac{\beta^2}{m^2\varepsilon}\right\}\left\{k\frac{m^4}{\beta^4}+\frac{2m^2}{\beta^2}(k+k\mu-\mu)+1\right\}+\\&+\frac{\beta^2}{m^2}\left(k\frac{m^4}{\beta^4}+\frac{2m^2}{\beta^2}\frac{k-\mu^2+k\mu+k\mu^2}{k(1+\mu)}+1\right)\end{aligned}\right]}{\left[\begin{aligned}&\frac{1}{2}\frac{r^2}{\varepsilon}\left(\frac{k-\mu^2}{k(1+\mu)}\right)\left\{k\frac{m^4}{\beta^4}+\frac{2m^2}{\beta^2}(k+k\mu-\mu)+1\right\}+\\&+r\left\{\frac{m^2}{\beta^2}\left(\frac{k}{\varepsilon}+\frac{k-\mu^2}{2k(1+\mu)}\right)+\left(1+\frac{k-\mu^2}{2k\varepsilon(1+\mu)}\right)\right\}+1\end{aligned}\right]} \quad . \quad (36)$$

Normally for a corrugated core sandwich D_{Qx} is many times greater than D_{Qy} and sufficient accuracy is obtained by putting ε equal to infinity. This is justified by Fig. 9. With this substitution equation (36) reduces to

$$-\frac{4N_x}{P_y}=\frac{\left[\begin{aligned}&\frac{r}{2}\frac{(k-\mu^2)}{k(1+\mu)}\left\{k\frac{m^4}{\beta^4}+\frac{2m^2}{\beta^2}(k+k\mu-\mu)+1\right\}+\\&+\frac{\beta^2}{m^2}\left(k\frac{m^4}{\beta^4}+\frac{2m^2}{\beta^2}\frac{k-\mu^2+k\mu+k\mu^2}{k(1+\mu)}+1\right)\end{aligned}\right]}{1+r\left\{1+\frac{m^2}{\beta^2}\frac{k-\mu^2}{2k(1+\mu)}\right\}} \quad . \quad (37)$$

The buckling parameter $-N_x/P_y$ is plotted against β in Fig. 3 for the case where $k=1{\cdot}25$ and $\mu=0{\cdot}25$.

The buckling end load per inch P_{cr}, of an infinitely long panel of width b is obtained by minimising (37) with respect to β/m. P_{cr} is plotted in Fig. 4, taking $\mu=0{\cdot}25$. The corresponding critical half wavelengths divided by the panel width (*i.e.* β/m) are plotted in Fig. 5.

6. Buckling in Compression of a Symmetrical Sandwich Panel having Zero Core Flexural Stiffnesses

For a symmetrical sandwich panel having equal flexural stiffnesses, $k=1{\cdot}0$, and the substitutions defined by equations (34) still hold. These reduce equation (33) to

$$-\frac{N_x}{P_y}=\frac{\frac{1}{4}\left(\frac{m}{\beta}+\frac{\beta}{m}\right)^2}{1+r\left\{\frac{1+\frac{1}{\varepsilon}\frac{m^2}{\beta^2}+\frac{1}{2}\frac{r}{\varepsilon}(1-\mu)\left(1+\frac{m^2}{\beta^2}\right)^2}{1+\frac{1}{2}r(1-\mu)\left(\frac{1}{\varepsilon}+\frac{m^2}{\beta^2}\right)}\right\}} \quad . \quad . \quad (38)$$

The buckling parameter, $-N_x/P_y$, is plotted against β for two values of ε in Fig. 6. P_{cr} for an infinitely long panel of width b is obtained by minimising (38) with respect to β/m and is plotted in Fig. 7, taking $\mu=0{\cdot}25$. The critical value of β/m is plotted against r in Fig. 8. It is possible in minimising the expression for $-N_x$ in equation (38) to obtain negative values for $(\beta/m)^2$. In these cases, β/m is taken as zero to obtain the critical values of P_{cr}, which will depend only on the shear stiffnesses of the panel.

To show the effect of the ratio of the shear stiffnesses, ε, on P_{cr}, a curve has been drawn in Fig. 9 for the case $r=0{\cdot}5$. From this curve it is seen that in increasing ε from 10 to infinity there is less than five per cent. change in the critical buckling end load per inch. This was the justification for taking ε equal to infinity for the corrugated core sandwich panel.

The buckling end load per inch for an isotropic core is obtained by putting $\varepsilon=1{\cdot}0$ in equation (38) which gives

$$-\frac{N_x}{P_y}=\frac{\frac{1}{4}\left(\frac{m}{\beta}+\frac{\beta}{m}\right)^2}{1+r\left(1+\frac{m^2}{\beta^2}\right)} \quad . \quad . \quad . \quad . \quad . \quad . \quad (39)$$

For an infinitely long panel P_{cr} is obtained by minimising (39) with respect to β/m and is given by

$$\frac{P_{cr}}{P_y}=\frac{1}{(1+r)^2} \quad . \quad . \quad . \quad . \quad . \quad . \quad . \quad (40)$$

This formula is similar to that derived by several authors for the critical buckling end load per inch of a simply-supported sandwich panel, with an isotropic core (for example, *see* Ref. 4).

7. Rectangular Panel Subjected to End Load Parallel to the x-axis and a Uniform Lateral Loading q

The uniform lateral loading can be represented by the double trigonometrical series

$$q = \sum_{m=1,3,5\ldots}^{\infty} \sum_{n=1,3,5\ldots}^{\infty} q_{mn} \sin\frac{m\pi x}{a} \sin\frac{n\pi y}{B} \quad . \quad . \quad . \quad . \quad (41)$$

where $$q_{mn} = \frac{16q}{\pi^2}\frac{1}{mn} \quad . \quad . \quad . \quad . \quad . \quad . \quad (42)$$

The equations for the deflected surface, shear forces and bending moments can also be represented by double trigonometrical series. Each term of these series is of the form given in equations (22), (24), (25).

The expressions for the bending moments only will be worked out in full. From (24) and (25) these can be expressed as

$$M_x = -\sum_{m=1,3\ldots}^{\infty} \sum_{n=1,3\ldots}^{\infty} \frac{1}{4} P_y k \left\{ W_{mn}\left(\frac{m^2}{\beta^2} + \frac{\mu_x}{k} n^2\right) + \frac{b}{\pi}\left(\frac{m}{\beta}\frac{X_{mn}}{D_{Qx}} - \frac{n\mu_x}{k}\frac{Y_{mn}}{D_{Qy}}\right)\right\} \times$$
$$\times \frac{q_{mn}}{Z_{mn}} \sin\frac{m\pi x}{a} \sin\frac{n\pi y}{b} \quad . \quad . \quad . \quad (43)$$

$$M_y = -\sum_{m=1,3,5\ldots}^{\infty} \sum_{n=1,3,5\ldots}^{\infty} \frac{1}{4} P_y \left\{ W_{mn}\left(\mu_x \frac{m^2}{\beta^2} + n^2\right) + \frac{b}{\pi}\left(\mu_x \frac{m}{\beta}\frac{X_{mn}}{D_{Qx}} - n\frac{Y_{mn}}{D_{Qy}}\right)\right\} \times$$
$$\times \frac{q_{mn}}{Z_{mn}} \sin\frac{m\pi x}{a} \sin\frac{n\pi y}{b} \quad . \quad . \quad . \quad (44)$$

Substituting the values of W_{mn}, X_{mn}, Y_{mn} from equations (28), (29), (30) into (43) and (44) gives

$$M_x = \frac{1}{4} P_y \sum_{m=1,3,5\ldots}^{\infty} \sum_{n=1,3,5\ldots}^{\infty} \left[k\frac{m^2}{\beta^2} + \mu_x n^2 + \frac{1}{2} r\left(1 - \frac{\mu_x^2}{k}\right)\left\{ k\eta\frac{m^4}{\beta^4} + \right.\right.$$
$$\left.\left. + \frac{m^2 n^2}{\beta^2}\left(2k - \frac{k\eta}{\varepsilon} - \eta\mu_x\right) + \frac{\eta\mu_x}{\varepsilon} n^4 \right\}\right] \frac{q_{mn}}{Z_{mn}} \sin\frac{m\pi x}{a} \sin\frac{n\pi y}{b} \quad . \quad . \quad (45)$$

$$M_y = \frac{1}{4} P_y \sum_{m=1,3,5\ldots}^{\infty} \sum_{n=1,3,5\ldots}^{\infty} \left[\mu_x\frac{m^2}{\beta^2} + n^2 + \frac{1}{2} r\left(1 - \frac{\mu_x^2}{k}\right)\left\{ \mu_x\eta\frac{m^4}{\beta^4} + \right.\right.$$
$$\left.\left. + \frac{m^2 n^2}{\beta^2}\left(\frac{2k}{\varepsilon} - \eta - \frac{\eta\mu_x}{\varepsilon}\right) + \frac{\eta}{\varepsilon} n^4 \right\}\right] \frac{q_{mn}}{Z_{mn}} \sin\frac{m\pi x}{a} \sin\frac{n\pi y}{b} \quad . \quad . \quad (46)$$

where

$$Z_{mn} = \frac{\pi^2}{b^2}\left[+ N_x\frac{m^2}{\beta^2}\left\{\frac{1}{2}\frac{r^2}{\varepsilon}\left(1 - \frac{\mu_x^2}{k}\right)\left(\eta k\frac{m^4}{\beta^4} + 2\frac{m^2 n^2}{\beta^2}(k - \eta\mu_x) + \eta n^4\right) + \right.\right.$$
$$+ r\left(\frac{m^2}{\beta^2}\left(\frac{k}{\varepsilon} + \frac{\eta(k - \mu_x^2)}{2k}\right) + n^2\left(1 + \frac{\eta(k - \mu_x^2)}{2k\varepsilon}\right)\right) + 1 \Big\} +$$
$$+ \frac{1}{4} P_y r\left(1 - \frac{\mu_x^2}{k}\right)\left(\frac{m^2}{\beta^2} + \frac{n^2}{\varepsilon}\right)\left(\frac{\eta k}{2}\frac{m^4}{\beta^4} + \frac{m^2 n^2}{\beta^2}(k - \eta\mu_x) + \frac{1}{2}\eta n^4\right) +$$
$$\left. + \frac{1}{4} P_y\left(k\frac{m^4}{\beta^4} + \frac{2m^2 n^2}{\beta^2}\left(\frac{\eta(k - \mu_x^2) + k\mu_x}{k}\right) + n^4\right)\right] \quad . \quad (47)$$

A corrugated core panel, with the corrugations running parallel to Ox, will now be considered. Substituting equations (34) and (35) and

$$\varepsilon=\infty \quad . \quad . \quad . \quad . \quad . \quad . \quad . \quad (48)$$

in equations (45), (46) and (47) gives

$$M_x=\frac{1}{4}P_y\sum_{m=1,3,5\ldots}^{\infty}\sum_{n=1,3,5\ldots}^{\infty}\left[k\frac{m^2}{\beta^2}+\mu n^2+\frac{1}{2}r\left(1-\frac{\mu^2}{k}\right)\left\{\frac{k}{1+\mu}\frac{m^4}{\beta^4}+\right.\right.$$
$$\left.\left.+\frac{m^2n^2}{\beta^2}\left(2k-\frac{\mu}{1+\mu}\right)\right\}\right]\frac{q_{mn}}{Z_{mn}}\sin\frac{m\pi x}{a}\sin\frac{n\pi y}{b} \quad . \quad . \quad (49)$$

$$M_y=\frac{1}{4}P_y\sum_{m=1,3,5\ldots}^{\infty}\sum_{n=1,3,5\ldots}^{\infty}\left[\mu\frac{m^2}{\beta^2}+n^2+\frac{1}{2}r\left(1-\frac{\mu^2}{k}\right)\left\{\frac{\mu}{1+\mu}\frac{m^4}{\beta^4}-\right.\right.$$
$$\left.\left.-\frac{m^2n^2}{\beta^2}\frac{1}{1+\mu}\right\}\right]\frac{q_{mn}}{Z_{mn}}\sin\frac{m\pi x}{a}\sin\frac{n\pi y}{b} \quad . \quad . \quad (50)$$

$$Z_{mn}=\frac{1}{4}\frac{\pi^2}{b^2}P_y\left[\frac{4N_x}{P_y}\frac{m^2}{\beta^2}\left\{r\frac{m^2}{\beta^2}\cdot\frac{k-\mu^2}{2k(1+\mu)}+rn^2+1\right\}+r\frac{m^2}{\beta^2}\left(1-\frac{\mu^2}{k}\right)\left(\frac{1}{2}\frac{k}{1+\mu}\frac{m^4}{\beta^4}+\right.\right.$$
$$\left.\left.+\frac{m^2n^2}{\beta^2}\left(k-\frac{\mu}{1+\mu}\right)+\frac{n^4}{2(1+\mu)}\right)+k\frac{m^4}{\beta^4}+\frac{2m^2n^2}{\beta^2}\left(\frac{(k-\mu^2)+k\mu(1+\mu)}{k(1+\mu)}\right)+n^4\right]$$
$$. \quad . \quad . \quad (51)$$

The maximum values of the bending moments, M_x and M_y can be expressed as

$$(M_y)_{\max}=\alpha_x qb^2. \quad . \quad . \quad . \quad . \quad . \quad . \quad (52)$$

$$(M_y)_{\max}=\alpha_y qb^2. \quad . \quad . \quad . \quad . \quad . \quad . \quad (53)$$

where α_x and α_y are functions of $-N_x/P_y$, r, k, and β. It can easily be shown that the position of maximum bending moments in the y-direction is on the centre line, $y=b/2$, but the position in the x-direction has to be found graphically. Fig. 10 gives the bending moment $(M_x)_{y=b/2}$ along the centre line of the panel for the case of $\beta=3{\cdot}0$, $r=0{\cdot}333$, and $k=1{\cdot}25$. For this case it is seen that the peak bending moment occurs at approximately one-sixth of the length of the panel from either end. The values of α_x and α_y for the case $\beta=3{\cdot}0$ and $k=1{\cdot}25$ are plotted in Figs. 11 and 12. The effect on α_x of changing the aspect ratio β of the panel is shown in Figs. 13 and 14.

For a sandwich panel having zero core flexural stiffnesses, the bending moments are obtained by substituting $k=1$ and equations (34) and (35) in equations (45), (46), and (47):—

$$M_x=\frac{1}{4}P_y\sum_{m=1,3,5\ldots}^{\infty}\sum_{n=1,3,5\ldots}^{\infty}\left[\frac{m^2}{\beta^2}+\mu n^2+\frac{1}{2}r(1-\mu)\left\{\frac{m^4}{\beta^4}+\frac{m^2n^2}{\beta^2}\left(2+\mu-\frac{1}{\varepsilon}\right)+\right.\right.$$
$$\left.\left.+\frac{\mu}{\varepsilon}n^4\right\}\right]\frac{q_{mn}}{Z_{mn}}\sin\frac{m\pi x}{a}\sin\frac{n\pi y}{b}. \quad . \quad (54)$$

$$M_y=\frac{1}{4}P_y\sum_{m=1,3,5\ldots}^{\infty}\sum_{n=1,3,5\ldots}^{\infty}\left[\mu\frac{m^2}{\beta^2}+n^2+\frac{1}{2}r(1-\mu)\left\{\mu\frac{m^4}{\beta^4}+\frac{m^2n^2}{\beta^2}\left(\frac{2+\mu}{\varepsilon}-1\right)+\right.\right.$$

$$\left.\left.+\frac{n^4}{\varepsilon}\right\}\right]\frac{q_{mn}}{Z_{mn}}\sin\frac{m\pi x}{a}\sin\frac{n\pi y}{b} \quad . \quad . \quad . \quad (55)$$

$$Z_{mn}=\frac{P_y\pi^2}{4b^2}\left[\frac{4N_x}{P_y}\frac{m^2}{\beta^2}\left\{\frac{1}{2}\frac{r^2}{\varepsilon}(1-\mu)\left(\frac{m^4}{\beta^4}+\frac{2m^2n^2}{\beta^2}+n^4\right)+r\left[\frac{m^2}{\beta^2}\left(\frac{1}{\varepsilon}+\frac{1-\mu}{2}\right)+\right.\right.\right.$$

$$\left.\left.\left.+n^2\left(1+\frac{1-\mu}{2\varepsilon}\right)\right]+1\right\}+\frac{1}{2}r(1-\mu)\left(\frac{m^2}{\beta^2}+\frac{n^2}{\varepsilon}\right)\left(\frac{m^2}{\beta^2}+n^2\right)^2+\left(\frac{m^2}{\beta^2}+n^2\right)^2\right]$$

$$. \quad . \quad . \quad . \quad . \quad . \quad (56)$$

Hence the maximum bending moments of the panel can again be expressed in the form

$$(M_x)_{max}=\alpha_x qb^2 \quad . \quad . \quad . \quad . \quad . \quad . \quad (57)$$

$$(M_y)_{max}=\alpha_y qb^2 \quad . \quad . \quad . \quad . \quad . \quad . \quad (58)$$

where α_x and α_y are functions of $-N_x/P_y$, r, ε, and β.

The Lift of Twisted and Cambered Wings in Supersonic Flow*

G. N. LANCE†, M.Sc., Ph.D.

(Department of Engineering, University of California)

SUMMARY: A generalised conical flow theory is used to deduce an integral equation relating the velocity potential on a delta wing (with subsonic leading edges) to the given downwash distribution over the wing. The complete solution of this integral equation is derived. This complete solution is composed of two parts, one being symmetric and the other anti-symmetric with respect to the spanwise co-ordinate; each part represents a velocity potential. For example, if y is the spanwise co-ordinate and x is measured in the free stream direction, then a downwash of the form $w = -\alpha_{11} Ux|y|$ is symmetric and will give rise to a symmetric potential, whereas $w = -\alpha_{11} Ux|y| \operatorname{sgn} y$ is anti-symmetric and gives rise to an anti-symmetric potential. The velocity potentials of such flows are given in the form of Tables for all downwashes up to and including homogenous cubics in the spanwise and streamwise co-ordinates. Table III gives similar formulae in the limiting case when the leading edges become transonic; these are compared with results given elsewhere[5] and serve as a check on the results of Tables I and II.

1. Introduction

In a recent paper[4] the author described a method of obtaining the lift on a twisted delta wing, with subsonic leading edges. The method was applied to obtain the lift distributions in the cases when the downwash w over the wing plan form was proportional to $x^r y^s$, with $0 \leqslant r+s \leqslant 3$. However, the results obtained therein were confined to the cases for which the velocity potential, and hence the lift distribution, had the *same* symmetry, with respect to the spanwise co-ordinate y, as had the downwash. For example, if $w = -\alpha_{01} y$ then the velocity potential obtained was an odd function of y; if $w = -\alpha_{12} x y^2$ the lift distribution was an even function of y. The present paper gives the extension required to obtain the potentials when the symmetry of the downwash distribution is carefully displayed.

For a delta wing with *supersonic* leading edges the velocity potentials have been calculated, for $w = -\alpha_{rs} x^r y^s$ by Hunn and the author[5]. The symmetric and the anti-symmetric velocity potentials were obtained for each downwash distribution. Such distributions are useful in flutter and aeroelastic problems when it is desired to describe the wing shape, approximately, by means of a power series expansion. The expansion must be even in y for symmetric motion and odd in y for anti-symmetric motion.

Received June 1954.

*This work was carried out under the auspices of the F.O.A. Scientific Research Project TA 01-101-3006 (OEEC 151).

†National Academy of Sciences Research Fellow.

The method described in Ref. 4 is not ideal when *both* the symmetric and anti-symmetric velocity potentials are required, so first a modification of this method is described. The present method has been partially described by Lomax and Heaslet[6] and by Lomax, Heaslet and Fuller[7]. To make the extension clear, the work of Refs. 6 and 7 is given, in outline, here. The lift distribution was obtained, in these two papers, as the solution of a certain integral equation. However, the solution given was not complete, a fact which explains why, in obtaining certain unknown constants, more equations were available than were required. (The same error was committed in Ref. 4). It is shown in this paper that there are, in fact, exactly the same number of equations as unknowns when the complete solution of the integral equation is used. (This point is discussed more fully in Section 3).

NOTATION

$a = B\tan\gamma$

$a_i, b_r, c_r, b_r', c_r'$ constants defined by equations (14), (15) and (20)

Δp difference in pressure between lower and upper surfaces of wing

t variable of integration

u, v, w components of perturbation velocity

x, y, z rectangular Cartesian co-ordinates (Fig. 1)

x_1, y_1 variables of integration

$B = (M^2-1)^{\frac{1}{2}}$

$D_1, \ldots, D_4$ functions of a defined in Tables I and II

$H(\theta, \eta)$ kernel function, *see* equations (11)

K, E complete elliptic integrals of the first and second kinds of modulus $(1-a^2)^{\frac{1}{2}}$

M Mach number

U free stream velocity

α_{rs} constants of proportionality for w given over the wing plan form, *see* equations (2)

γ semi-angle of the delta wing

$\eta = By/x$

$\eta_1 = By_1/x$

κ degree of the downwash distribution

ρ density of free stream

θ variable of integration

$\operatorname{sgn} y \equiv y/|y|$

$\mathcal{F}\int$ denotes the "finite part" of the integral

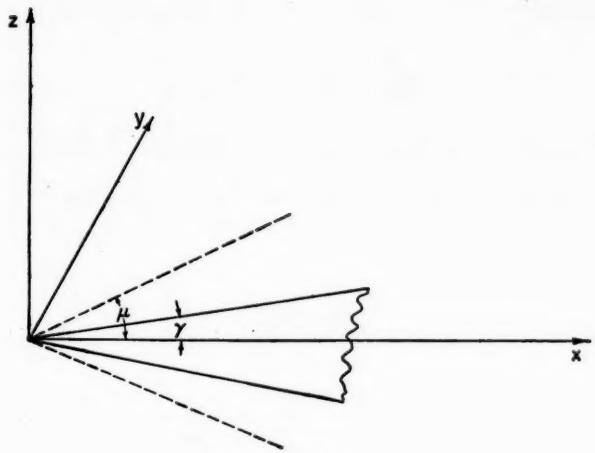

Fig. 1.
The co-ordinate system and notation relevant to the delta wing.

2. The Integral Equation

The co-ordinate system is shown in Fig. 1. The assumptions made here are the same as those of Ref. 4. Attention is confined to an unyawed delta wing placed in a supersonic flow whose free stream velocity is U; linearised supersonic theory is used and the flow is of generalised conical type.

The equations of the leading edges are

$$y = \pm x \tan \gamma \quad . \quad . \quad . \quad . \quad . \quad (1)$$

which is written $\eta = \pm a,$

where the non-dimensional co-ordinate

$$\eta = By/x,$$

$$a = B \tan \gamma$$

and $B = (M^2 - 1)^{\frac{1}{2}}.$

Since subsonic edges only are considered, $a < 1$.

The downwash, which is known over the wing, will be of the form

$$w = -\alpha_{rs} U x^r |y|^s \quad . \quad . \quad . \quad . \quad (2a)$$

for symmetric deformation of the wings, or

$$w = -\alpha_{rs} U x^r |y|^s \operatorname{sgn} y \, . \quad . \quad . \quad . \quad (2b)$$

for anti-symmetric deformations.

The local load coefficient can be written, according to linearised theory,

$$\frac{\Delta p}{\frac{1}{2}\rho U^2} = \frac{p_l - p_u}{\frac{1}{2}\rho U^2} = \frac{4}{U}\frac{\partial \phi}{\partial x}, \qquad (3)$$

where p_l and p_u are the pressures on the lower and upper surfaces, respectively.

Consider an elementary ray of the wing (Fig. 2) emanating from the apex O and inclined at an angle δ to the x-axis. Suppose that the load carried by this element is

$$\frac{\Delta p}{\frac{1}{2}\rho U^2} = Cy^\kappa, \qquad (4)$$

where C is a constant. Then the upwash field due to a complete triangle with one side along $y=0$ and the other along $y = x\tan\delta$ is given by[8]

$$w = \frac{U}{4\pi}\mathscr{F}\int_\tau dy_1 \int \frac{(x-x_1)\,\Delta p\,(x_1, y_1)\,dx_1}{\frac{1}{2}\rho U^2 (y-y_1)^2 [(x-x_1)^2 - B^2(y-y_1)^2]^{\frac{1}{2}}}. \qquad (5)$$

where τ is the area of the wing plan form that lies inside the fore Mach cone from the point $(x, y, 0)$. The generalised principal part of the integral is to be evaluated, as indicated by the symbol $\mathscr{F}\int$.

Writing $\eta_1 = By_1/x$ and performing the integration with respect to x_1, after using (4), we obtain

$$\left(\frac{B}{x}\right)^\kappa \frac{w}{U} = \frac{BC}{4\pi}\int_0^{\frac{a(1+\eta)}{(1+a)}} \frac{\eta_1^\kappa}{(\eta-\eta_1)^2}\left[\left(1-\frac{\eta_1}{a}\right)^2 - \left(\eta-\eta_1\right)^2\right]^{\frac{1}{2}} d\eta_1;\ 0<a,\ -1<\eta<a \qquad (6a)$$

$$= \frac{BC}{4\pi}\int_0^{\frac{a(1-\eta)}{(1-a)}} \frac{\eta_1^\kappa}{(\eta-\eta_1)^2}\left[\left(1-\frac{\eta_1}{a}\right)^2 - \left(\eta-\eta_1\right)^2\right]^{\frac{1}{2}} d\eta_1;\ 0<a,\ a<\eta<1, \qquad (6b)$$

with slight modification if a is negative.

The element of upwash produced by the ray of angle $d\delta$ is obtained by subtracting two such expressions. Let the upwash of the plan form with vertex angle δ be

$$w = f(a, \eta). \qquad (7)$$

Then $$dw = f(a+da, \eta) - f(a, \eta) = \frac{\partial f}{\partial a}da.$$

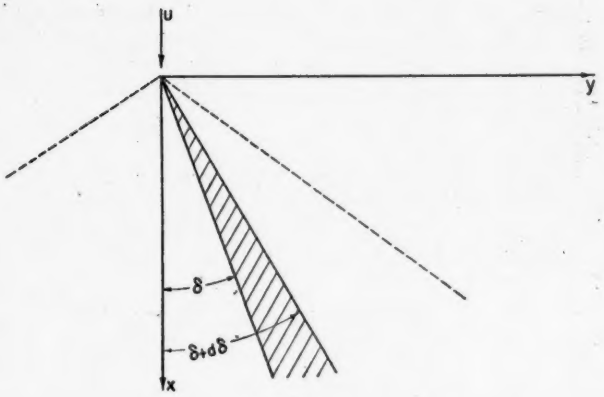

Fig. 2.
The elementary ray, of apex angle $d\delta$, emanating from the apex of the wing.

If this differentiation is applied to (6) and η_1 is replaced by

$$\eta_1 = \frac{a(\eta - t)}{(a - t)} \quad . \quad . \quad . \quad . \quad . \quad . \quad (8)$$

there results

$$\left(\frac{B}{x}\right)^{\kappa} \frac{dw}{U} = \frac{-BCda(\kappa+1)a^{\kappa}}{4\pi} \int_{-1}^{\eta} \frac{(\eta - t)^{\kappa}(1-t^2)^{\frac{1}{2}}\,dt}{t(a-t)^{\kappa+2}}, \quad -1 < \eta < a < 1 \quad . \quad (9a)$$

and $$\left(\frac{B}{x}\right)^{\kappa} \frac{dw}{U} = \frac{-BCda(\kappa+1)a^{\kappa}}{4\pi} \int_{1}^{\eta} \frac{(\eta - t)^{\kappa}(1-t^2)^{\frac{1}{2}}\,dt}{t(a-t)^{\kappa+2}}, \quad -1 < a < \eta < 1 \ldots \quad (9b)$$

In one of these integrals the Cauchy principal part is required.

Hence the total downwash contribution from all such triangular elements lying between $-a$ and $+a$ is

$$\left(\frac{B}{x}\right)^{\kappa} \frac{w}{U} = \frac{-B(\kappa+1)}{4\pi} \mathscr{F} \int_{-a}^{a} \theta^{\kappa} C(\theta) H(\theta, \eta)\, d\theta, \quad . \quad . \quad (10)$$

where $$H(\theta, \eta) = \int_{1}^{\eta} \frac{(\eta - t)^{\kappa}(1-t^2)^{\frac{1}{2}}\,dt}{t(\theta - t)^{\kappa+2}}, \qquad -a \leqq \theta < \eta \quad . \quad . \quad (11a)$$

$$= \int_{-1}^{\eta} \frac{(\eta - t)^{\kappa}(1-t^2)^{\frac{1}{2}}\,dt}{t(\theta - t)^{\kappa+2}}, \qquad \eta < \theta \leqq a \ldots \quad . \quad (11b)$$

By expressions (2*a*) and (2*b*) it is seen that the boundary condition to be satisfied by (10) is that $B^{\kappa}w/(x^{\kappa}U)$ is a polynomial of, at most, degree κ in the variable $|\eta|$ for symmetric deformations and a polynomial in $|\eta|$ multiplied by $\operatorname{sgn}\eta\,(=\eta/|\eta|)$ for anti-symmetric deformations. Hence

$$\frac{B(\kappa+1)}{4\pi}\,\mathscr{F}\int_{-a}^{a}\theta^{\kappa}C(\theta)\left(\frac{\partial}{\partial\eta}\right)^{\kappa+1}H(\theta,\eta)\,d\theta=0. \quad . \quad . \quad . \quad (12)$$

Performing the differentiation with respect to η gives

$$\frac{(1-\eta^2)^{\frac{1}{2}}}{\eta}\,\mathscr{F}\int_{-a}^{a}\frac{\theta^{\kappa}C(\theta)\,d\theta}{(\theta-\eta)^{\kappa+2}}=0$$

which may be written

$$\left(\frac{\partial}{\partial\eta}\right)^{\kappa+1}\mathscr{F}\int_{-a}^{a}\frac{\theta^{\kappa}C(\theta)\,d\theta}{(\theta-\eta)}=0. \quad . \quad . \quad . \quad . \quad (13)$$

Thus the function $C(\theta)$ is found to be a solution of the integral equation

$$\mathscr{F}\int_{-a}^{a}\frac{\theta^{\kappa}C(\theta)\,d\theta}{(\theta-\eta)}=\sum_{i=0}^{\kappa}a_i|\eta|^i, \text{ for symmetric deformations} \quad . \quad (14)$$

$$=\sum_{i=0}^{\kappa}a_i|\eta|^i\frac{\eta}{|\eta|}, \text{ for anti-symmetric deformations.}$$

3. The Solution of the Integral Equation

It is shown in the Appendix that the complete solution of (14) can be written in the form

$$\theta^{\kappa}C(\theta)=\sum_{0}^{\kappa+1}\frac{b_r\theta^r}{(a^2-\theta^2)^{\frac{1}{2}}}+\sum_{1}^{\kappa}c_r\theta^r\cosh^{-1}\left|\frac{v}{\theta}\right| \quad . \quad . \quad . \quad (15)$$

and it remains to show how the constants b_r and c_r may be obtained.

Since

$$\mathscr{F}\int_{-1}^{\eta}\frac{(\eta-t)^{\kappa}(1-t^2)^{\frac{1}{2}}\,dt}{t(\theta-t)^{\kappa+2}}=\mathscr{F}\int_{1}^{\eta}\frac{(\eta-t)^{\kappa}(1-t^2)^{\frac{1}{2}}\,dt}{t(\theta-t)^{\kappa+2}} \quad . \quad . \quad . \quad (16)$$

(10) can be written

$$\left(\frac{B}{x}\right)^{\kappa}\frac{w}{U}=-\frac{B(\kappa+1)}{4\pi}\int_{-a}^{a}\theta^{\kappa}C(\theta)\,d\theta\,\mathscr{F}\int_{1}^{\eta}\frac{(\eta-t)^{\kappa}(1-t^2)^{\frac{1}{2}}\,dt}{t(\theta-t)^{\kappa+2}},\ \eta>0 \quad . \quad (17)$$

with a similar expression if $\eta<0$.

The order of integration in (17) may be reversed and a careful analysis[6] shows that

$$\left(\frac{B}{x}\right)^{\kappa}\frac{w}{U}=\frac{B}{4\kappa!}\mathscr{F}\int_{1}^{a}\frac{(\eta-t)^{\kappa}(1-t^2)^{\frac{1}{2}}}{t}\left(\frac{\partial}{\partial t}\right)^{\kappa+1}\left[\sum_{1}^{\kappa}c_r t^r\cos^{-1}\frac{a}{t}-\sum_{0}^{\kappa+1}\frac{b_r t^r}{(t^2-a^2)^{\frac{1}{2}}}\right]dt,\quad \eta>0. \qquad (18)$$

Now $B^{\kappa}w/(x^{\kappa}U)$ is simply a power of $|\eta|$ or a power of $|\eta|$ multiplied by $\eta/|\eta|$; thus, by equating like powers of this co-ordinate on each side of (18) it is seen that there are *exactly* the same number of equations and unknowns, once it has been decided whether the odd or even solutions are being sought. For example, if $\kappa=2$, there are just three equations and the six unknown constants b_0, b_1, b_2, b_3, c_1, c_2. In seeking, say, the anti-symmetric load distribution only the constants with odd subscripts are selected, and the remainder are equated to zero. Thus the unknowns are reduced to exactly three.

4. Examples

Two examples are given which bring out the technique for obtaining the constants. As a final result the velocity potential ϕ_{r_a} is required for downwash distributions given by equations (2). Since $\eta=By/x$, $dx=-Byd\eta/\eta^2$, and thus, by (3),

$$\frac{\Delta p}{\frac{1}{2}\rho U^2}=-\frac{4\eta^2}{UBy}\frac{\partial\phi}{\partial\eta}. \qquad (19)$$

It follows that we must assume an expression for ϕ of the form

$$\phi=\alpha Ux^{\kappa+1}\left[\sum_{1}^{\kappa+1}c_r'\eta^r\cosh^{-1}\left|\frac{a}{\eta}\right|+\sum_{0}^{\kappa}b_r'\eta^r\left(a^2-\eta^2\right)^{\frac{1}{2}}\right], \qquad (20)$$

which, when substituted in (19), will give an expression for

$$\theta^{\kappa}C(\theta)=\frac{\theta^{\kappa}\Delta p}{\frac{1}{2}\rho U^2 y^{\kappa}} \qquad (21)$$

which is of the correct type, namely expression (15).

For illustrative purposes, only the cases

(*a*) $w=-\alpha_{11}Ux|y|$

and (*b*) $w=-\alpha_{11}Ux|y|\operatorname{sgn}y,$

are considered, in which case $\kappa=2$. Case (*a*) corresponds to the symmetric and case (*b*) to the anti-symmetric velocity potentials.

Case (a)

From (20), the expression for ϕ is

$$\phi_{11}=\frac{\alpha_{11}Ux^3}{B^2}\left[\left(b_0'+b_2'\eta^2\right)\left(a^2-\eta^2\right)^{\frac{1}{2}}+c_2'\eta^2\cosh^{-1}\left|\frac{a}{\eta}\right|\right], \quad . \quad (22)$$

where only the coefficients of even powers of η have been selected and the factor B^{-2} is inserted to simplify b_0', b_2' and c_2'.

Now (19) and (21) show that

$$\eta^2 C(\eta)=\frac{\eta^2\Delta p}{\frac{1}{2}\rho U^2y^2}=4\alpha_{11}\left[\frac{b_0'(3a^2-2\eta^2)}{(a^2-\eta^2)^{\frac{1}{2}}}+\frac{b_2'a^2\eta^2}{(a^2-\eta^2)^{\frac{1}{2}}}+c_2'\eta^2\left(\cosh^{-1}\left|\frac{a}{\eta}\right|+\frac{a}{(a^2-\eta^2)^{\frac{1}{2}}}\right)\right] \quad . \quad . \quad . \quad . \quad (23)$$

Comparing this equation with (15) shows that

$$b_0=12a^2b_0',$$

$$b_2=4(a^2b_2'+ac_2'-2b_0')$$

and

$$c_2=4c_2'.$$

Thus (18) becomes

$$-\eta=\tfrac{1}{2}\mathscr{F}\int_1^a\frac{(\eta-t)^2(1-t^2)^{\frac{1}{2}}}{t}\frac{\partial^3}{\partial t^3}\left[c_2't^2\cos^{-1}\frac{a}{t}-\frac{(3a^2b_0'+t^2\{a^2b_2'+ac_2'-2b_0'\})}{(t^2-a^2)^{\frac{1}{2}}}\right]dt.$$

By equating the coefficients of η on each side, the following three equations are obtained:—

$$\mathscr{F}\int_1^a\frac{(1-t^2)^{\frac{1}{2}}}{t}\frac{\partial^3}{\partial t^3}\left[c_2't^2\cos^{-1}\frac{a}{t}-\frac{(3a^2b_0'+t^2\{a^2b_2'+ac_2'-2b_0'\})}{(t^2-a^2)^{\frac{1}{2}}}\right]dt=0 \quad (24)$$

$$\mathscr{F}\int_1^a(1-t^2)^{\frac{1}{2}}\frac{\partial^3}{\partial t^3}\left[c_2't^2\cos^{-1}\frac{a}{t}-\frac{(3a^2b_0'+t^2\{a^2b_2'+ac_2'-2b_0'\})}{(t^2-a^2)^{\frac{1}{2}}}\right]dt=1 \quad (25)$$

$$\mathscr{F}\int_1^a t(1-t^2)^{\frac{1}{2}}\frac{\partial^3}{\partial t^3}\left[c_2't^2\cos^{-1}\frac{a}{t}-\frac{(3a^2b_0'+t^2\{a^2b_2'+ac_2'-2b_0'\})}{(t^2-a^2)^{\frac{1}{2}}}\right]dt=0. \quad (26)$$

With the substitution $t^2=a^2\,\mathrm{nd}^2 u$ equations (24) and (26) reduce to

$$ab_0'[2a^2\mathrm{K}-(1+a^2)\mathrm{E}]+ab_2'[a^2\mathrm{K}(3-5a^2)-2\mathrm{E}(3-5a^2+a^4)]-$$
$$-c_2'[2a^2\mathrm{K}(3-5a^2+a^4)-\mathrm{E}(12-21a^2+7a^4)]=0 \quad . \quad (27)$$

$$ab_0'[a^2\mathrm{K}(5-3a^2)+2\mathrm{E}(1-5a^2+3a^4)]+ab_2'[2a^4\mathrm{K}-(a^2+a^4)\mathrm{E}]+$$
$$+a^2c_2'[a^2\mathrm{K}(1+a^2)-2a^2\mathrm{E}]=0 \quad . \quad . \quad . \quad . \quad (28)$$

respectively, while (25) can be evaluated in terms of elementary functions and gives

$$c_2'=1/\pi. \quad . \quad . \quad . \quad . \quad . \quad . \quad (29)$$

The tables of integrals of elliptic functions by Byrd and Friedman[2] were found most useful in all these evaluations; throughout this work K and E denote the complete elliptic integrals of the first and second kinds, respectively, whose modulus is $(1-a^2)^{\frac{1}{2}}$.

After substituting for c_2' from (29) in (27) and (28), we solve for b_0' and b_2' and obtain

$$b_0'=a[3a^4\mathrm{K}^2-8a^2\mathrm{KE}+(4+a^2)\mathrm{E}^2]/D_1 \quad . \quad . \quad . \quad . \quad (30)$$

and
$$b_2'=-2a[a^4\mathrm{K}^2-2a^2(1+a^2)\mathrm{KE}+3a^2\mathrm{E}^2]/D_1, \quad . \quad . \quad . \quad (31)$$

where
$$D_1=5a^4\mathrm{K}^2-8a^2(1+a^2)\mathrm{KE}-(4-19a^2+4a^4)\mathrm{E}^2; \quad . \quad . \quad (32)$$

this completes the derivation of ϕ_{11} of Table I.

Case (b)

The anti-symmetric solution of (20) is now required, namely

$$\phi_{11}=\frac{\alpha_{11}Ux^3\eta}{B^2}\left[b_1'\left(a^2-\eta^2\right)^{\frac{1}{2}}+\left(c_1'+c_3'\eta^2\right)\cosh^{-1}\left|\frac{a}{\eta}\right|\right]. \quad . \quad (33)$$

From (19) and (21), we have

$$\eta^2C(\eta)=\frac{\eta^2\Delta\rho}{\frac{1}{2}\rho U^2y^2}=4\alpha_{11}\eta\left[\frac{b_1'(2a^2-\eta^2)}{(a^2-\eta^2)^{\frac{1}{2}}}+c_1'\left(2\cosh^{-1}\left|\frac{a}{\eta}\right|+\frac{a}{(a^2-\eta^2)^{\frac{1}{2}}}\right)+\frac{c_3'a\eta^2}{(a^2-\eta^2)^{\frac{1}{2}}}\right]$$
$$. \quad . \quad . \quad . \quad (34)$$

and (18) gives, in this case,

$$-\eta=\tfrac{1}{2}\mathscr{H}\int_1^a\frac{(\eta-t)^2(1-t^2)^{\frac{1}{2}}}{t}\frac{\partial^3}{\partial t^3}\left[c_1't\left(2\cos^{-1}\frac{a}{t}-\frac{a}{(t^2-a^2)^{\frac{1}{2}}}\right)-\right.$$
$$\left.-\frac{b_1't(2a^2-t^2)}{(t^2-a^2)^{\frac{1}{2}}}-\frac{c_3'at^3}{(t^2-a^2)^{\frac{1}{2}}}\right]dt, \quad . \quad (35)$$

Equating coefficients of η on both sides of this equation, we have

$$\mathscr{F}\int_1^a \frac{(1-t^2)^{\frac{1}{2}}}{t}\frac{\partial^3}{\partial t^3}\left[c_1't\left(2\cos^{-1}\frac{a}{t}-\frac{a}{(t^2-a^2)^{\frac{1}{2}}}\right)-\frac{b_1't(2a^2-t^2)}{(t^2-a^2)^{\frac{1}{2}}}-\frac{c_3'at^3}{(t^2-a^2)^{\frac{1}{2}}}\right]dt=0 \quad . \quad . \quad . \quad . \quad (36)$$

$$\mathscr{F}\int_1^a (1-t^2)^{\frac{1}{2}}\frac{\partial^3}{\partial t^3}\left[c_1't\left(2\cos^{-1}\frac{a}{t}-\frac{a}{(t^2-a^2)^{\frac{1}{2}}}\right)-\frac{b_1't(2a^2-t^2)}{(t^2-a^2)^{\frac{1}{2}}}-\frac{c_3'at^3}{(t^2-a^2)^{\frac{1}{2}}}\right]dt=1 \quad . \quad . \quad . \quad . \quad (37)$$

$$\mathscr{F}\int_1^a t(1-t^2)^{\frac{1}{2}}\frac{\partial^3}{\partial t^3}\left[c_1't\left(2\cos^{-1}\frac{a}{t}-\frac{a}{(t^2-a^2)^{\frac{1}{2}}}\right)-\frac{b_1't(2a^2-t^2)}{(t^2-a^2)^{\frac{1}{2}}}-\frac{c_3'at^3}{(t^2-a^2)^{\frac{1}{2}}}\right]dt=0. \quad . \quad . \quad . \quad . \quad (38)$$

In the present case (36) and (38) can be evaluated in terms of elementary functions and they show that

$$c_1'=c_3'=0. \quad . \quad . \quad . \quad . \quad . \quad . \quad . \quad (39)$$

With the elliptic function substitution $t^2=a^2\,\mathrm{nd}^2\,u$, (37) gives

$$b_1'=\frac{(1-a^2)^2}{[a^2(1+a^2)\mathrm{K}-2(1-a^2+a^4)\mathrm{E}]}. \quad . \quad . \quad . \quad . \quad (40)$$

This completes the derivation of ϕ_{11} of Table II.

5. Results

The results for the symmetric velocity potentials are listed in Table I. They are valid for $-a\leqslant\eta\leqslant a$. The velocity potentials which are anti-symmetric in η are listed in Table II; these also are valid for $-a\leqslant\eta\leqslant a$. (In all tables $|\eta|$ is used in the argument of the $\cosh^{-1}$ terms). It is apparent from these complicated results that their derivation is long and tedious. A check is desirable; it is applied by taking the limit as a tends to 1 from below, and comparing these much simpler formulae with the corresponding limiting values derived from the supersonic formulae[5] by letting a tend to 1 from above. In every case the results agree, so it is unlikely that any errors are now present.

6. Conclusions

The formulae listed in Tables I and II give the symmetric and anti-symmetric velocity potentials ϕ_{rs}, respectively, when the downwash over the wing plan form is given in the form $w=-\alpha_{rs}Ux^ry^s$. Table III gives the formulae for wings with transonic leading edges.

The Tables can be used for flutter calculations as described in Ref. 5, Table I being used for symmetric modes of vibration and Table II for anti-symmetric modes. The formulae given herein can also be used in aeroelastic calculations, the shape being specified in a power series of the form $\Sigma\alpha_{rs}x^ry^s$. The technique used is similar to that of Ref. 3 for swept wings with moderate aspect ratio.

The method presented can, in principle, be extended to values of $\kappa > 3$, but the algebraic work gets more and more laborious, and it is doubtful whether any useful purpose would be served by carrying this work further. A slight extension only would be required to include thickness effects, and this will form the subject of another paper.

ACKNOWLEDGMENTS

The author wishes to express his gratitude to Professor John W. Miles from whom he has received many helpful suggestions, and also to Dr. H. Lomax for his criticisms of the original manuscript.

REFERENCES

1. BIERENS DE HAAN, D. *Nouvelles Tables d'Intégrales Définiés.* G. E. Stechert, New York, 1939.

2. BYRD, P. F. and FRIEDMAN, M. D. *Handbook of Elliptic Integrals for Engineers and Physicists.* Springer, Berlin, 1954.

3. HUNN, B. A. and LANCE, G. N. An Aspect of the Deformation of Swept Wings in Steady Supersonic Flight. *Journal of the Royal Aeronautical Society,* November 1954.

4. LANCE, G. N. The Delta Wing in a Non-Uniform Supersonic Stream. *The Aeronautical Quarterly,* Volume V, May 1954.

5. LANCE, G. N. and HUNN, B. A. The Three Dimensional Aerodynamic Forces on Oscillating Swept Wings with Supersonic Leading Edges. Hawker Aircraft Design Department Report No. 1189 (unpublished).

6. LOMAX, H. and HEASLET, M. A. Generalised Conical-Flow Fields in Supersonic Wing Theory. N.A.C.A. T.N. 2497, September 1951.

7. LOMAX, H., HEASLET, M. A. and FULLER, F. B. Integrals and Integral Equations in Linearized Wing Theory. N.A.C.A. Report 1054, 1951.

8. LOMAX, H., HEASLET, M. A. and FULLER, F. B. Formulas for Source, Doublet, and Vortex Distributions in Supersonic Wing Theory. N.A.C.A. T.N. 2252, 1950.

Appendix

It is required to show that

$$f(\theta) = \sum_{0}^{\kappa+1} \frac{b_r \theta^r}{(a^2 - \theta^2)^{\frac{1}{2}}} + \sum_{1}^{\kappa} c_r \theta^r \cosh^{-1}\left|\frac{a}{\theta}\right| . \quad . \quad . \quad . \quad (41)$$

is a solution of the integral equation

$$\mathscr{F}\int_{-a}^{a} \frac{f(\theta)\,d\theta}{(\theta - \eta)} = \sum_{i=0}^{\kappa} a_i |\eta|^i \quad \text{for symmetric deformations} \quad . \quad . \quad (42)$$

$$= \sum_{i=0}^{\kappa} a_i |\eta|^i \frac{\eta}{|\eta|} \quad \text{for anti-symmetric deformations.}$$

The first summation in (41) is the usual solution and the fact that it satisfies (42) will not be proved.

Consider the expression

$$I_0 = \mathscr{F}\int_{-a}^{a} \frac{\cosh^{-1}\left|\frac{a}{\theta}\right| d\theta}{(\theta-\eta)} = \int_0^a \frac{\cosh^{-1}\frac{a}{\theta}\,d\theta}{(\theta-\eta)} - \int_0^a \frac{\cosh^{-1}\frac{a}{\theta}\,d\theta}{(\theta+\eta)},$$

Thus
$$I_0 = \mathscr{F}\int_0^1 \frac{2a\eta\cosh^{-1}\frac{1}{t}\,dt}{(a^2t^2-\eta^2)} \qquad (43)$$

$$= 2a\eta\left\{\mathscr{F}\int_0^{\eta/a} \frac{\cosh^{-1}\frac{1}{t}\,dt}{(a^2t^2-\eta^2)} + \mathscr{F}\int_{\eta/a}^1 \frac{\cosh^{-1}\frac{1}{t}\,dt}{(a^2t^2-\eta^2)}\right\}.$$

Integration by parts gives

$$I_0 = \left\{\mathscr{F}\int_0^{\eta/a} \log\left(\frac{\eta-at}{\eta+at}\right)\frac{dt}{t(1-t^2)^{\frac{1}{2}}} + \mathscr{F}\int_{\eta/a}^1 \log\left(\frac{at-\eta}{at+\eta}\right)\frac{dt}{t(1-t^2)^{\frac{1}{2}}}\right\}$$

$$= \left\{\mathscr{F}\int_0^1 \log\left(\frac{\eta-at}{\eta+at}\right)\frac{dt}{t(1-t^2)^{\frac{1}{2}}} - i\pi\int_{\eta/a}^1 \frac{dt}{t(1-t^2)^{\frac{1}{2}}}\right\}.$$

These two integrals can be found in tables (*e.g.* Ref. 1) and we get

$$I_0 = -\pi\left\{\sin^{-1}\frac{a}{\eta} + i\cosh^{-1}\frac{a}{\eta}\right\} = -\tfrac{1}{2}\pi^2\frac{\eta}{|\eta|}, \quad \text{if } \eta \neq 0 \qquad (44)$$

If $\eta=0$, (43) shows that $I_0=0$. The exact value of I_0 is unimportant in this context, the important point being that it is a function of $\eta/|\eta|$ only.

Now $\theta^r = \{\eta+(\theta-\eta)\}^r = \sum_{k=0}^{r}\binom{r}{k}\eta^{r-k}(\theta-\eta)^k$ so that

$$c_r\mathscr{F}\int_{-a}^{a} \frac{\theta^r\cosh^{-1}\left|\frac{a}{\theta}\right| d\theta}{(\theta-\eta)} = c_r\left\{\eta^r I_0 + \sum_{k=1}^{r}\binom{r}{k}\eta^{r-k}\mathscr{F}\int_{-a}^{a}(\theta-\eta)^{k-1}\cosh^{-1}\left|\frac{a}{\theta}\right| d\theta\right\},$$

the expression in { } is clearly a polynomial of degree r in $|\eta|$ or a polynomial of degree r in $|\eta|$ multiplied by $\eta/|\eta|$ according as the motion is symmetric or anti-symmetric. Hence it follows that the second summation in (41) gives a contribution, to the integral equation (42), of the form $\sum_1^{\kappa} a_i'|\eta|^i$ for symmetric, or $\sum_1^{\kappa} a_i'|\eta|^i(\eta/|\eta|)$ for anti-symmetric motions, which is thus of the correct form.

Thus it has been shown that the complete solution of the integral equations (13) or (14) may be written in the form (15), despite the fact that the left hand side of (10) and its derivatives may be discontinuous at $\eta=0$. It has been shown, by Lomax*, that the solution of (13), having a discontinuity at $\theta=l$, where $-a<l<a$ may be derived from the standard Söhngen inversion formula.

*Private communication to the author.

TABLE I

EXPRESSIONS FOR THE SYMMETRIC POTENTIALS

ϕ_{rs} is the velocity potential for the flow whose downwash is of the form

$$w = -\alpha_{rs} U x^r \left| y \right|^s.$$

$$\phi_{00} \quad \frac{\alpha_{00} U x (a^2-\eta^2)^{\frac{1}{2}}}{BE}$$

$$\phi_{01} \quad \frac{\alpha_{01} U x^2 a\,(E-a^2K)\,(a^2-\eta^2)^{\frac{1}{2}}}{\pi B^2\,[a^2K+(1-2a^2)\,E]} + \frac{\alpha_{01} U x^2 \eta^2 \cosh^{-1}\left|\frac{a}{\eta}\right|}{\pi B^2}$$

$$\phi_{10} \quad \frac{\alpha_{10} U x^2\,(1-a^2)\,(a^2-\eta^2)^{\frac{1}{2}}}{B\,[a^2K+(1-2a^2)\,E]}$$

$$\phi_{02} \quad \frac{2\,\alpha_{02} U x^3 \{a^2\,[2a^2K-(1+a^2)\,E]-\eta^2\,[a^2K\,(5-3a^2)+2E\,(1-5a^2+3a^4)]\}\,(a^2-\eta^2)^{\frac{1}{2}}}{3B^3 D_1}$$

$$\phi_{11} \quad \frac{\alpha_{11} U x^3 a\,\{3a^4K^2-8a^2KE+(4+a^2)\,E^2-2\eta^2\,[a^4K^2-2a^2KE\,(1+a^2)+3E^2a^2]\}\,(a^2-\eta^2)^{\frac{1}{2}}}{\pi B^2 D_1} + \frac{\alpha_{11} U x^3 \eta^2 \cosh^{-1}\left|\frac{a}{\eta}\right|}{\pi B^2}$$

$$\phi_{20} \quad \frac{2\,\alpha_{20} U x^3\,\{a^2K\,(3-5a^2)-2E\,(3-5a^2+a^4)+\eta^2\,[2a^2K-E\,(1+a^2)]\}\,(a^2-\eta^2)^{\frac{1}{2}}}{3BD_1}$$

where $\quad D_1 = 5a^4K^2-8a^2KE\,(1+a^2)-E^2\,(4-19a^2+4a^4)$

$$\phi_{03} \quad \frac{\alpha_{03} U x^4 a}{2\pi B^4 D_2}\left\{\begin{array}{l} a^2\,[2a^4K^2\,(3a^2-7)+4a^2KE\,(8-a^2-3a^4)-2E^2\,(4+11a^2-11a^4)]+ \\ +\eta^2\,[a^4K^2\,(27-55a^2+48a^4)-a^2KE\,(48-58a^2-46a^4+96a^6)- \\ -E^2\,(12-119a^2+239a^4-152a^6)] \end{array}\right\}(a^2-\eta^2)^{\frac{1}{2}} + \frac{\alpha_{03} U x^4 \eta^4 \cosh^{-1}\left|\frac{a}{\eta}\right|}{2\pi B^4}$$

$$\phi_{12} \quad \frac{2\,\alpha_{12} U x^4\,(1-a^2)}{3B^3 D_2}\left\{\begin{array}{l} a^2\,[a^2K\,(9-a^2)-E\,(3+7a^2-2a^4)]- \\ -\eta^2\,[a^2K\,(27-31a^2+12a^4)+E\,(6-55a^2+65a^4-24a^6)] \end{array}\right\}(a^2-\eta^2)^{\frac{1}{2}}$$

$$\phi_{21} \quad -\frac{\alpha_{21} U x^4 a}{12\pi B^2 D_2}\left\{\begin{array}{l} 2\,[a^4K^2\,(78-88a^2-13a^4+3a^6)-2a^2KE\,(96-98a^2-16a^4-5a^6+3a^8)+ \\ +E^2\,(72-10a^2-84a^4-9a^6+11a^8)]+\eta^2\,[a^4K^2\,(306-511a^2+41a^4+ \\ +48a^6)-2a^2KE(312+10a^2-559a^4+73a^6+48a^8)+E^2\,(24+974a^2- \\ -1107a^4-159a^6+152a^8)] \end{array}\right\}(a^2-\eta^2)^{\frac{1}{2}} + \frac{\alpha_{21} U x^4 \eta^2\,[12+(2-a^2)\,\eta^2]\cosh^{-1}\left|\frac{a}{\eta}\right|}{12\pi B^2}$$

$$\phi_{30} \quad \frac{2\,\alpha_{30} U x^4\,(1-a^2)}{BD_2}\left\{\begin{array}{l} a^2K\,(3-9a^2-2a^4)-E\,(6-15a^2+5a^4-4a^6)+ \\ +\eta^2\,[a^2K\,(9-a^2)-E\,(3+7a^2-2a^4)] \end{array}\right\}(a^2-\eta^2)^{\frac{1}{2}}$$

where

$$D_2 = a^4K^2\,(27-31a^2-8a^4)-2a^2KE\,(24-5a^2-15a^4-16a^6)- -E^2\,(12-119a^2+151a^4-64a^6+32a^8)$$

TABLE II

EXPRESSIONS FOR THE ANTI-SYMMETRIC POTENTIALS

ϕ_{rs} is the velocity potential for the flow whose downwash is of the form

$$w = -\alpha_{rs} U x^r \,|\, y \,|^s \operatorname{sgn} y.$$

ϕ_{00}

$$\frac{2\alpha_{00} U x \eta \cosh^{-1}\left|\frac{a}{\eta}\right|}{\pi B}$$

ϕ_{01}

$$\frac{-\alpha_{01} U x^2 (1-a^2)\,\eta\,(a^2-\eta^2)^{\frac{1}{2}}}{B^2\,[a^2\mathrm{K}-(2-a^2)\,\mathrm{E}]}$$

ϕ_{10}

$$\frac{-2\alpha_{10} U x^2 a \eta\,[a^2\mathrm{K}-\mathrm{E}]\,(a^2-\eta^2)^{\frac{1}{2}}}{\pi B\,[a^2\mathrm{K}-(2-a^2)\,\mathrm{E}]} + \frac{2\alpha_{10} U x^2 \eta \cosh^{-1}\left|\frac{a}{\eta}\right|}{\pi B}$$

ϕ_{02}

$$\frac{2\alpha_{02} U x^3 a \eta\,[a^2\mathrm{K}\,(1-3a^2)-2(1-2a^2)\,\mathrm{E}]\,(a^2-\eta^2)^{\frac{1}{2}}}{3\pi B^3 D_3} + \frac{2\alpha_{02} U x^3 \eta^3 \cosh^{-1}\left|\frac{a}{\eta}\right|}{3\pi B^3}$$

ϕ_{11}

$$\frac{\alpha_{11} U x^3 (1-a^2)^2 \eta\,(a^2-\eta^2)^{\frac{1}{2}}}{B^2 D_3}$$

ϕ_{20}

$$\frac{-\alpha_{20} U x^3 a \eta\,[a^2\mathrm{K}\,(23-9a^2)-2\mathrm{E}\,(8-a^2)]\,(a^2-\eta^2)^{\frac{1}{2}}}{3\pi B D_3} + \frac{\alpha_{20} U x^3 \eta\,(6+\eta^2) \cosh^{-1}\left|\frac{a}{\eta}\right|}{3\pi B}$$

where $\quad D_3 = a^2\mathrm{K}\,(1+a^2)-2\mathrm{E}\,(1-a^2+a^4).$

ϕ_{03}

$$\frac{-2\alpha_{03} U x^4 (1-a^2)\,\eta\,\left\{\begin{array}{l} a^2[a^2\mathrm{K}\,(1-9a^2)-\mathrm{E}\,(2-7a^2-3a^4)]+ \\ +\eta^2\,[a^2\mathrm{K}\,(2+9a^2-3a^4)-\mathrm{E}\,(4-5a^2+15a^4-6a^6)] \end{array}\right\}(a^2-\eta^2)^{\frac{1}{2}}}{B^4 D_4}$$

ϕ_{12}

$$\frac{2\alpha_{12} U x^4 a \eta}{3\pi B^3 D_4}\left\{\begin{array}{r} a^4\mathrm{K}^2\,(8-57a^2+45a^4)-2a^2\mathrm{KE}\,(16-89a^2+69a^4)+ \\ +\mathrm{E}^2\,(32-128a^2+83a^4+9a^6)+2a^2\eta^2\,[a^4\mathrm{K}^2\,(7-3a^2)- \\ -2a^2\mathrm{KE}\,(8-a^2-3a^4)+\mathrm{E}^2\,(4+11a^2-11a^4)] \end{array}\right\}(a^2-\eta^2)^{\frac{1}{2}}+$$

$$+\frac{2\alpha_{12} U x^4 \eta^3 \cosh^{-1}\left|\frac{a}{\eta}\right|}{3\pi B^3}$$

ϕ_{21}

$$\frac{-2\alpha_{21} U x^4 (1-a^2)\,\eta\,\left\{\begin{array}{r} a^2\mathrm{K}\,(12-31a^2+27a^4)-(24-65a^2+55a^4-6a^6)\,\mathrm{E}+ \\ +\eta^2\,[a^2\mathrm{K}(1-9a^2)-(2-7a^2-3a^4)\,\mathrm{E}] \end{array}\right\}(a^2-\eta^2)^{\frac{1}{2}}}{3B^2 D_4}$$

ϕ_{30}

$$\frac{-\alpha_{30} U x^4 a \eta}{\pi B D_4}\left\{\begin{array}{r} a^4\mathrm{K}^2\,(160-187a^2+63a^4)-2a^2\mathrm{KE}\,(200-223a^2+71a^4-12a^6)+ \\ +\mathrm{E}^2\,(160-84a^2-31a^4-9a^6)+2\,(1-a^2)\,\eta^2\,[a^4\mathrm{K}^2\,(13+3a^2)- \\ -2a^2\mathrm{KE}\,(16+5a^2+3a^4)+\mathrm{E}^2\,(12+13a^2+7a^4)] \end{array}\right\}(a^2-\eta^2)^{\frac{1}{2}}+$$

$$+\frac{\alpha_{30} U x^4 \eta\,(2+\eta^2) \cosh^{-1}\left|\frac{a}{\eta}\right|}{\pi B}$$

where

$$D_4 = a^4\mathrm{K}^2\,(8+31a^2-27a^4)-2a^2\mathrm{KE}\,(16+15a^2+5a^4-24a^6)+\mathrm{E}^2(32-64a^2-151a^4-119a^6+12a^8)$$

TABLE III

EXPRESSIONS FOR THE POTENTIALS WHEN THE LEADING EDGES ARE TRANSONIC

	(*a*) *Symmetric*	(*b*) *Anti-symmetric*
ϕ_{00}	$\dfrac{2\alpha_{00}Ux(1-\eta^2)^{\frac{1}{2}}}{B\pi}$	$\dfrac{2\alpha_{00}Ux\eta\cosh^{-1}\left\lvert\dfrac{1}{\eta}\right\rvert}{\pi B}$
ϕ_{01}	$\dfrac{\alpha_{01}Ux^2(1-\eta^2)^{\frac{1}{2}}}{3\pi B^2}+\dfrac{\alpha_{01}Ux^2\eta^2\cosh^{-1}\left\lvert\dfrac{1}{\eta}\right\rvert}{\pi B^2}$	$\dfrac{4\alpha_{01}Ux^2\eta(1-\eta^2)^{\frac{1}{2}}}{3\pi B^2}$
ϕ_{10}	$\dfrac{4\alpha_{10}Ux^2(1-\eta^2)^{\frac{1}{2}}}{3\pi B}$	$-\dfrac{2\alpha_{10}Ux^2\eta(1-\eta^2)^{\frac{1}{2}}}{3\pi B}+\dfrac{2\alpha_{10}Ux^2\eta\cosh^{-1}\left\lvert\dfrac{1}{\eta}\right\rvert}{\pi B}$
ϕ_{02}	$\dfrac{4\alpha_{02}Ux^3(1+11\eta^2)(1-\eta^2)^{\frac{1}{2}}}{45\pi B^3}$	$\dfrac{2\alpha_{02}Ux^3\eta(1-\eta^2)^{\frac{1}{2}}}{5\pi B^3}+\dfrac{2\alpha_{02}Ux^3\eta^3\cosh^{-1}\left\lvert\dfrac{1}{\eta}\right\rvert}{3\pi B^3}$
ϕ_{11}	$\dfrac{\alpha_{11}Ux^3(3-2\eta^2)(1-\eta^2)^{\frac{1}{2}}}{15\pi B^2}+\dfrac{\alpha_{11}Ux^3\eta^2\cosh^{-1}\left\lvert\dfrac{1}{\eta}\right\rvert}{\pi B^2}$	$\dfrac{16\alpha_{11}Ux^3\eta(1-\eta^2)^{\frac{1}{2}}}{15\pi B^3}$
ϕ_{20}	$\dfrac{4\alpha_{20}Ux^3(11+\eta^2)(1-\eta^2)^{\frac{1}{2}}}{45\pi B}$	$\dfrac{-19\alpha_{20}Ux^3\eta(1-\eta^2)^{\frac{1}{2}}}{15\pi B}+\dfrac{\alpha_{20}Ux^3\eta(6+\eta^2)\cosh^{-1}\left\lvert\dfrac{1}{\eta}\right\rvert}{3\pi B}$
ϕ_{03}	$\dfrac{\alpha_{03}Ux^4(2+27\eta^2)(1-\eta^2)^{\frac{1}{2}}}{70\pi B^4}+\dfrac{\alpha_{03}Ux^4\eta^4\cosh^{-1}\left\lvert\dfrac{1}{\eta}\right\rvert}{2\pi B^4}$	$\dfrac{16\alpha_{03}Ux^4\eta(1+5\eta^2)(1-\eta^2)^{\frac{1}{2}}}{105\pi B^4}$
ϕ_{12}	$\dfrac{16\alpha_{12}Ux^4(1+17\eta^2)(1-\eta^2)^{\frac{1}{2}}}{315\pi B^3}$	$\dfrac{2\alpha_{12}Ux^4\eta(15-2\eta^2)(1-\eta^2)^{\frac{1}{2}}}{105\pi B^3}+\dfrac{2\alpha_{12}Ux^4\eta^3\cosh^{-1}\left\lvert\dfrac{1}{\eta}\right\rvert}{3\pi B^3}$
ϕ_{21}	$\dfrac{\alpha_{21}Ux^4(54-125\eta^2)(1-\eta^2)^{\frac{1}{2}}}{420\pi B^2}+\dfrac{\alpha_{21}Ux^4(12+\eta^2)\eta^2\cosh^{-1}\left\lvert\dfrac{1}{\eta}\right\rvert}{12\pi B^2}$	$\dfrac{16\alpha_{21}Ux^4\eta(17+\eta^2)(1-\eta^2)^{\frac{1}{2}}}{315\pi B^2}$
ϕ_{30}	$\dfrac{16\alpha_{30}Ux^4(5+\eta^2)(1-\eta^2)^{\frac{1}{2}}}{105\pi B}$	$-\dfrac{\alpha_{30}Ux^4\eta(187+32\eta^2)(1-\eta^2)^{\frac{1}{2}}}{105\pi B}+\dfrac{\alpha_{30}Ux^4\eta(2+\eta^2)\cosh^{-1}\left\lvert\dfrac{1}{\eta}\right\rvert}{\pi B}$

Review

Studies in Mathematics and Mechanics, *presented to Richard von Mises by Friends, Colleagues and Pupils, and edited by Garrett Birkhoff, Gustav Kuerti and Gabor Szegö. New York Academic Press,* 1954. 353 *pp.* $9.00.

This tribute to the eminent work of Richard von Mises in applied mathematics and mechanics takes the admirable form of a series of 42 articles, on branches of these subjects in which he had worked, by " friends, colleagues and pupils." It is preceded by a valuable bibliography of von Mises's writings, and a brief but penetrating study by Philipp Frank of the views and aims which governed the selection by von Mises of a wide variety of scientific, mathematical, philosophical and literary subject-matter for investigation. Here are noticed briefly only four articles in the volume, which seem to be those of most interest to aeronautical scientists.

Professor Temple contributes an article on his very important concept of " weak functions " or " generalised functions," which is treated further in *J. London Math. Soc.* 28, 134 (1953) and *Proc. Roy. Soc.* 228, 175 (1955). In these investigations he gives a simple and rigorous foundation to the theory of delta functions, principal values and finite parts of integrals, and the Fourier analysis of singular functions of all kinds. Much of this work greatly simplifies the analysis in many well-known kinds of aerodynamical calculation.

A simple model of shear flow turbulence based on considering the motion from a Lagrangian point of view and postulating certain resistances and rotations for fluid elements depending on their difference of velocity from the mean and on the local mean shear is put forward by Dr. J. M. Burgers.

The oscillating vortex wake behind an obstacle at Reynolds numbers of order 10^2 is studied by means of the Oseen approximation in a paper by Professor C. C. Lin.

Professor Howard Emmons derives a general correlation for experimental results on natural convection, film condensation, film boiling and film melting, by re-analysing the significance of the relevant Rayleigh and Reynolds numbers.

M. J. LIGHTHILL.

Errata

It is regretted that in the paper by L. E. Fraenkel " On the Unsteady Motion of a Slender Body through a Compressible Fluid " published in the February 1955 issue of The Aeronautical Quarterly (Vol. VI, p. 59), the printed impression of some of the pages was very poor.

The most serious result of this was that the identity between equations (16) and (17), page 65, *which should read*

$$K_0(z)=\tfrac{1}{2}\int_0^\infty \exp\left(-u-\frac{z^2}{4u}\right)\frac{du}{u},$$

apparently contained " z " and not " z^2 " in the expression on the right hand side.

In addition the letter " d " should have appeared before the " θ " at the very end of equations (76) and (77) on p. 80.